SCHüRMANN L W

THE GEOCHEMISTRY AND PETROLOGY OF THE UPPER CRITICAL ZONE IN THE BOSHOEK SECTION, OF THE WESTERN BUSHVELD COMPLEX

MSc UP 1991

The geochemistry and petrology of the upper critical zone in the Boshoek section, of the western Bushveld Complex.

by

L.W. Schürmann

Thesis submitted in fulfilment of the requirements for the degree of MASTER OF SCIENCE in the Department of Geology, University of Pretoria

July 1991

To the memory of my brother Martin,
for the bright years.

ABSTRACT

The Boshoek section is located in the mafic part of the southwestern Bushveld Complex. The tectonic setting of the section is characterized by two deformational stages prior and during emplacement of the lower and critical zones. The warped floor of the southwestern Bushveld Complex resulted in lithological differences of the lower zone sequences in the Rustenburg and Marikana sections, and the subsequent transgression northwards towards the Boshoek section in response to the addition of fresh magma into the magma chamber.

The upper critical zone in the Boshoek section is stratigraphically subdivided into several units on the basis of lithological features and geochemical trends. The Intermediate and Merensky Footwall units are further subdivided into sub-units on the basis of modal-mineral proportions and whole rock geochemical trends.

The mechanism introduced for the formation of the upper critical zone is based on mineralogical and geochemical trends, together with the characteristics of the potential parental magmas to the lower and critical zones. The feldspathic pyroxenite layers are produced by the slumping of B1 magma from an elevated position down to the floor, while the sub-units of the Intermediate and Merensky Footwall units are initiated by periodic, gentle influxes of B2/B3 magma. Such an influx of magma can cause an increase in temperature and thus the return to plagioclase as the only mineral phase on the liquidus, in order to produce a mottled anorthosite. On cooling, orthopyroxene will join plagioclase on the liquidus to produce the noritic rocks.

The formation of the Merensky and Bastard units is initiated by the emplacement of the main zone magma, B4, together with the slumping of B1 magma from an elevated position. The B1 magma is responsible for the feldspathic pyroxenite layers, while the hybrid magma consisting of B1 and B4, together with the B4 magma produced the more felsic layers by crystal settling.

SAMEVATTING

Die Boshoekseksie is geleë in die mafiese gedeelte van die suidwestelike Bosveldkompleks. Die gebied word tektonies gekenmerk deur twee vervormingsfases voor en gedurende inplasing van die Laer- en Kritieke Sones. Die golwende vloer van die suidwestelike Bosveldkompleks het die magma-inplasing in so 'n mate beïnvloed dat litologiese verskille in die opeenvolgings van die Laersone in die Rustenburg- en Marikanaseksies, en die daaropvolgende transgressie noordwaards in die rigting van die Boshoek- seksie, prominent is.

Die boonste Kritieke Sone in die Boshoekseksie is stratigrafies in verskeie eenhede ingedeel op grond van litologiese kenmerke en geochemiese neigings. Die Oorgangs- en die Merensky-vloereenhede is verder onderverdeel in subeenhede op grond van modale mineraalproporsies en geochemiese neigings.

Die meganisme wat vir die formasie van die boonste Kritieke Sone voorgestel is, is gebaseer op die opwaardse verplasing van B1-magma (hoër likwidustemperatuur, maar 'n laer digtheid as B2/B3-magma) deur die toevoeging van B2/B3-magma in die magmakamer. Die B1-magma kristalliseer ortopirokseen, wat aanleiding gee tot 'n ortopirokseen-houdende mengsel met 'n digtheid wat hoër is as die onderliggende B2/B3-magma. Insakking van die B1-magmamengsel in die onderliggende B2/B3-magma is dus verantwoordelik vir die veldspatiese piroksenietlae. Die subeenhede van die Oorgangs- en Merensky-vloereenhede word voortgebring deur periodieke, stadige toevoegings van B2/B3-magma bokant die vloer van die magmakamer. So 'n inplasing kan verantwoordelik wees vir 'n toename in temperatuur, en dus 'n terugkeer na plagioklaas as die enigste mineraalfase op die liquidus, ten einde 'n gevlekte anortosiet op te lewer. Namate die magma afkoel, sal ortopirokseen terugkeer na die liquidus om saam met plagioklaas, leukonoriet en waarskynlik noriet, te produseer.

Die Merensky- en Bastardeenhede is voortgebring deur die inplasing van die Hoofsone-magma, B4, tesame met die insakking van die B1-magma. Die B1-magma is verantwoordelik vir die veldspatiese piroksenietlae, terwyl 'n magma bestaande uit hibriede B1 en B4, en B4-magma die meer felsiese-lae (noriet, leukonoriet en gevlekte anortosiet) deur kristaluitsakking voortgebring het.

CONTENTS

LIST OF FIGURES

LIST OF TABLES

1. INTRODUCTION

During the past decade a number of investigations characterized the geological setting of the Merensky Reef and UG2 chromitite layer, the two important platiniferious layers in the upper critical zone of the western Bushveld Complex. These investigations include the studies in the Union and Rustenburg sections of the Rustenburg Platinum Mine (De Klerk, 1982; Eales **et al.**, 1986; Kruger, 1982; Naldrett **et al.**, 1986, 1987; and Viljoen **et al.**, 1986a, 1986b) and in the Maandagshoek area of the eastern Bushveld (Gain, 1985). Although Leeb du Toit (1986) described the upper critical zone succession in the Boshoek section of the southwestern Bushveld Complex, this work contains no compositional data of minerals or rock layers. Consequently, it was decided to investigate a representative lithological section through the upper critical zone in the Boshoek section in detail and to compare geochemical and mineralogical data of this sequence with published data on equivalent sections in the Union and Rustenburg areas. It was hoped that this study would also elucidate the petrogenesis of the important mineralized layers in this part of the succession.

The Impala lease area is situated in the Boshoek section north of Rustenburg in the Republic of Bophuthatswana and covers approximately 10 700 hectares (**Fig. 1.1**). Four mines are operational, with the Wildebeestfontein South Mine, from which the samples studied here were obtained, situated approximately 5 kilometres north of Rustenburg in the southern part of the lease area.

1.1 Geological setting

The rocks of the Rustenburg Layered Suite are poorly exposed in the southwestern Bushveld Complex. The marginal zone is marked by the presence of quartzite xenoliths and reflects the transgressive relationship between the Rustenburg Layered Suite and its floor. Marked undulations in the sedimentary floor, which consists of quartzite and minor hornfels, subdivide the southwestern Bushveld Complex into the Boshoek, Rustenburg and Marikana sections (mapping of Coertze, 1974) and appear to be responsible for lateral variations in thickness of the pyroxenites of the lower and lower critical zones (Viljoen and Hieber, 1986).

In the Boshoek section the Rustenburg Layered Suite is represented by the marginal, critical and main zones. The lower zone is not developed in the area (Coertze, 1974) and the lower critical zone rests directly on marginal lithologies (**Fig. 1.1**).

The lease area has a low relief and lies between the Magaliesberg Formation in the south and west, the upper zone gabbro in the east and the Pilanesberg Alkaline Complex in the northwest (**Fig. 1.1**).

Rock units of the Layered Suite strike predominantly north- northwest but locally may strike east-west (Leeb du Toit, 1986). The average dip is approximately 9 to 10 degrees northeast. Minor faults, with displacements ranging from 1 to 20 metres are present (Leeb du Toit, 1986). Lamprophyre and dolerite dykes, with thicknesses varying from 0,2 to 2 metres and up to 40 metres respectively, are frequently encountered in the mine workings. Several dunite pipes occur in the lease area.

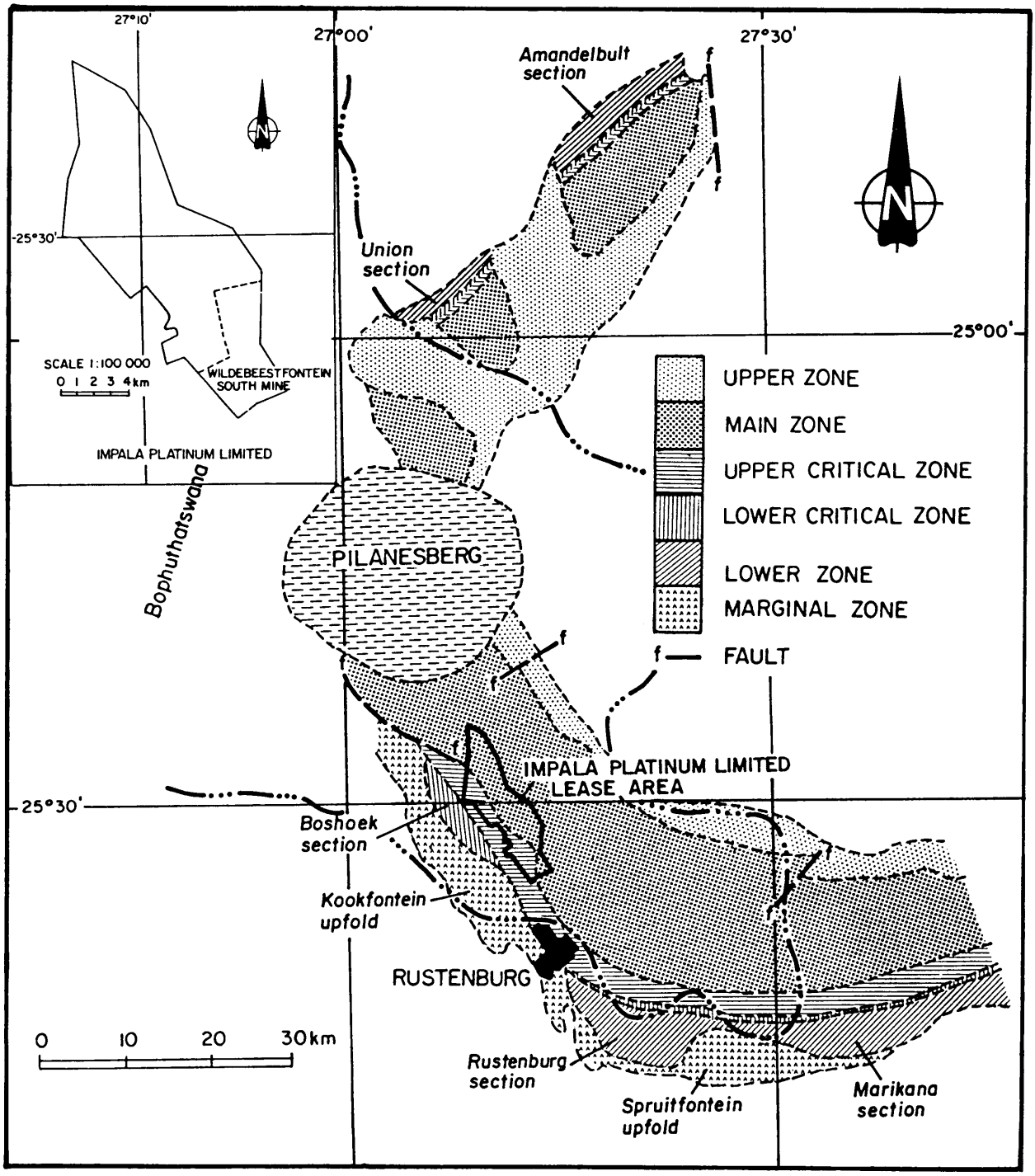

Figure 1.1 Map showing the location of the study area.

1.2 Previous work

The western Bushveld Complex has been studied by various researchers over the past century. Publications concerning the geochemistry, mineralogy, petrogenesis and mining activities are numerous and this review of previous work concentrates only on those publications of direct relevance to this investigation.

The structure of the Bushveld Complex was described by Hall (1932) as a lopolith due to its inclined footwall and sheet-like form. Truter (1955) expressed his doubt regarding the lopolithic form and suggested that there were several intrusion centres connected laterally along an east-west axis. Emplacement was confined to four or five loci with an additional centre located slightly to the south of Potgietersrus.

On the basis of geophysical and geological data, Cousins (1959) suggested that the Bushveld Complex was not a lopolith but consisted of two curved troughs of mafic rocks with a superficial synclinal structure. He suggested that the configuration of the mafic rocks along the inner margins of these postulated troughs are obscured by granitic intrusives and by overlying younger rocks. He also noted that the mafic rocks were never emplaced in the central area of the Bushveld Complex and that the troughs of mafic rocks may have had dyke-like central feeders.

The chromitite layers in the Rustenburg-Boshoek section were described by Fourie (1959) who correlated them on the basis of the type of host rock, presence of markers and individual layer thicknesses. Furthermore, mineralogical, physical and chemical characteristics of the individual chromitite layers were described. Subsequently Cousins and Feringa (1964) found the thicker layers to be continuous along strike and persistent to depths of over 1600 metres vertically below surface. They subdivided the chromitite layers of the critical zone into the Lower, Middle and Upper Groups and introduced a system of symbols designating the different chromitite layers.

On the basis of field relations, Coertze (1974) subdivided the western Bushveld Complex into eight rock units: viz. the basal norite unit (marginal zone), harzburgite and pyroxenite units (lower and lower critical zones), anorthosite, norite and porphyritic pyroxenite units (upper critical zone), gabbro unit (main zone) and ferrogabbro unit (upper zone). He found that within individual units the pyroxenes become more iron-rich and plagioclase more sodic upwards in the sequence and that reversals in the compositional trends are confined to contacts between successive units. A model describing the emplacement of the Bushveld magma which was regulated by conditions of tension and compression, is presented. He also proposed that sagging of the floor and tilting towards the centre of the Complex resulted in a tilted, funnel-shaped structure.

The pegmatoid nodules in the Boulder Bed at Impala Platinum Mines were studied by Jones (1976). These were found to have approximately the same mineralogy and chemistry as the pegmatoid associated with the UG2 and Merensky Reef. Jones suggested that the nodules formed as a result of the break-up of a pyroxenitic layer and equated the position of the Boulder Bed with the Pseudo Reef at the Union section in the northwestern Bushveld Complex.

Mostert **et al.** (1982) investigated the platinum-group mineralogy of the Merensky Reef at Impala Platinum Mines. On the basis of the textures observed they concluded that the platinum-group minerals were formed at a relatively late stage in the crystallization history. They suggested that these elements were concentrated in the original monosulphide solid-solution and that they crystallized subsequent to the associated chalcopyrite.

Leeb du Toit (1986) described the succession from the UG1 chromitite layer to the top of the Bastard unit in the Impala lease area and introduced a terminology by which characteristic rock layers are numbered sequentially from the Merensky Reef down, i.e. the footwall (FW) layers, and from the Reef up, i.e. the hanging wall (HW) layers. Because the Merensky Reef is extensively potholed in the area three types of Reef are distinguished depending on the immediate footwall layer of the Reef. Merensky "A" Reef, which can be pegmatoidal or pyroxenitic, is underlain by the FW1 norite **(Fig. 1.2A)**. Types "B" and "C" are associated with potholes where the "B" Merensky Reef lies on FW2 and the "C" Reef on the FW3 or lower layers **(Figs. 1.2B and 1.2C)**. The "B" type Merensky Reef is commonly pegmatoidal and the "C" type may either be pegmatoidal or pyroxenitic. The Merensky Reef is underlain in places by pothole-like features filled with fine-grained, brown norite which contains xenoliths of pegmatoidal pyroxenite and lenses of fine-grained chromite. This norite, also known as the brown sugar norite (BSN) is regarded by Leeb du Toit (1986) as remnants of a pre-Merensky footwall sequence which was subjected to erosion and assimilation prior to and during the emplacement of the magma from which the Merensky unit crystallized. No satisfactory explanation is offered for the distribution or origin of the downwarped footwall structures, except that relatively unstable conditions could have prevailed in the magma chamber prior to or during the formation of the Merensky unit.

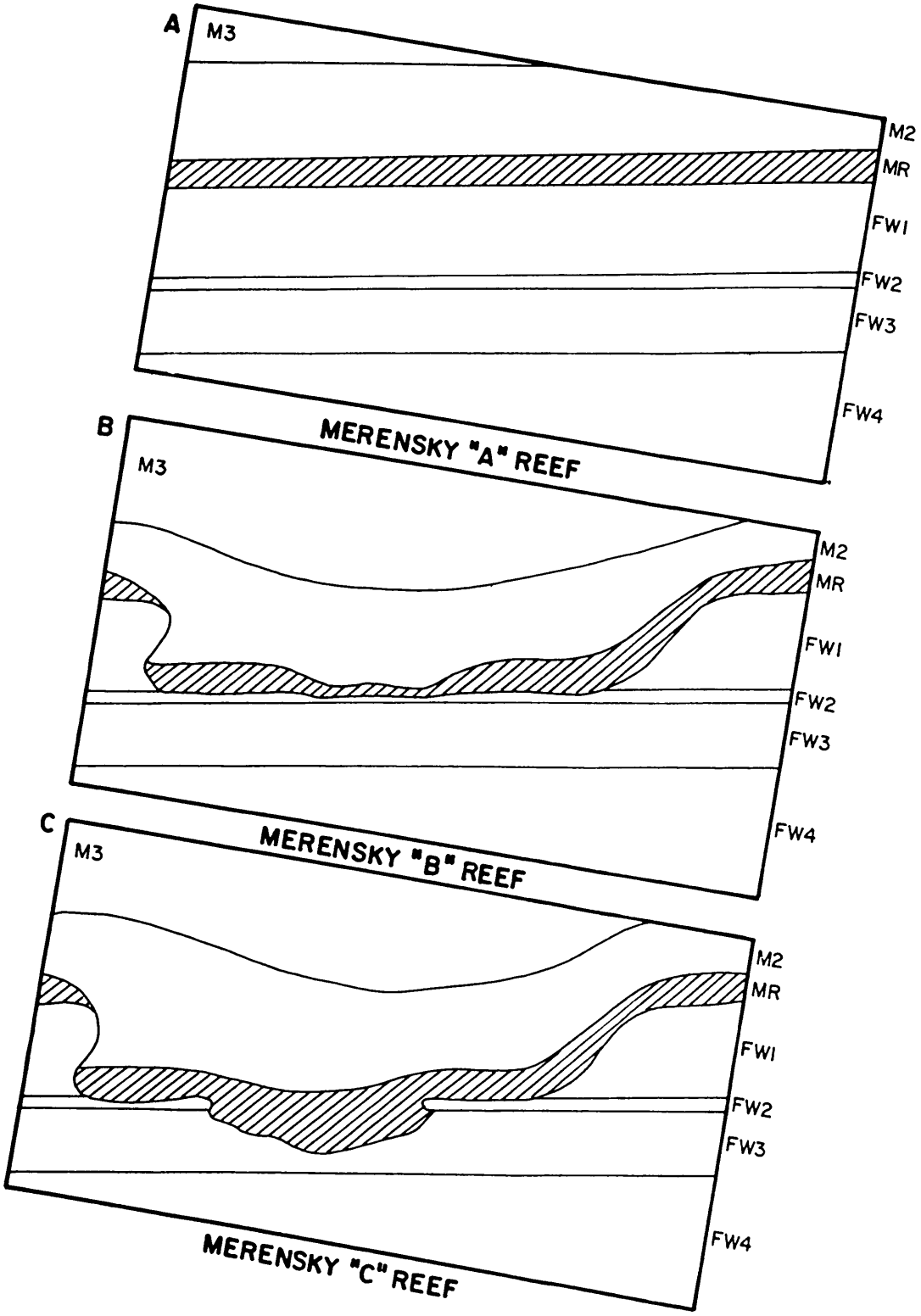

Figure 1.2 Classification of the Merensky Reef according to Leeb du Toit (1986).

2. TECTONIC FRAMEWORK OF THE SOUTHWESTERN BUSHVELD COMPLEX

Mapping of the area west and southwest of the Impala lease area, revealed that the floor rocks of the southwestern Bushveld Complex display increasingly varied degrees of deformation towards the contact with the Layered Suite.

The structure of the adjacent floor rocks in the southwestern Bushveld Complex is dominated by the NW-trending (160 degrees) post-Bushveld Rustenburg fault **(Fig. 2.1 in Folder)**. This normal fault with a downthrow to the east extends northwards towards the west of the Pilanesberg Complex. A second set of smaller faults and joints, striking approximately 73 degrees and dipping at either 76 degrees SSE or 88 degrees NNW is related to the Rustenburg fault as well as its northern extension, the Lilliput fault (Du Plessis and Walraven, 1990). The faults and joints post-date the main zone rocks and earlier folding of the Transvaal sediments. Vermaak (1976) considers the folding and faulting due to the emplacement of the Bushveld Complex which were subsequently reactivated during the intrusion of the Pilanesberg Complex. Dykes, associated with the Pilanesberg Complex intruded along these faults and joints.

Two stages of folding can be recognized in the area from west and southwest of the lease area towards the Olifantsnek Dam in the south. The first stage is represented by fold structures that are mainly confined to the Magaliesberg Quartzite Formation. Fold-axes are parallel to the contact between the Layered Suite and the Magaliesberg Quartzite Formation **(Fig. 2.1 in Folder)**. In the marginal zone these structures (stage 1 folds) can be subdivided into attached and detached folds (Sharpe and Chadwick, 1982). Quartzitic xenoliths are present close to the contact between the Rustenburg Layered Suite and the sedimentary floor. Examples of the attached floor folds are the Boekenhoutfontein, Rietvly and Olifantsnek anticlines. This stage 1 folding was initiated by compressional stresses generated by isostatic subsidence of the Transvaal Sequence during sedimentation and the emplacement of the pre-Bushveld sills (Sharpe and Snyman, 1980).

The second stage of deformation comprises large-scale folds, represented by the undulating contact between the floor and the Rustenburg Layered Suite **(Figs. 2.1 in Folder and 2.2)**. Their fold-axes trend at approximately right angles to the first folding event (stage 1). Deformation during the emplacement of the Bushveld Complex was largely ductile and the formation of basins by sagging and upfolding of the floor exerted a strong influence on the subsequent evolution of the lower and critical zones and the associated chromitite layers (Sharpe and Chadwick, 1982).

The subdivision of the southwestern Bushveld Complex into the Marikana, Rustenburg and Boshoek sections is based on **(a)** the presence of the Spruitfontein and Kookfontein upfolds **(b)** stratigraphic differences between the lower and lower critical zones and **(c)** lateral variations of the associated chromitite layers (Hatton and Von Gruenewaldt, 1985). Work done by Coertze (1974) has shown that the lower zone is not developed in the Boshoek section but that it is prominent in the Rustenburg and Marikana sections **(Fig. 2.2)**. The Lower Group chromitite layers occur sporadically in the Boshoek section together with the prominent LG6 and LG6a chromitite layers. In the Rustenburg section, all the Lower Group chromitite layers are developed, although the silicate sequence is much thinner than that hosting the Lower Group chromitite layers in other parts of the Bushveld Complex (Fourie, 1959; Cousins and Feringa, 1964). Thin chromitite layers are present in the lower critical zone of the Marikana section but they can not be correlated with the

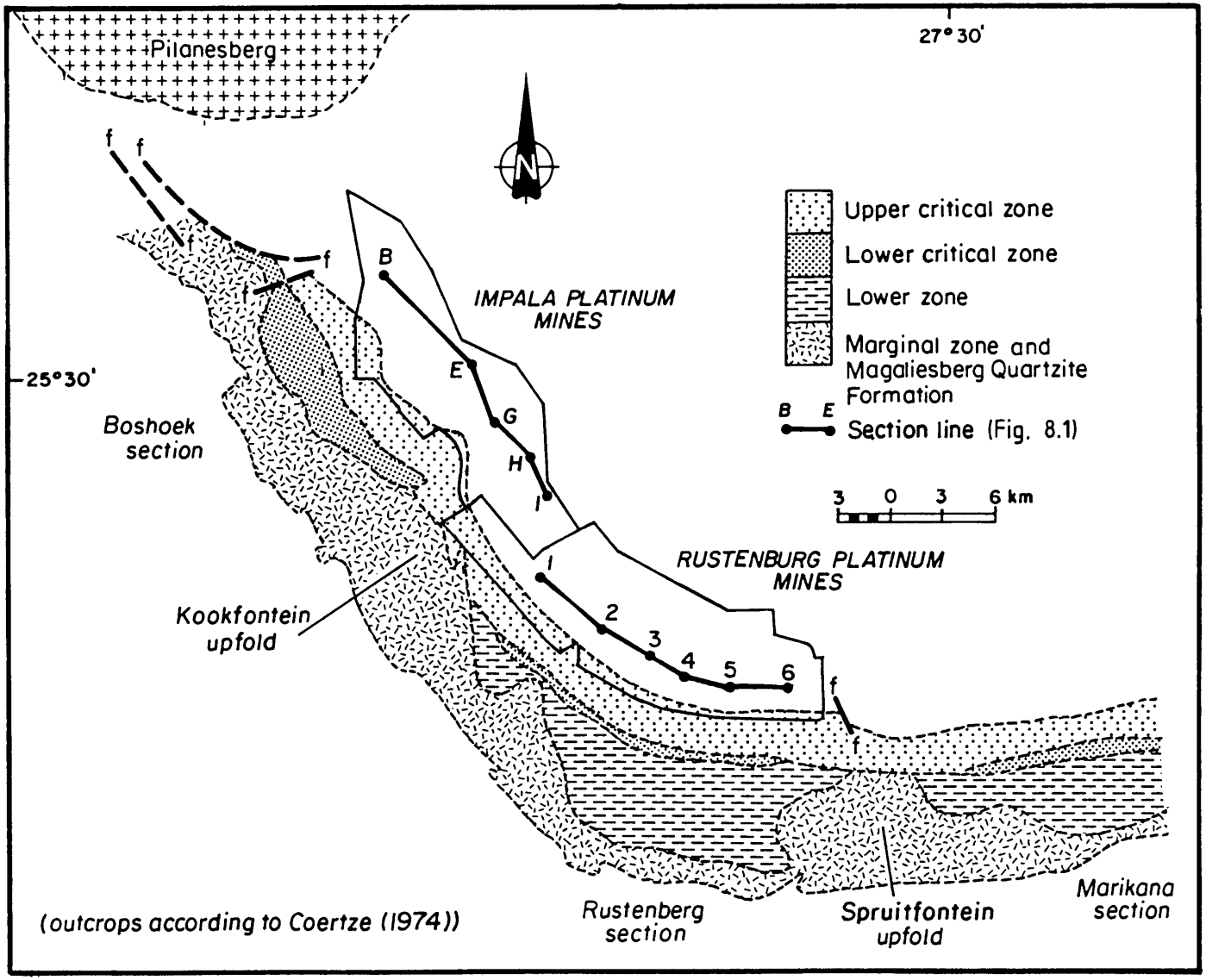

Figure 2.2 Simplified geological map of the southwestern Bushveld Complex showing the floor folds in the Magaliesberg Quartzite Formation in relation to the Impala and Rustenburg Lease areas.

Lower Group chromitite layers elsewhere in the Complex. The Middle Group chromitite layers in the Rustenburg section are single, rather than multiple layers, while the amount of chromite present is distinctly less than in the Marikana section (Hatton and Von Gruenewaldt, 1985). In the Boshoek section the amount of chromite decreases further and a change in the associated silicate stratigraphy is also prominent. The Upper Group chromitite layers correlate well in all the southwestern sections.

Figure 2.3a to 2.3c is a simplified schematic representation of the proposed structural evolution to explain the relationship between the lower and critical zones of the southwestern Bushveld Complex and its floor. The second folding stage is considered mainly to be due to an increase in ductility of the floor below the magma chamber. The first of these to form was the Spruitfontein upfold which developed during the formation of the lower zone **(Figs. 2.3a and 2.3b)** in order to produce two lithologically different lower zone sequences in the Rustenburg and Marikana sections (Cousins and Feringa, 1964). Subsequent to crystallization of the lower zone in these two sections, the magma chamber evidently transgressed northwards towards the Boshoek section in response to the addition of pulses of fresh magma into the magma chamber. The Kookfontein upfold, therefore only developed during the crystallization of the lower critical zone.

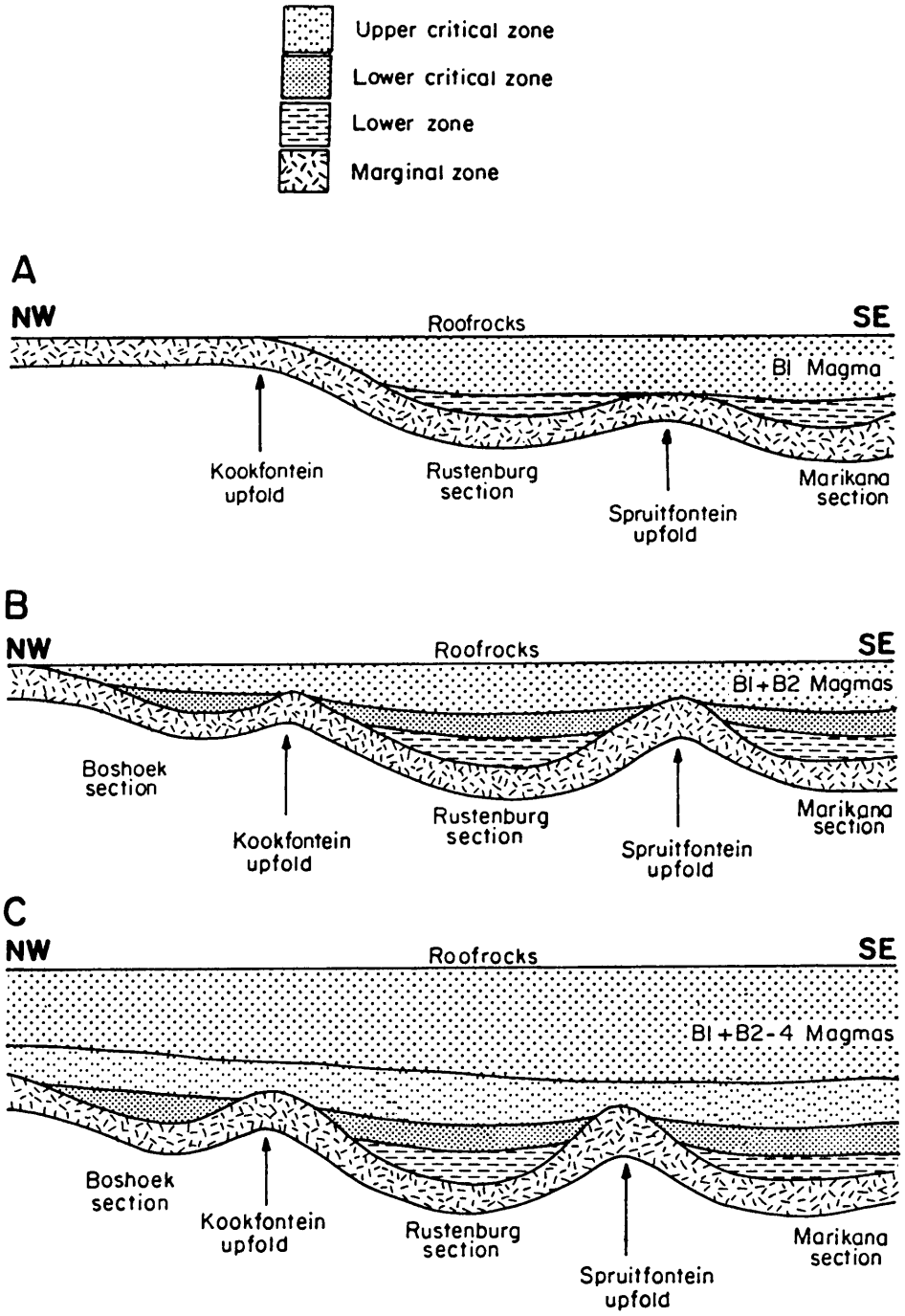

Figure 2.3 Simplified structural model to explain the relationship between the lower and critical zones of the southwestern Bushveld Complex to the floor rocks.

3. STRATIGRAPHY OF THE UPPER CRITICAL ZONE

3.1 Introduction

Plagioclase and plagioclase-pyroxene cumulates, mostly norites, leuconorites and anorthosites, are the most common rock types in the upper critical zone. They have, on the basis of characteristic lithological features, been assigned numbers according to their position with respect to the Merensky unit (Leeb du Toit, 1986). The footwall layers range from FW14 beneath the UG1 chromitite layer to FW1 directly below the Merensky Reef. Hanging wall layers are those above the Bastard Reef and range from HW1 to HW5, the uppermost layer generally exposed in underground workings. The layers within the Merensky unit are the Merensky feldspathic pyroxenite at the base, followed by a leuconorite and a mottled anorthosite at the top. The latter are referred to as the Middling 2 and Middling 3 respectively. The feldspathic pyroxenite layers (pyroxene cumulates) are named according to the "reef" that they host, hence, from the base upwards the UG1, UG2 (upper and lower), Merensky and Bastard pyroxenites.

For purposes of this study the succession is divided into six units on the basis of lithological features and geochemical trends. They are the UG1, UG2, Intermediate, Merensky Footwall or "Pseudo", Merensky and Bastard units.

The Intermediate and Merensky Footwall units are further subdivided into sub-units on the basis of modal-mineral proportions and whole rock geochemical trends. A sub-unit is recognized by an overall upward increase in the modal amount of orthopyroxene and or olivine. Mottled anorthosite invariably occurs at the base of these sub-units and is overlain by layers of leuconorite and or norite. Sharp contacts occur predominantly between the mottled anorthosite and the underlying leuconorite or norite while the contact of the mottled anorthosite and the overlying leuconorite or norite is usually gradational. Two sub-units are present within the Intermediate unit while four less prominent ones are present in the Merensky Footwall unit **(Fig. 3.1)**.

3.2 UG1 unit

The UG1 chromitite layer at the base of the unit is approximately one metre thick and overlies the 10 metre thick FW14 mottled anorthosite. The chromitite layer bifurcates to form two or more layers in the mottled anorthosite footwall, while lenses of anorthosite are also found within these chromitite layers. The overlying pyroxenite consists of cumulus orthopyroxene with clinopyroxene oikocrysts and intercumulus plagioclase. A chromitite layer (1 to 10 centimetre thick) with sharp top and bottom contacts separates the UG1 pyroxenite and the overlying FW13 leuconorite, which is between 7 and 8 metres thick **(Fig. 3.1)**.

3.3 UG2 unit

The UG2 unit commences with a 4,5 metre thick feldspathic pyroxenite at the base. An orthopyroxene pegmatoid layer, 0,2 to 2 metres thick, overlies the lower pyroxenite with a sharp contact. Disseminated chromite and chromitite stringers are present in the pegmatoid.

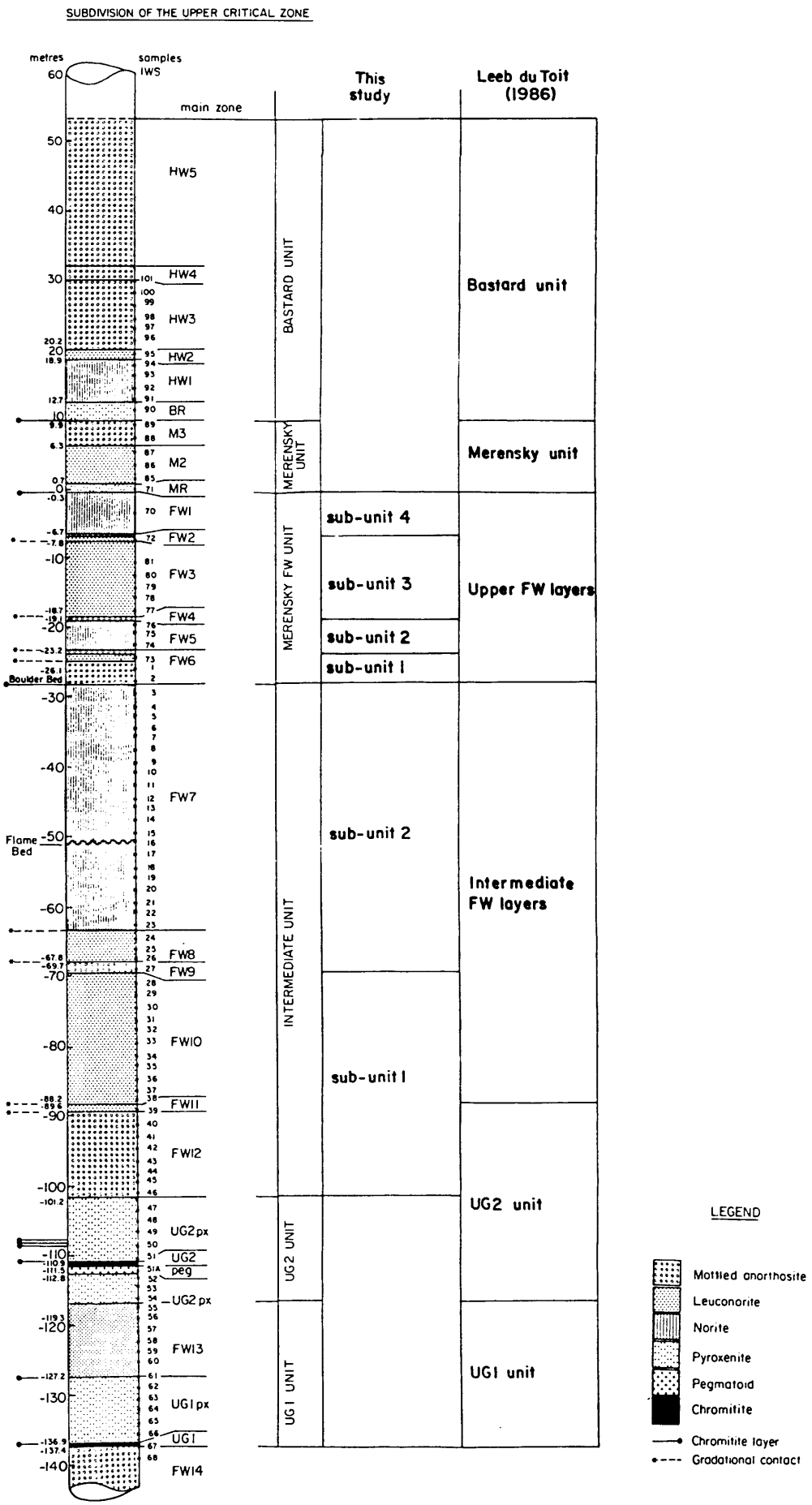

Figure 3.1 Lithological and stratigraphic subdivision of the upper critical zone in the Boshoek section according to Leeb du Toit (1986) and this investigation.

Its contact with the overlying 0,50 to 0,80 metre thick chromitite layer is irregular. Poikilitic bronzite grains give the chromitite layer a spotted appearance. A 9 metre thick feldspathic pyroxenite overlies the UG2 chromitite layer **(Fig. 3.1)**. The upper and lower feldspathic pyroxenite layers have sharp contacts with FW12 and 13 respectively. The upper pyroxenite layer hosts the "Leader triplets" which are situated between 0,2 to 3 metres above the main UG2 chromitite layer.

3.4 Intermediate unit

The Intermediate unit overlies the upper pyroxenite of the UG2 unit and extends to the FW7/FW6 contact. The lowermost layer of this unit is the 10 metre thick FW12 mottled anorthosite, which overlies the UG2 upper pyroxenite with a sharp contact. Footwall 11, an approximately 1 metre thick leuconorite, has gradational contacts with the under- and overlying footwall layers. Footwall 10 consists of an 18 metre thick leuconorite layer. Although Footwall 11 and 10 are both leuconorite layers, distinction between the two layers is based on the texture and subtle differences in the modal composition of the individual rock layers. Leeb du Toit (1986), termed FW11 a spotted anorthosite and FW10 an anorthositic norite. Footwall 12, 11 and 10 constitute the first Intermediate sub-unit in the investigated succession **(Fig. 3.1)**.

The FW9 mottled anorthosite overlies the FW10 leuconorite with a sharp contact. The layer is 2 metres thick and underlies the FW8 leuconorite and FW7 norite which are 3 and 37 metres thick respectively. The FW9/FW8 and FW8/FW7 contacts are gradational but distinct. The contorted "flame bed" is present 15 metres above the FW8/FW7 contact and comprises a 1,5 metre thick, highly contorted layer of mottled anorthosite. According to Vermaak (1976), this contorted marker layer formed as a result of differential loading, assumed to be caused by magma movements during tectonic adjustments of the floor. The second Intermediate sub-unit consists of FW9, 8 and 7 **(Fig. 3.1)**.

3.5 Merensky Footwall unit

The Merensky Footwall unit contains the succession between the FW7/FW6 and the FW1/MR pyroxenite contacts. Where the entire FW6 layer is thicker than 3 metres it usually consists of four well defined rock-types (Leeb du Toit, 1986). The mottled anorthosite layer FW6(c) is not developed in the Wildebeestfontein South area, even though the entire FW6 sequence is about 4.8 metres thick. The lowermost sublayer, FW6(d), is a mottled anorthosite with mottles between 30 and 40 millimetres in diameter, and characterized by the presence of "boulders" or nodules. It is commonly referred to as the "Boulder Bed" (Jones, 1976; Lee and Sharpe, 1979; Leeb du Toit, 1986). The nodules are "muffin" shaped, 5 to 25 centimetre in diameter, have convex lower contacts and consist of cumulus olivine and orthopyroxene with intercumulus plagioclase. Other common minerals are chromite, clinopyroxene and biotite. One chromitite stringer, 2 to 10 millimetres thick, is present at the base of the FW6(d) sublayer. Footwall 6(b) is a leuconorite containing pyroxene oikocrysts 10 to 20 millimetres in diameter. Two layers, 2 to 3 centimetres thick, which consist of fine-grained orthopyroxene and minor olivine, define the upper and lower contacts. The uppermost sublayer footwall 6(a) is a mottled anorthosite **(Fig. 3.1)**.

A uniform norite (FW5), with a thickness of 4,1 metres, overlies FW6. It is noted by Leeb du Toit (1986) that the thickness of FW5 is 3,5 metres in the south and 1 metre in the north. Such a lateral variation in thickness is typical of many of the layers in the Merensky Footwall unit. Footwall 4 is a mottled anorthosite, 40 centimetres thick with distinct layering at its base. Footwall 3 is an 11 metre thick uniform leuconorite. In the Wildebeestfontein South area, FW2 is 1,1 metre thick and consists of two sublayers. The lowermost sublayer, FW2(b), is a 76 centimetre thick leuconorite and is overlain by a 33 centimetre thick mottled anorthosite layer FW2(a). The two leuconorite layers, FW3 and sublayer FW2(b), are distinguished on the basis of their texture. Where FW2 attains a maximum thickness of 2 metres a third layer, viz. a 1 to 2 centimetre thick pyroxenite or pegmatitic pyroxenite (FW2(c)), is developed at the base (Leeb du Toit, 1986). In the studied profile FW2(c) is absent. Footwall 1 is a 6,7 metre thick norite layer.

The Merensky Footwall unit can be subdivided into four sub- units. The lowest, sub-unit 1, consists of sublayers FW6(d) and FW6(b). The Merensky Footwall sub-unit 2, which overlies sub-unit 1, commences with FW6(a) at the base and grades upward into FW5. The FW5/FW4 contact is sharp and divides sub-units 2 and 3. Sub-unit 3 consists of FW4, FW3 and sublayer FW2(b)**(Fig. 3.1)**. Sub-unit 4, which consists of the FW2(a) and FW1 is the uppermost sub-unit of the Merensky Footwall unit.

3.6 Merensky unit

The Merensky unit, with the Merensky Reef at its base, is the most consistent unit within the critical zone (Vermaak, 1976). In the Impala lease area, the pegmatoid and chromitite layer between the pegmatoid and pyroxenite are not always present. At Wildebeestfontein South the Merensky unit is 10 metres thick and consists of a 2 centimetre thick chromitite layer, which is developed on the contact between the FW1 norite and the overlying Merensky pyroxenite **(Fig. 3.1)**. Overlying the pyroxenite layer are layers M2 (a leuconorite) and M3 (a mottled anorthosite layer).

3.7 Bastard unit

This unit comprises a basal pyroxenite, approximately 3 metres thick with a thin chromitite layer (the uppermost chromitite layer in the critical zone) developed on the lower contact **(Fig. 3.1)**. Overlying the pyroxenite is a 6,5 metre thick norite layer (HW1) separated from the overlying 1,5 metre thick leuconorite layer (HW2) by two thin mottled anorthosite layers. HW3 is a 10 metre thick mottled anorthosite layer, and constitutes the base of the "Giant Mottled" anorthosite. The mottled anorthosite layers HW4 and HW5 are 2 and approximately 37 metres thick respectively. The distinction between HW3, 4 and 5 is based on the size of the mottles of the respective layers. HW4 has small mottles (0,75 centimetre diameter) interspersed with larger mottles of up to 4 centimetres in diameter. The overlying HW5 contains mottles 5 to 7 centimetres in diameter set in a matrix of dirty-grey plagioclase grains, compared to the clean white matrix of the HW3 layer. HW5 represents the upper part of the "Giant Mottled" anorthosite, the top of which is the contact between the upper critical and the main zones.

4. SAMPLING PROCEDURE AND ANALYTICAL TECHNIQUES

During the early part of 1987 underground samples were collected from shafts no. 9 and no. 1 of the Wildebeestfontein South Mine. The interval from the FW6 to the UG1 footwall was sampled on level 17 (cross-cut east) at the no. 9 shaft and FW6 to HW4 on level 12 (cross-cut west) and 1247 travelling way at the no. 1 shaft **(Figs. 4.1, 4.2 and 4.3)**.

Although a pothole of approximately 30 metres in diameter was intersected in 12 cross-cut west, samples of FW1, FW2 and the Merensky Reef were taken in the 1247 travelling way to ensure stratigraphic completeness. Samples of 2 to 3 kilograms were taken at 10 metre intervals in the cross-cuts which represent a vertical interval of approximately every 1,8 metres. A stratigraphic profile was compiled with the aid of these samples and underground maps supplied by the company geologists **(Fig. 3.1)**.

Polished thin sections of all samples were petrographically examined with transmitted and reflected light microscopes. The results of point count analyses to determine the modal proportions of plagioclase, orthopyroxene, clinopyroxene and olivine, are schematically represented in **Figure 4.4.**

Whole rock major element compositions as well as the trace element concentrations for Co, Cu, Ni, Zr, Rb, Sr, Ga, Sc, V, Y, U, Th, Nb, Cr, Zn and Ba of 103 samples were obtained by XRF technique on equipment housed at the University of Pretoria. Standard preparation techniques were used, and the values obtained are within the normal limits of analytical uncertainty. The results are listed in **Appendix 1.**

Microprobe analyses were obtained for plagioclase, orthopyroxene, chromite and olivine by using a JEOL 733 SUPERPROBE. Sample numbers and positions are shown in **Figure 4.5.** Operating conditions and standards used are summarized in **Table 4.1.** All analyses are listed in **Appendix 2.**

Operating conditions for chromite analyses were as follows:
Counting times for the elements Ti, Mn, Fe and Al were 20 seconds while for Cr and V it was 50 seconds. Lower limits of detection for Cr, V and Al were 0,027 wt%, 0,052 wt% and 0,019 wt% respectively. For full ZAF correction the program FZAFO was used. The Fe^{3+} content was calculated from the analysis by assuming stoichiometry. The effect of interferences between the Ti-K_B X-ray emission line and the V-K_x line was determined by Butcher and Merkle (1986) who analyzed for V in pure TiO_2 and found it to be 0,47 wt% V_2O_3. Similarly the effect of the interference between the V-K_B and Cr-K_x lines was found to be 12,0 wt% Cr_2O_3 in pure V_2O_5.

Sulphur content was determined on 103 samples at the Geological Survey on a LECO CS244 infrared absorption spectrometer with a HF100 induction furnace in an oxygen stream at approximately 1200 to 1400 °C.

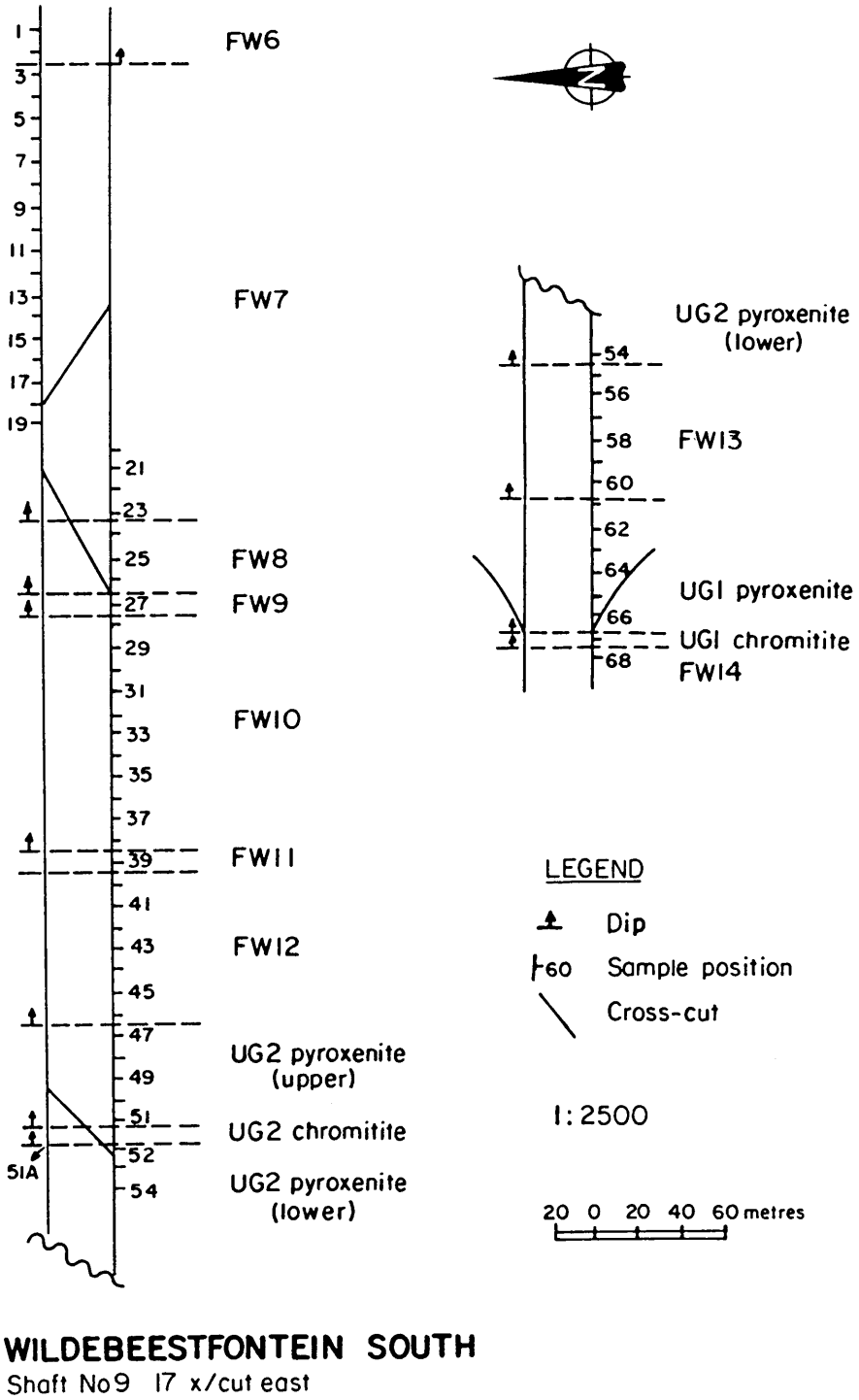

Figure 4.1 Diagram showing sampling positions of the FW14-FW6 sequence on the 17th level, cross-cut east of shaft No. 9, Wildebeestfontein South.

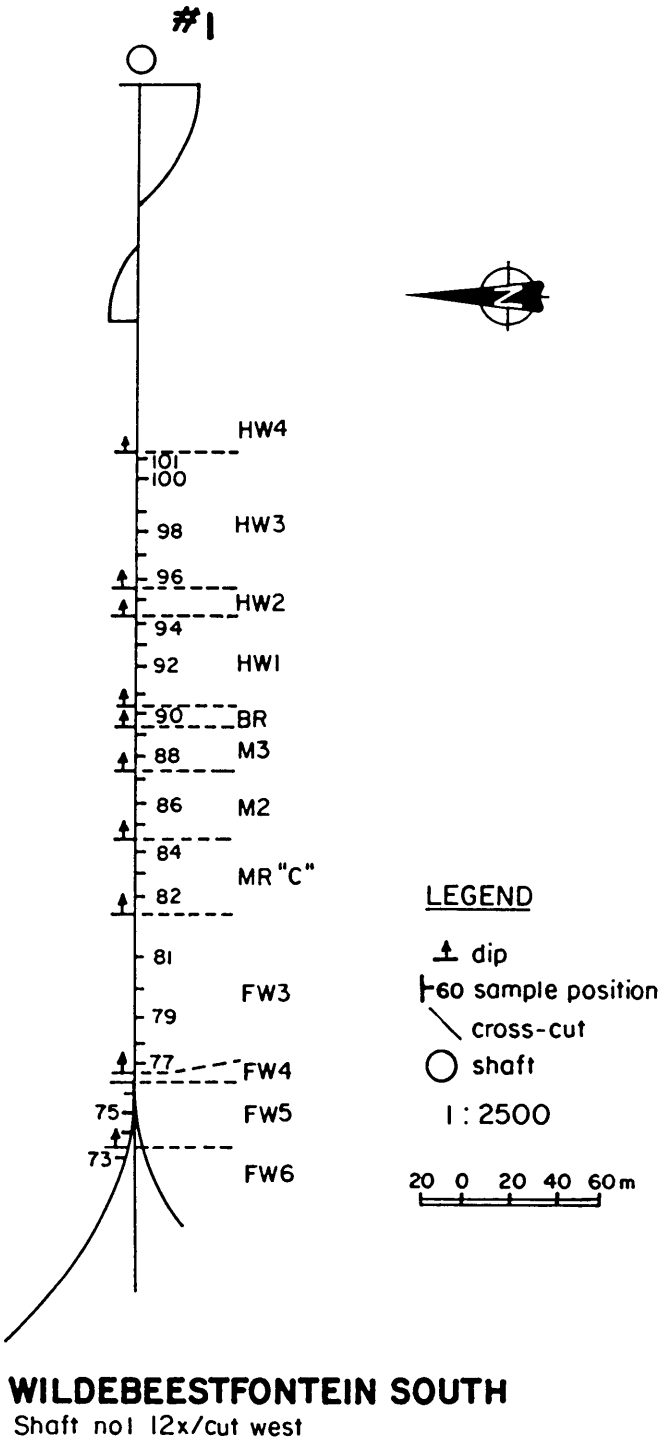

Figure 4.2 Diagram showing sampling positions of the FW6-HW4 sequence on the 12th level, cross-cut west of shaft No. 1, Wildebeestfontein South.

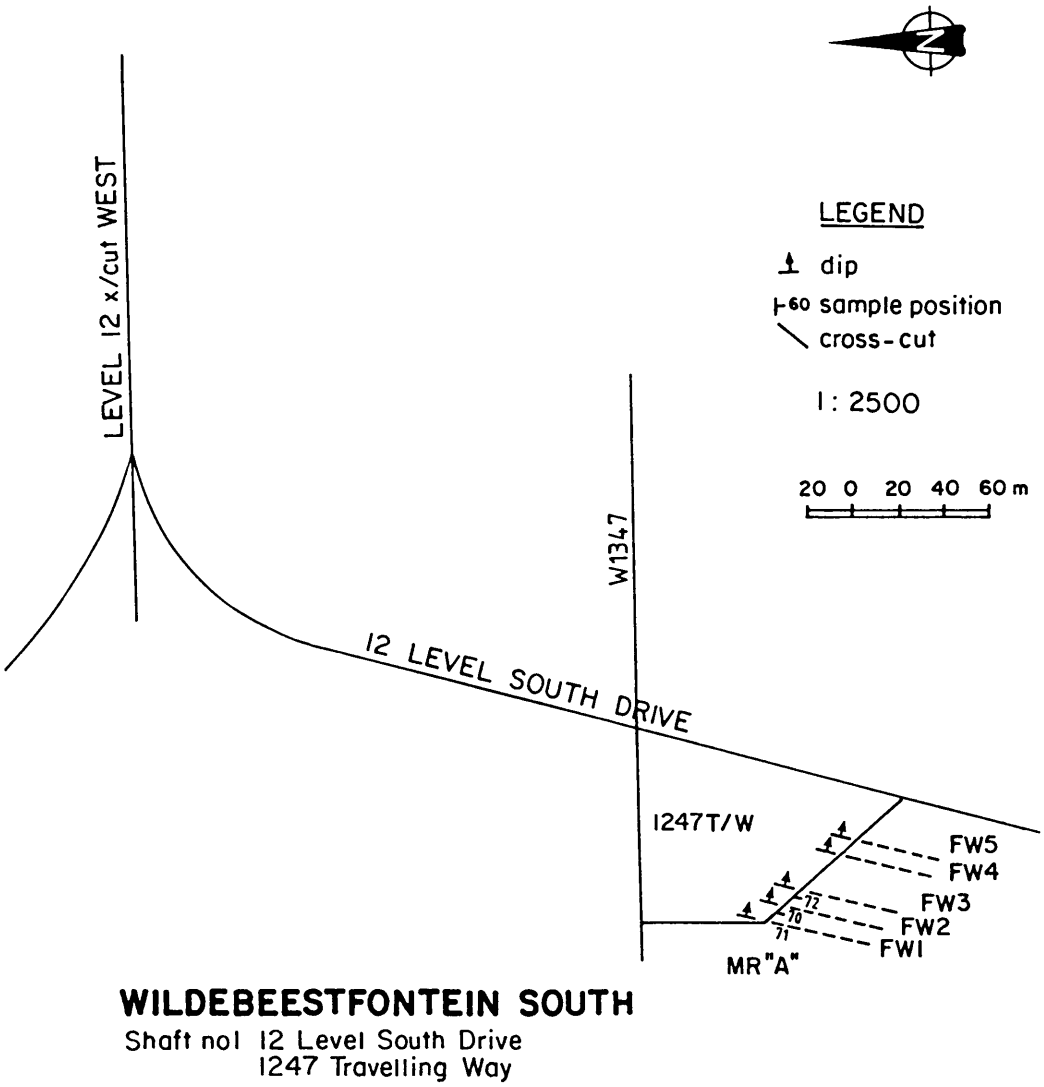

Figure 4.3 Diagram showing sampling positions of FW2, FW1 and Merensky Reef in 1247 travelling way, 12th level south drive of shaft No. 1, Wildebeestfontein South.

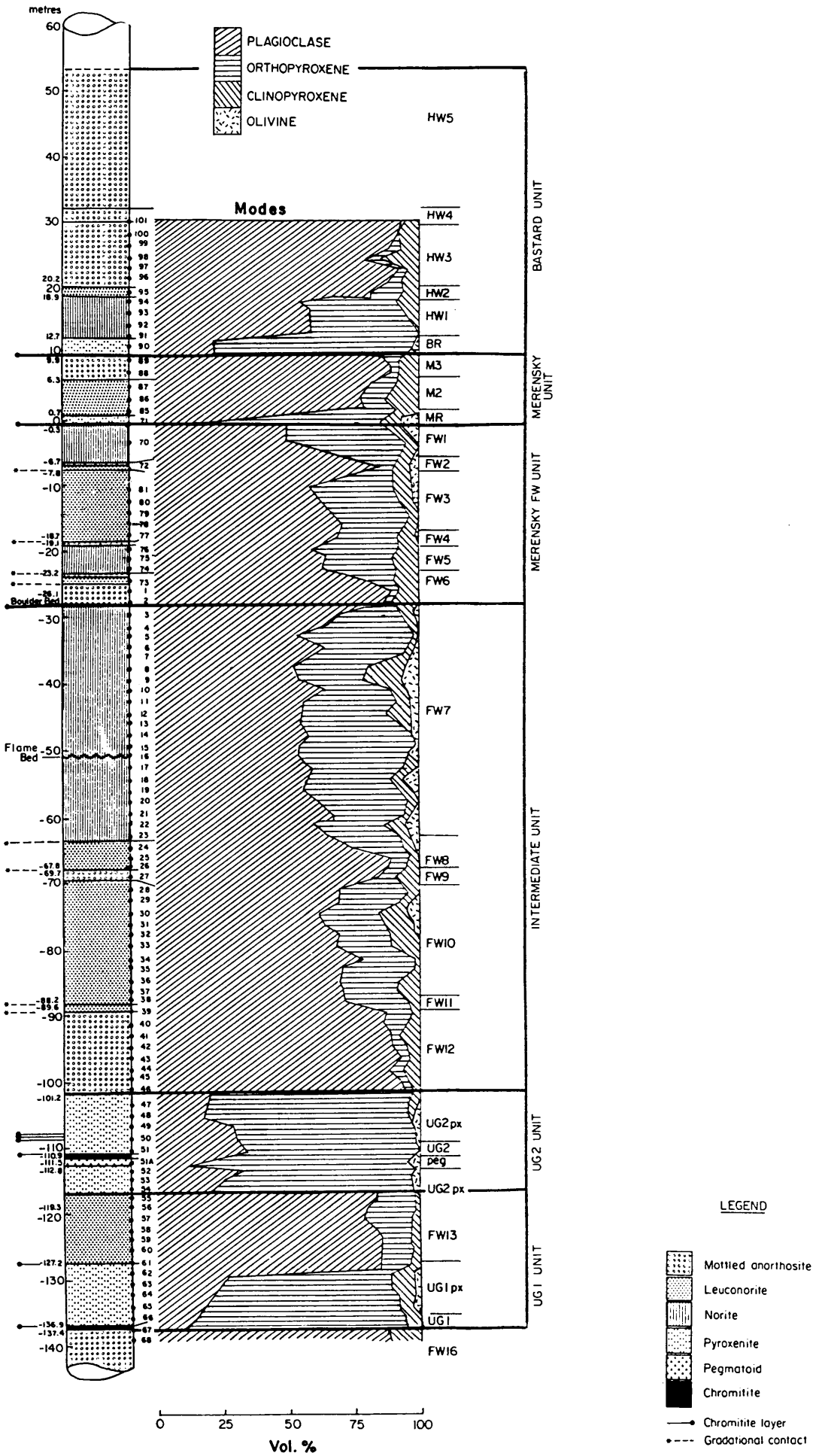

Figure 4.4 The modal proportions of plagioclase, orthopyroxene, clinopyroxene and olivine for part of the upper critical zone of the Boshoek section.

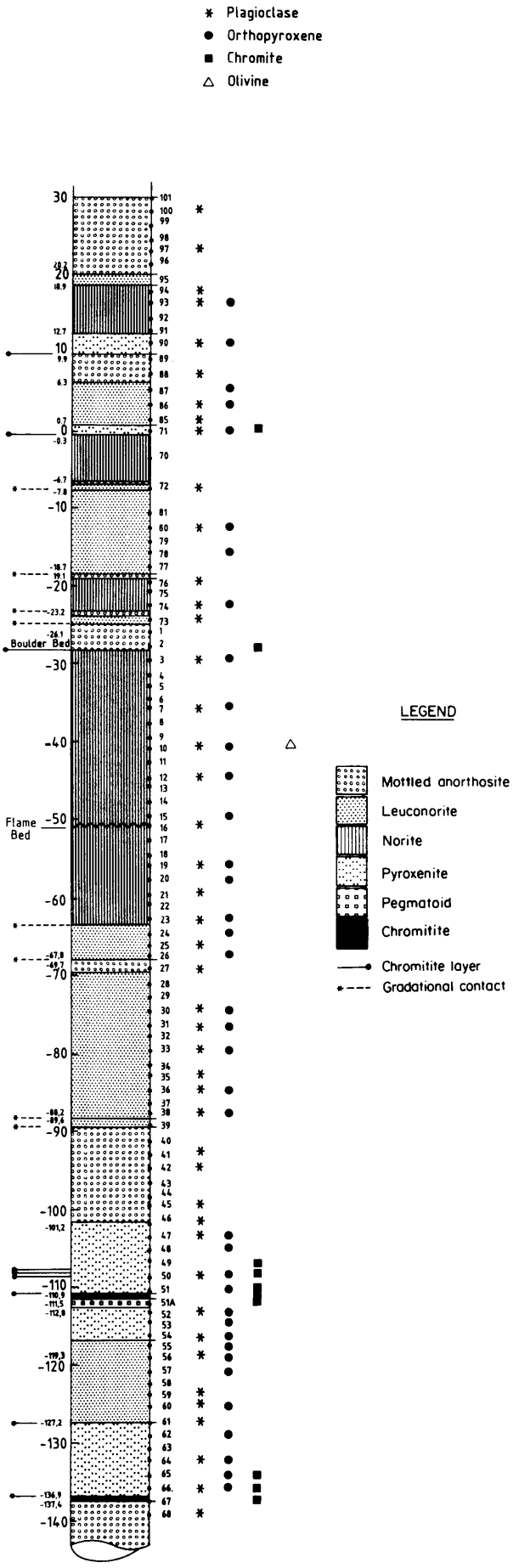

Figure 4.5 Samples used for plagioclase, orthopyroxene, chromite and olivine microprobe analyses.

Table 4.1 Technical information for microprobe analyses of plagioclase, orthopyroxene, olivine and chromite.

Mineral	No. of sections	No. of grains/ section	KV	nA	Beam r^2	Standards
Plag	45	10-30	15	20	10	SiO_2 quartz Al_2O_3 pure oxide FeO hematite CaO wollastonite Na_2O albite K_2O sanidine V_2O_3 VO_2 Cr_2O_3 pure oxide MgO pure oxide MnO pure oxide TiO_2 pure oxide
Opx **Ol**	37 1	10 15	15	40	10	SiO_2 quartz Al_2O_3 pure oxide FeO hematite CaO wollastonite Na_2O albite K_2O sanidine V_2O_3 VO_2 Cr_2O_3 pure oxide MgO pure oxide MnO pure oxide TiO_2 pure oxide
Chr	10	5	20	20	10	Pure oxides for FeO, TiO_2, MnO, MgO, Al_2O_3, Cr_2O_3 and 100% VO_2 for V_2O_3

5. PETROGRAPHY

5.1 Introduction

The rocks in the study area are classified according to the nomenclature and recommendations of the IUGS Subcommission on Igneous Rocks (Streckeisen, 1976) **(Fig. 5.1)**. The prefixes mela- and leuco- in melanorite or leuconorite are used by Streckeisen to distinguish between mafic and more felsic rock types. Traditional descriptive names of Bushveld rocks are also used to illustrate their texture, for example, "spotted" and "mottled" anorthosite, and their composition, e.g. feldspathic pyroxenite for a pyroxenite with approximately 10% plagioclase.

5.2 Anorthosite

In the UG1 FW - Bastard unit interval several layers of mottled anorthosite can be distinguished **(Fig. 3.1)**. The mottles, which vary from 2 to 5 centimetres in diameter, consist of intercumulus orthopyroxene and small amounts of clinopyroxene which may contain euhedral plagioclase inclusions. According to De Klerk (1982) the correct petrological name for such a rock is poikilitic anorthosite. An average volumetric mineral composition for a mottled anorthosite is:

plagioclase	90%
orthopyroxene	5%
clinopyroxene	4%

and minor biotite and sulphides 1%.

Plagioclase occurs in two different sizes. Small (<1,8 millimetre), sub- to euhedral cumulus crystals occur together with plagioclase crystals which are larger than 1,8 millimetre in diameter. Zoning has not been seen **(Fig. 5.2)**.

The intercumulus clinopyroxene, which gives rise to the mottled texture, usually displays optical continuity **(Fig. 5.2)**. The anhedral plagioclase crystals (<0,4 mm in diameter) in the clinopyroxene display no preferred orientation.

Biotite is present as small intercumulus grains. Chromite grains are euhedral and occur in the vicinity of chromitite layers or stringers. Disseminated chromite is found on crystal boundaries or as inclusions in orthopyroxene and plagioclase. Sample IWS46, a mottled anorthosite, contains euhedral magnetite grains up to 18 micron in diameter, with exsolution lamellae of ilmenite.

Disseminated sulphides, mostly chalcopyrite and minor amounts of pentlandite, are present along grain boundaries and as inclusions in plagioclase and pyroxenes. In sample IWS44, a mottled anorthosite, anhedral grains of chalcopyrite (14 micron in diameter) are present as inclusions in plagioclase and in cumulus pyroxenes, while in sample IWS68, also a mottled anorthosite, the chalcopyrite, with an average diameter of 21 micron, is restricted to crystal boundaries. Pentlandite tends to be euhedral, has an average size of 10 microns, and is present on crystal boundaries.

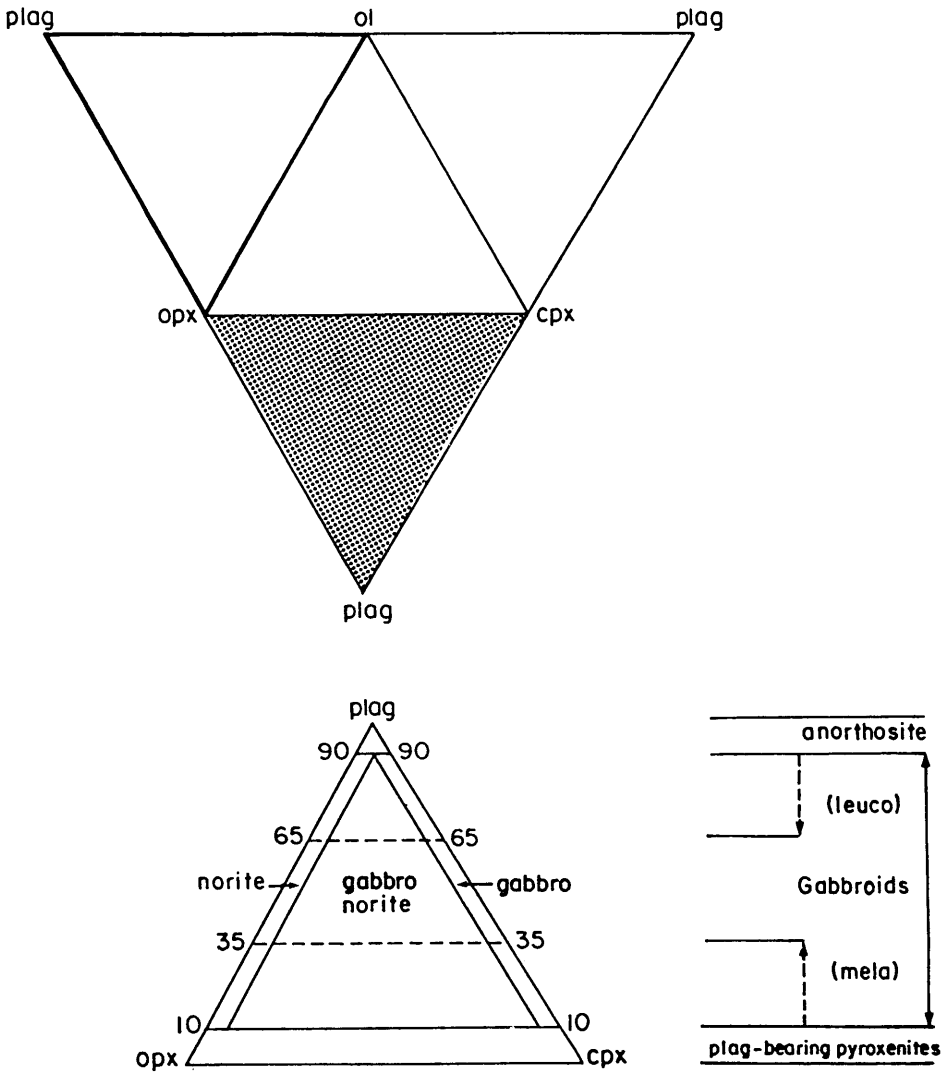

Figure 5.1 Nomenclature and classification system of Schreckeisen (1976) for the rocks most frequently encountered in this investigation.

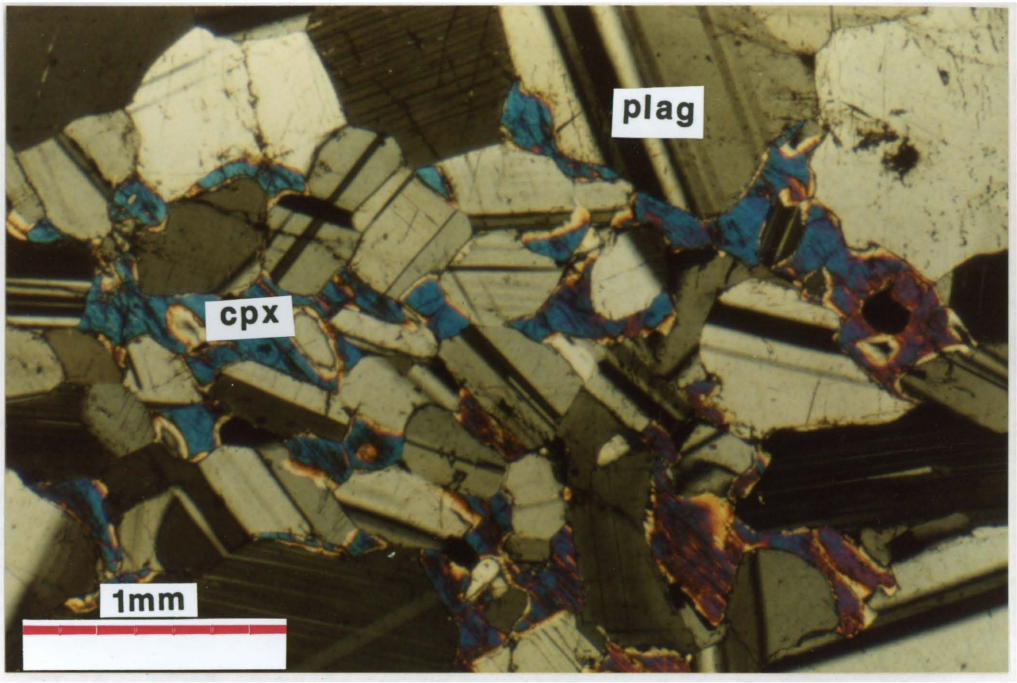

Figure 5.2 Cumulus, anhedral plagioclase crystals within an intercumulus clinopyroxene "mottle". Inclusions are <0,4 mm in diameter. Mottled anorthosite sample IWS45. Transmitted light, crossed nicols.

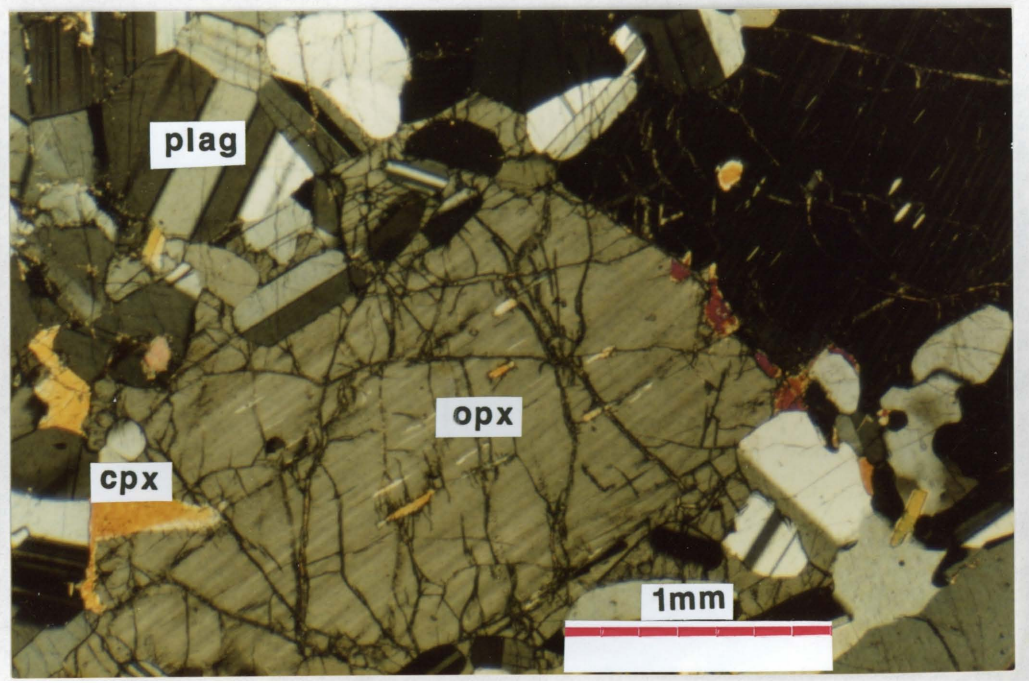

Figure 5.3 Subhedral orthopyroxene with exsolution lamellae of augite. Postcumulus overgrowth is indicated by a zone rich in small plagioclase inclusions. Norite sample IWS11. Transmitted light, crossed nicols.

The mottled anorthosites can, on the account of the texture and the absence of zoning in the plagioclase and the associated intercumulus pyroxene, be described as adcumulates (Cox **et al.,** 1979).

5.3 Norites

Norites and leuconorites consist of cumulus plagioclase and orthopyroxene. The average modal composition of the norite is:

plagioclase	57%
orthopyroxene	36%
clinopyroxene	3%
olivine, sulphides and biotite	4%.

The FW10 leuconorite, has a modal composition of:

plagioclase	70%
orthopyroxene	18%
clinopyroxene	9%
olivine and minor sulphides	3%.

As in the case of mottled anorthosite, distinct textural types of plagioclase are developed. Included in the first type are the plagioclase grains enclosed in postcumulus overgrowths of the cumulus orthopyroxene **(Figs. 5.3 and 5.4)**.

The plagioclase inclusions within these zones of postcumulus overgrowth are generally smaller than the anhedral plagioclase crystals which surround the orthopyroxene. Bimodal size variation of plagioclase grains in the leuconorite layer (FW8) is prominent with the larger grains measuring 2,8 mm in diameter compared to the smaller grains which are 0,9 mm in diameter **(Figs. 5.5 and 5.6)**.

Orthopyroxene occurs as cumulus grains which commonly contain small inclusions of plagioclase and sulphide which tend to predominate in the postcumulus overgrowth **(Fig. 5.7)**. Cumulus olivine with embayments, probably due to resorption, usually contain small plagioclase inclusions. The olivine is irregularly cracked and shows indications of alteration to serpentine **(Figs. 5.8 and 5.9)**.

All clinopyroxene is intercumulus and usually surrounds cumulus orthopyroxene grains. Biotite is seen as small intercumulus grains associated with clinopyroxene and sulphides.

Chromite and sulphide grains occur in the FW13 leuconorite. The sulphides are dominantly chalcopyrite with minor amounts of pentlandite and millerite. These minerals are frequently present as inclusions in the plagioclase, pyroxenes and on the plagioclase/orthopyroxene crystal boundaries **(Figs. 5.10 and 5.11)**. The leuconorite of FW10 and the norite of FW7 contain chalcopyrite with minor amounts of pyrrhotite and pentlandite between the plagioclase grains. Inclusions of chromite and chalcopyrite are present in a large, altered, anhedral olivine grain (sample IWS24)**(Fig. 5.12)**.

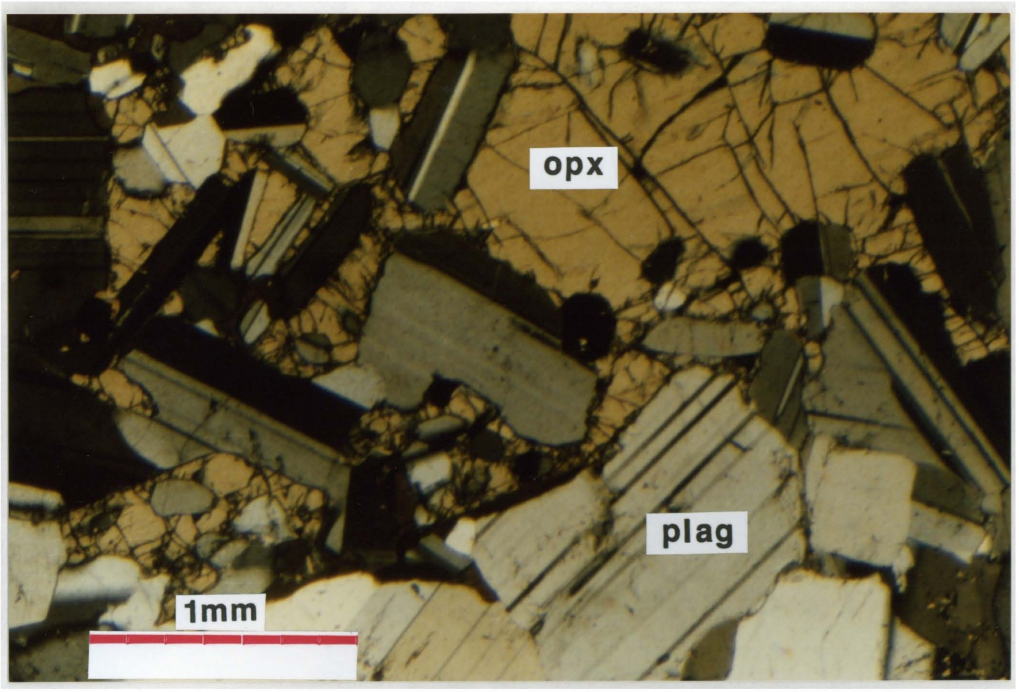

Figure 5.4 Intercumulus overgrowths on cumulus orthopyroxene poikilitically enclosing plagioclase grains which range in size from 0,1 to 0,8 mm. Surrounding the intercumulus orthopyroxene are larger anhedral plagioclase crystals. Leuconorite sample IWS25. Transmitted light, crossed nicols.

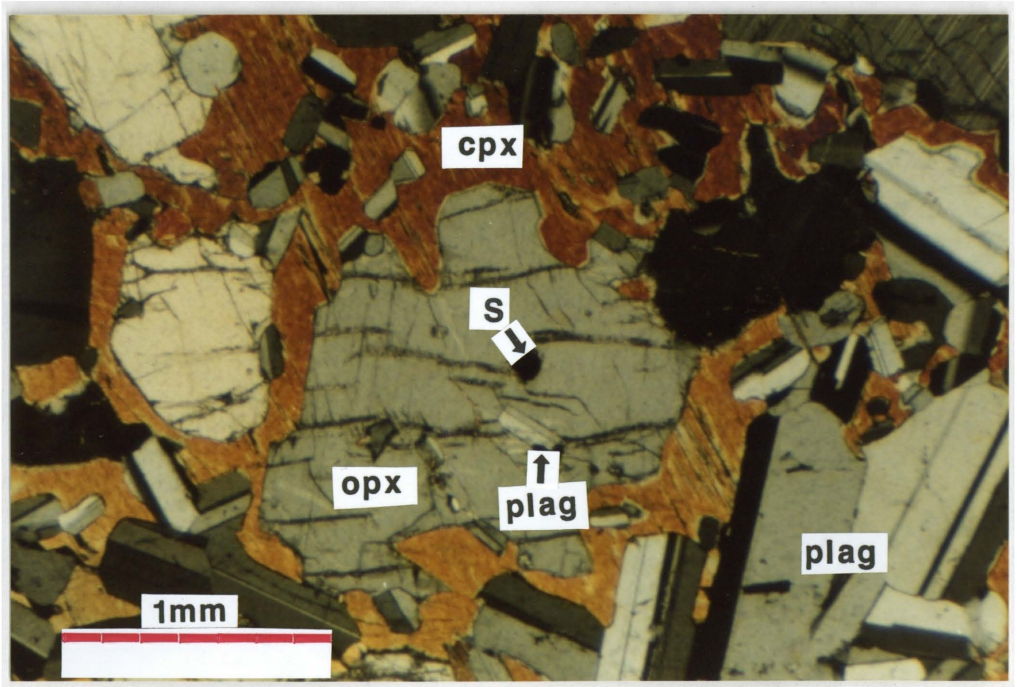

Figure 5.5 Anhedral orthopyroxene grains with small (<0,2 mm in diameter) plagioclase and sulphide inclusions. The orthopyroxene, which is surrounded by postcumulus clinopyroxene, is resorbed. Larger plagioclase crystals surround the poikilitic clinopyroxene. Norite sample IWS12. Transmitted light, crossed nicols.

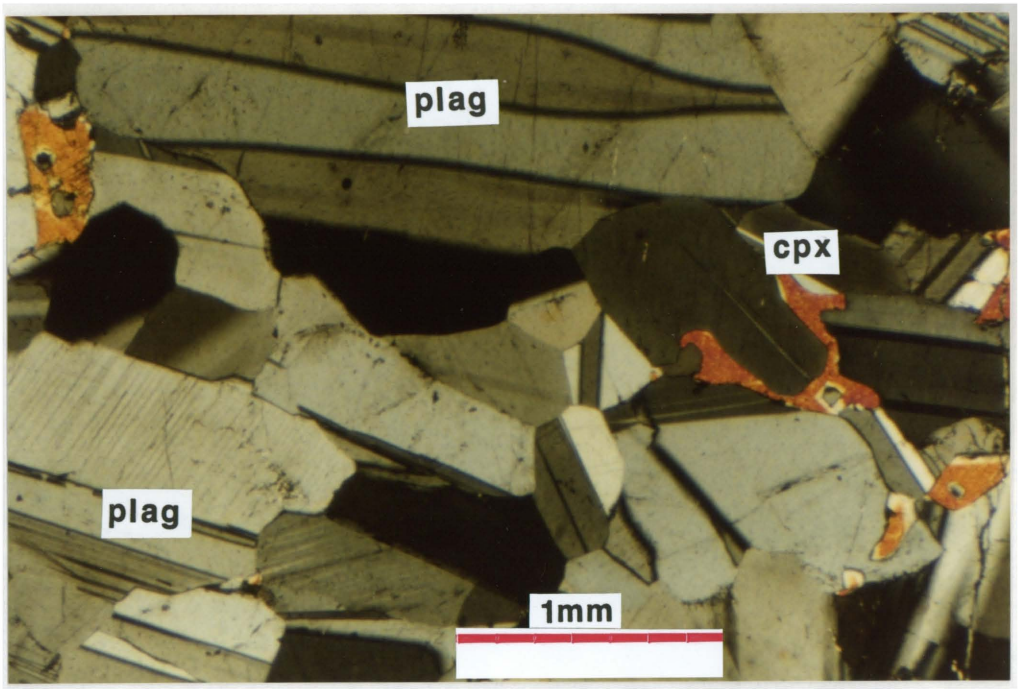

Figure 5.6 Large, subhedral plagioclase crystals (2,8 mm in diameter) accompanied by smaller plagioclase crystals. Small plagioclase crystals display prominent resorption rims. Leuconorite sample IWS26. Transmitted light, crossed nicols.

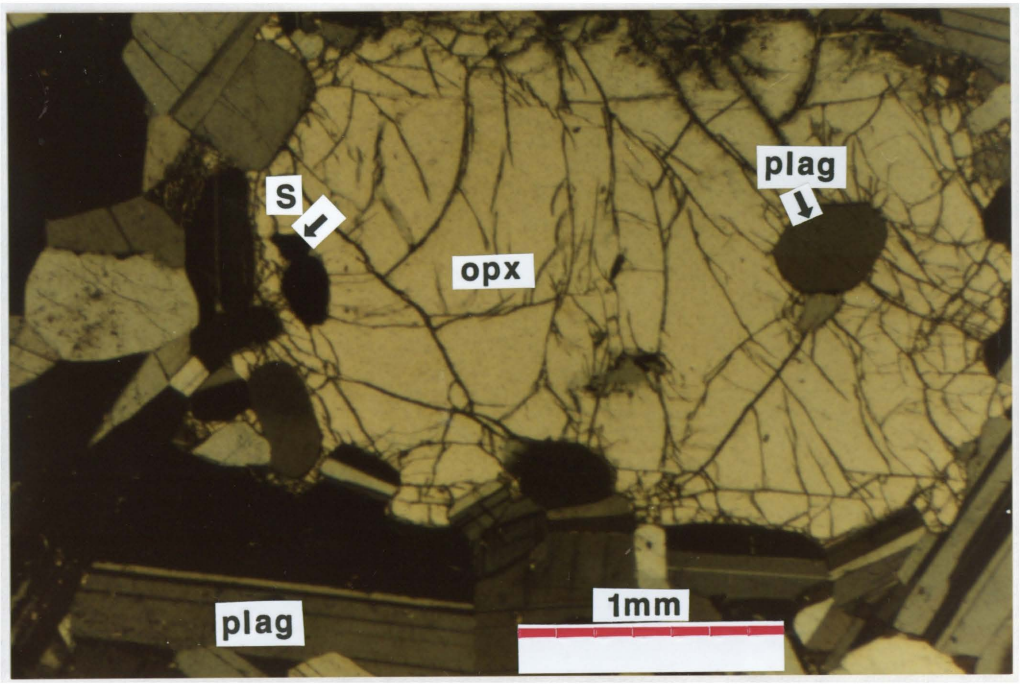

Figure 5.7 A large (2,4 mm in diameter), subhedral orthopyroxene crystal with plagioclase and sulphide inclusions. Plagioclase inclusions tend to predominate in the postcumulus overgrowth. Norite sample IWS7. Transmitted light, crossed nicols.

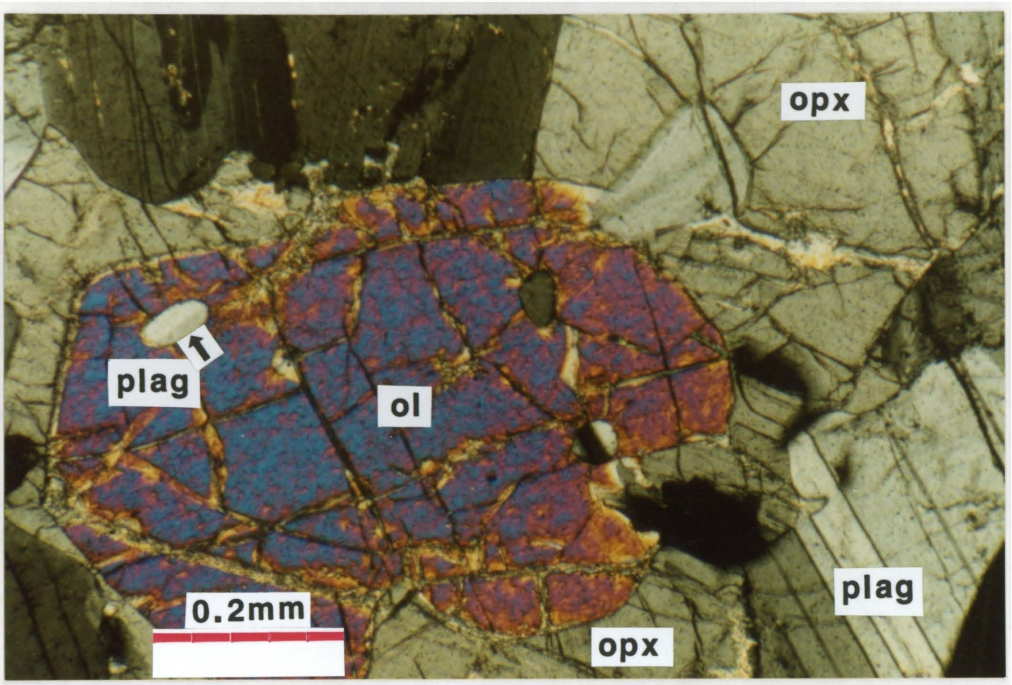

Figure 5.8 Cumulus olivine with embayments which may be due to resorption. Note the small inclusions of plagioclase. Irregular cracks in the olivine show indications of alteration to serpentine. Norite sample IWS11. Transmitted light, crossed nicols.

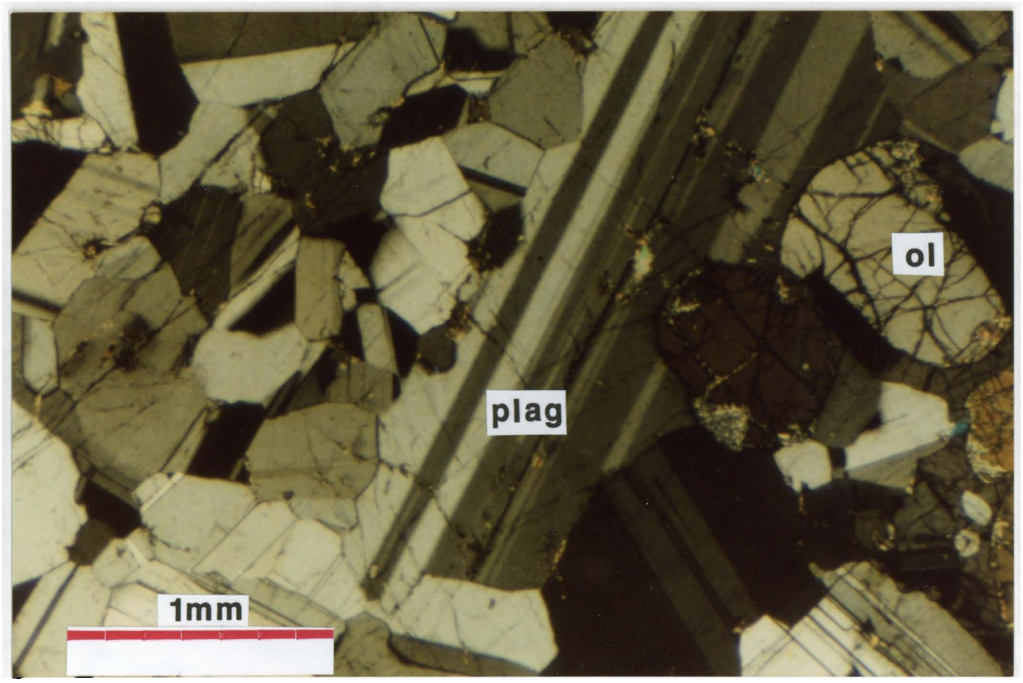

Figure 5.9 Large subhedral plagioclase crystals (2,4 mm long) surrounded by smaller (0,4 mm) plagioclase crystals. Anhedral olivine crystals are partially altered to serpentine along cracks. Leuconorite sample IWS30. Transmitted light, crossed nicols.

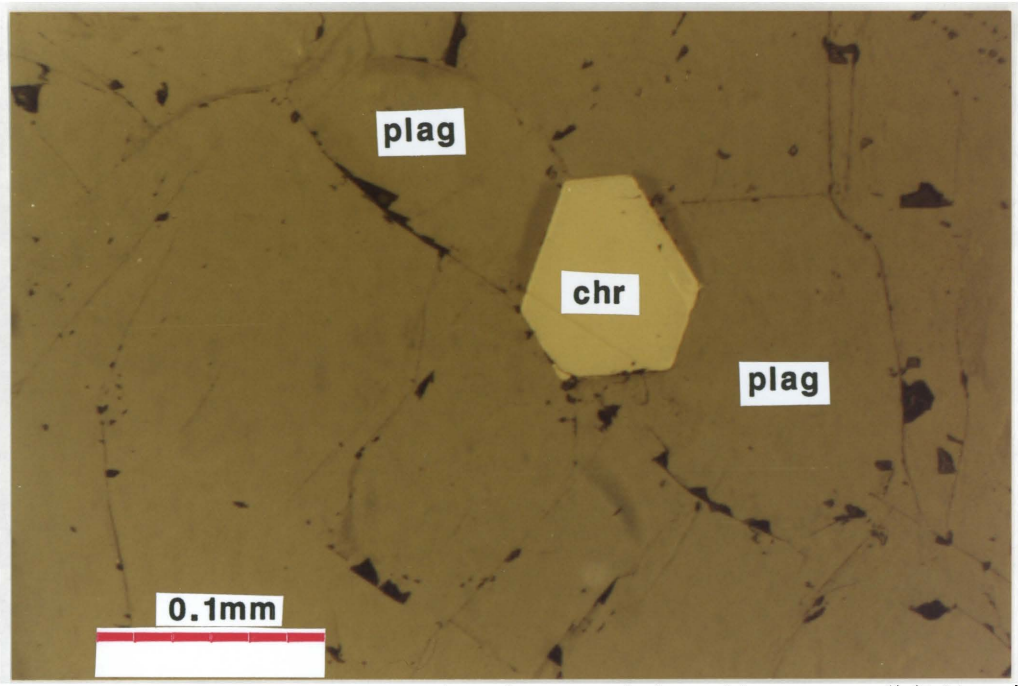

Figure 5.10 Euhedral chromite grains (size approximately 0,08 mm) situated between small (0,14 mm) plagioclase crystals. Leuconorite sample IWS26. Reflected light.

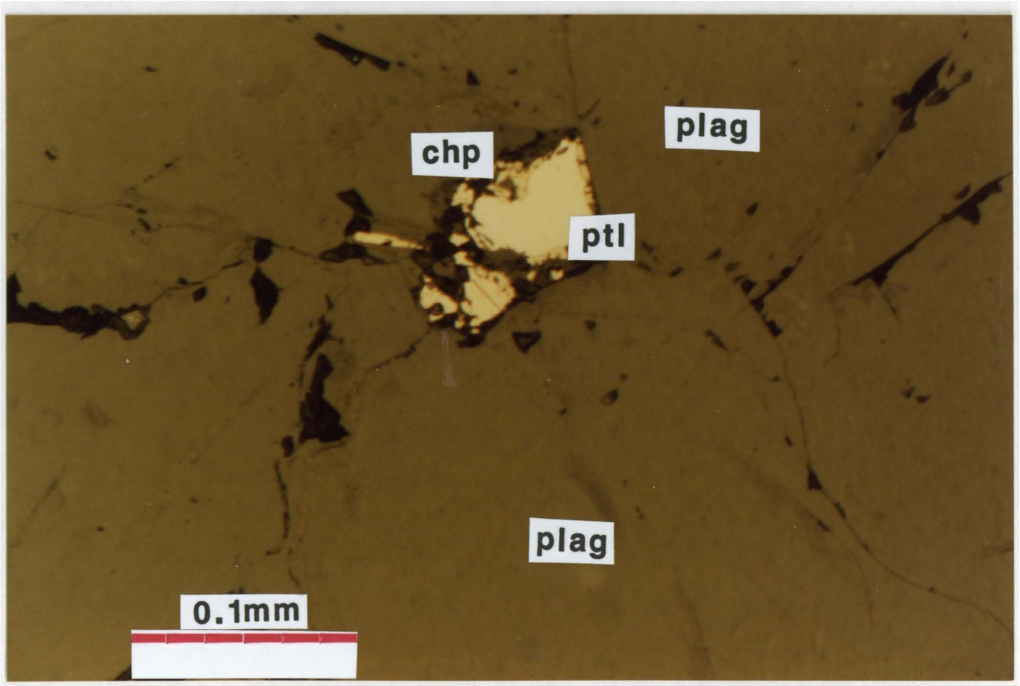

Figure 5.11 Sub- to anhedral pentlandite (ptl) enclosed by chalcopyrite and situated between plagioclase crystals of approximately 0,4 mm in diameter. Norite sample IWS17. Reflected light.

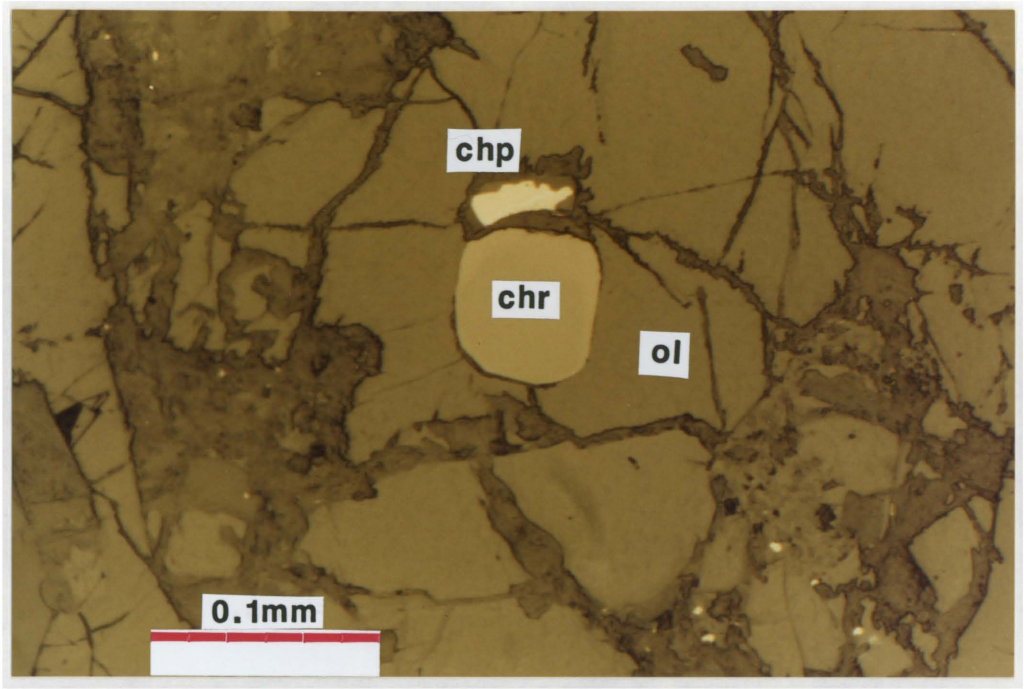

Figure 5.12 A large, anhedral olivine grain partially altered along cracks in a leuconorite. Subhedral chromite and anhedral chalcopyrite inclusions (0,07 and 0,04 mm in diameter respectively) are present. Small disseminated sulphide grains occur in the altered portions. Leuconorite sample IWS24. Reflected light.

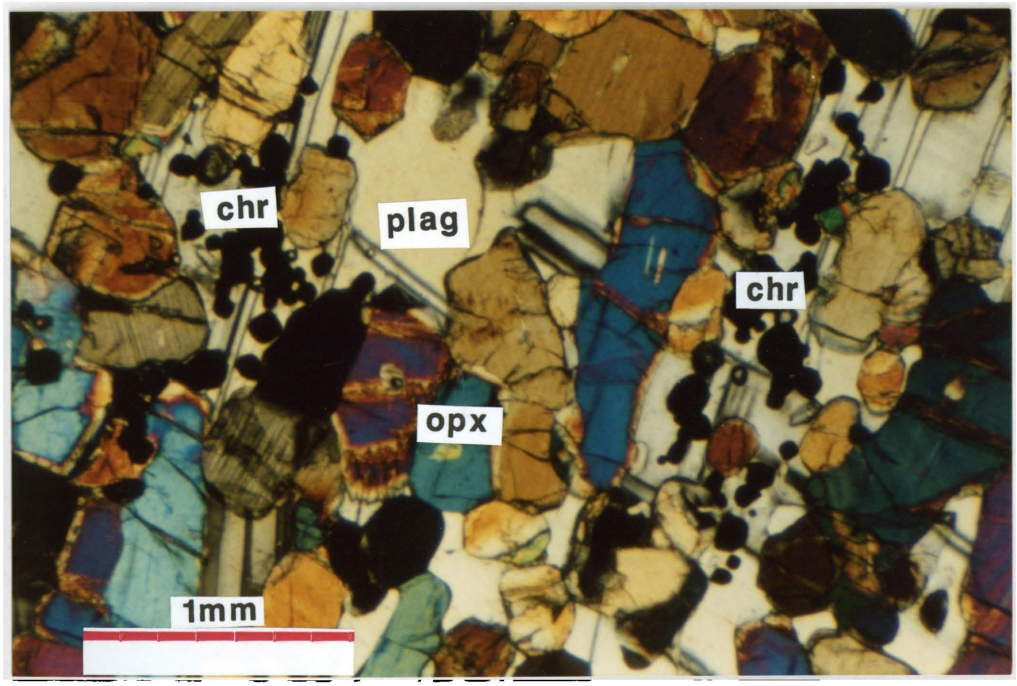

Figure 5.13 Anhedral to subhedral orthopyroxene crystals and intercumulus plagioclase of a chromite-bearing feldspathic pyroxenite. Subhedral chromite grains are aligned parallel to the igneous layering. Feldspathic pyroxenite sample IWS62. Transmitted light, crossed nicols.

On account of the limited adcumulate growth the norite and the leuconorite are classified as mesocumulates.

5.4 Pyroxenite

Several feldspathic pyroxenite layers are present in the studied interval. The modal composition of these rocks varies from:

orthopyroxene	65% to 80%
plagioclase	32% to 14%
clinopyroxene	3% to 5%.

According to the IUGS classification of a pyroxenite, the rock should contain less than 10% plagioclase (Streckeisen, 1976). In this study this limit is exceeded by 4% to 22% and are, according to the Streckeisen nomenclature, melanorites. However, due to the high modal percentage of plagioclase, which is invariably intercumulus, the rock is referred to as a "feldspathic pyroxenite". De Klerk (1982) described these rocks as poikilitic feldspathic pyroxenites due to the high modal percentage of plagioclase and the poikilitic nature of the clinopyroxene. Apart from cumulus orthopyroxene and intercumulus plagioclase **(Fig. 5.13)** these rocks also contain minor amounts of clinopyroxene, biotite, chromite and sulphides.

The cumulus orthopyroxene grains are subhedral to euhedral in form, vary from 1 to 4 millimetres in diameter and contain thin exsolution lamellae of augite. Clinopyroxene is present either as large, anhedral oikocrysts (5 to 10 millimetres in diameter) or as smaller intercumulus grains. The large oikocrysts contain anhedral, cumulus orthopyroxene inclusions which do not display any preferred orientation. Plagioclase is an interstitial phase which poikilitically encloses the orthopyroxene, clinopyroxene and chromite.

Feldspathic pyroxenites in close proximity to chromitite layers have high concentrations of cumulus chromite disseminated in plagioclase, orthopyroxene and clinopyroxene. Chromite grains enclosed in cumulus phases are euhedral compared to the subhedral to anhedral shape of the grains between cumulus silicates **(Fig. 5.14)**.

The sulphides are predominantly pyrrhotite, pentlandite and chalcopyrite and are mainly interstitial to the silicates. Small amounts of sulphides occur as inclusions in the intercumulus plagioclase and are closely associated with the cumulus chromite grains.

The modal amount of orthopyroxene decreases from the base to the top of the UG1 and the UG2 lower pyroxenite layers. For the UG2 upper pyroxenite layer the modal amount of orthopyroxene increases from the base to the top. The feldspathic pyroxenites can be classified according to their texture as heteradcumulates.

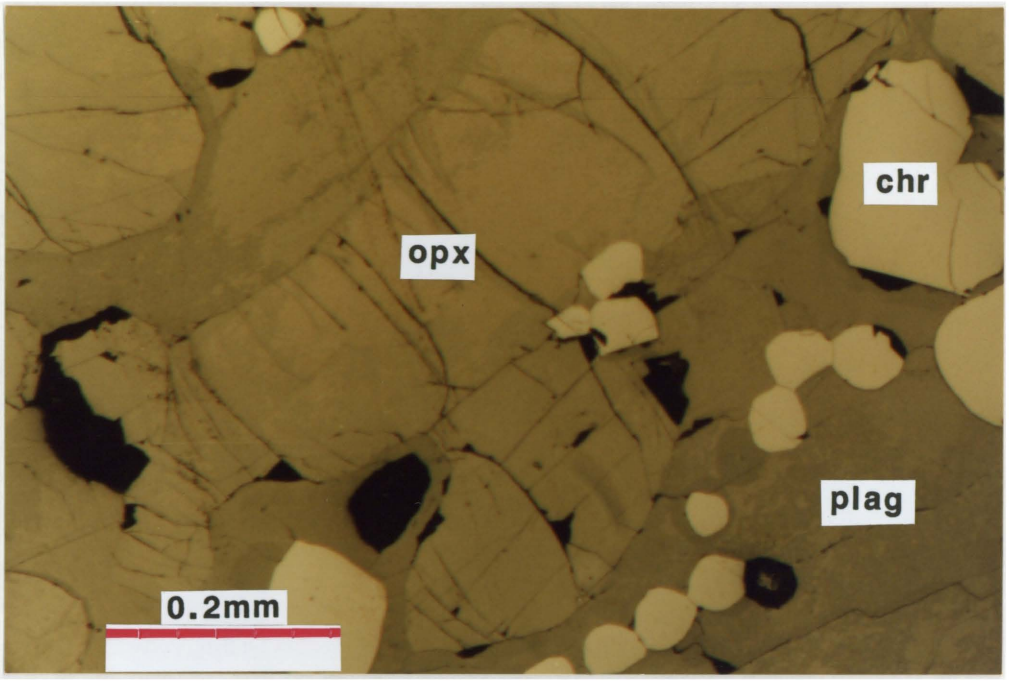

Figure 5.14 Sub- to anhedral chromite grains, ranging from 0,03 to 0,17 mm in diameter in intercumulus plagioclase, on grain boundries and included in the subhedral orthopyroxene. Feldspathic pyroxenite sample IWS50. Reflected light.

6. MINERAL CHEMISTRY

6.1 Introduction

Representative thin sections of the different layers and units were selected for mineral analyses to ensure a complete as possible representation of chemical and mineralogical trends. Sample numbers and positions are indicated in **Figure 4.5**, whilst analytical data used to compile the compositional trends for plagioclase, orthopyroxene, chromite and olivine are listed in **Appendix 2.**

6.2 Plagioclase

The cumulus plagioclase in the UG1 unit has a constant An content while in the Merensky unit the An content increases with height from an average of An 75,8 at the base to An 78,2 at the top of the unit. The Bastard unit displays an upward decrease in An content **(Fig. 6.1).**

Intercumulus plagioclase within all feldspathic pyroxenite layers has a lower An content than the under- and overlying rocks which contain cumulus plagioclase. Variations in An content within layers containing intercumulus plagioclase (UG1 and UG2 feldspathic pyroxenite) do not display trends from the base upwards **(Fig. 6.1).** The exception at the FW13/lower UG2 feldspathic pyroxenite contact is probably due to infiltration metasomatism or mixing of interstitial liquid from the top of the FW13 leuconorite layer and the overlying lower UG2 feldspathic pyroxenite layer (Eales **et al.,** 1986).

The An content of the plagioclase also reflects the cyclic nature of the Intermediate sub-units 1 and 2. Sample IWS27 (Footwall 9) at the base of Intermediate sub-unit 2, contains plagioclase with a lower mean An content and a smaller range in composition than the over- and underlying samples. For both Intermediate sub-units 1 and 2, the average An content of the plagioclase increases slightly with height. At the top of Intermediate sub-unit 2 the An content decreases markedly **(Fig. 6.1).**

A poorly defined upward increase in the An content is evident from the Boulder Bed at the base of the Merensky Footwall unit to the top of FW5, which demarcates the Merensky Footwall sub-units 1 and 2. The limited data for the remainder of the Merensky Footwall unit suggests an upward decrease in An content **(Fig. 6.1).**

Plagioclase inclusions in cumulus orthopyroxene, e.g. samples IWS3 and IWS7, are distinctly enriched in calcium compared to the surrounding cumulus plagioclase. No systematic compositional difference between cores and rims with height was detected **(Fig 6.1).** Cumulus plagioclase grains generally display inconsistent zonation patterns with rims either more or less calcic than the cores.

The upward increase in the An content within cyclic units of the critical zone is not unusual and has been documented by several workers (Cameron, 1980; De Klerk, 1982; Kruger, 1982; Eales **et al.,** 1986; Naldrett **et al.,** 1987 and Hatton, 1989). An exception seems to be the upper part of the upper critical zone at the Union section where distinct decreases in the An content for the cumulus

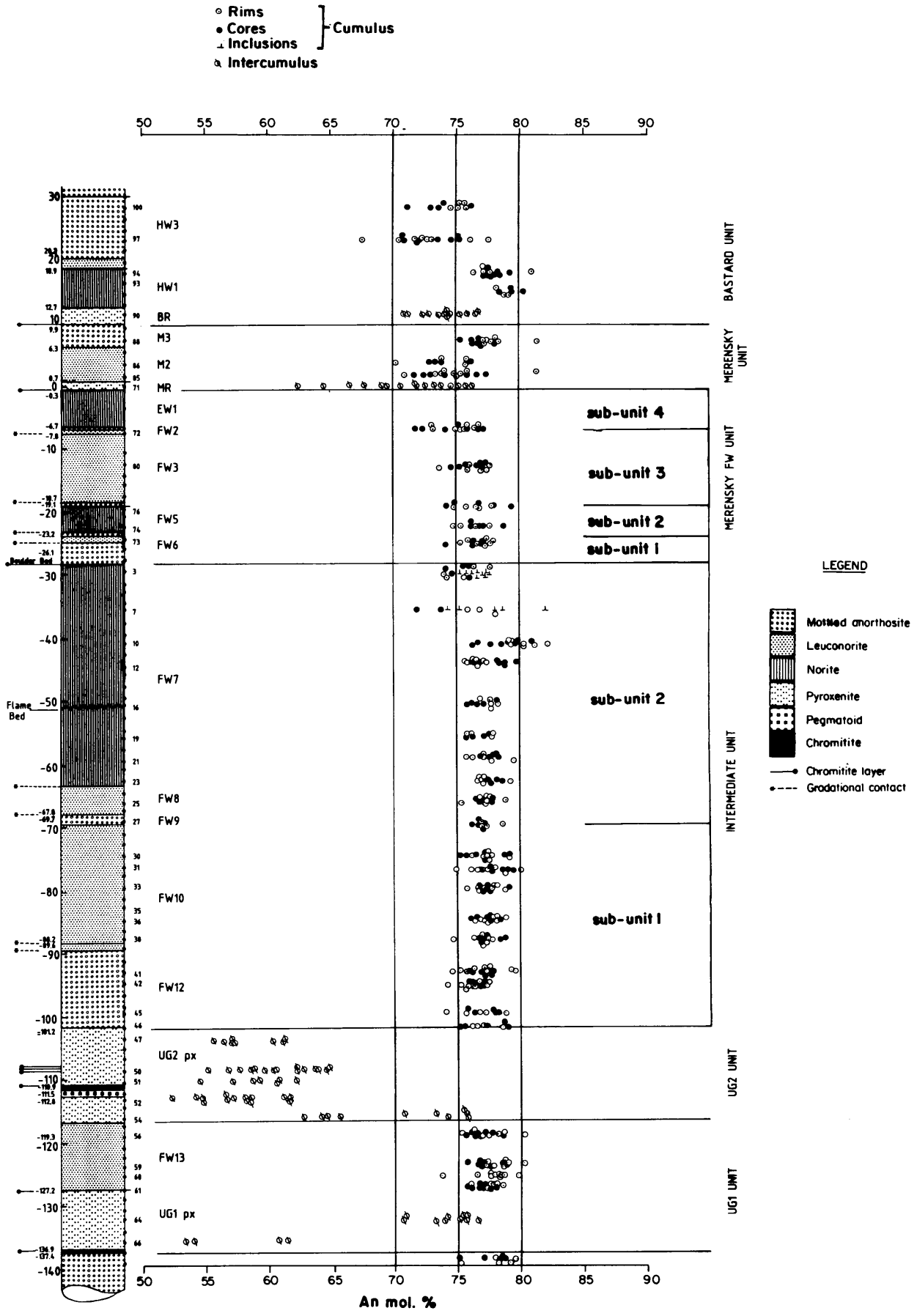

Figure 6.1 Plot of An content of plagioclase against stratigraphic height.

plagioclase from the bases of the Pseudo, Merensky and Bastard units upwards have been documented by Naldrett **et al.** (1986)**(Fig. 6.2)**. The corresponding units at the Rustenburg section (Boulder Bed sequence, Merensky and Bastard), display slight increases in the An content to the top of the Boulder Bed sequence, while prominent increases are evident in the Merensky and lower part of the Bastard units (Kruger, 1982; Naldrett **et al.**, 1987).

The Sr content of plagioclase is plotted against stratigraphic height in **Figure 6.3** in order to determine whether compositionally different parental magmas were involved in the crystallization of the upper critical zone, as was suggested by Kruger and Marsh (1982) and Naldrett **et al.** (1986). The Sr content of plagioclase was calculated from whole rock data according to the method outlined by Naldrett **et al.** (1987), who argued that in rocks consisting primarily of combinations of plagioclase and bronzite, all Sr would be contained in the plagioclase. In such rocks the amount of plagioclase can readily be determined from the MgO content of the rock which is inversely proportional to the amount of plagioclase.

Seeing that the partition coefficient for Sr into plagioclase within the sequence under consideration can be considered to be constant (Naldrett **et al.**, 1984), any variation in the Sr content of the plagioclase must be ascribed to changes in the Sr content of the magma from which the plagioclase has crystallized. Some interesting trends have emerged from this data. In general, the rock sequence below the Merensky Reef contains plagioclase with >445 ppm Sr **(Fig. 6.3)**. In the Intermediate unit however, there is a gradual decrease in the Sr content from the base of the FW12 mottled anorthosite to the top of FW10 leuconorite. The Sr content of plagioclase in the overlying FW9 mottled anorthosite and FW8 leuconorite displays a slight increase and decrease respectively from where the Sr content gradually increases to a value of 525 ppm at the top of the FW3 leuconorite. Here values decrease more gradually to the base of the Merensky unit. At the base of the Merensky unit, there is another abrupt decrease of about 50 ppm in the Sr content of the plagioclase, with a further gradual decrease upward through the Bastard unit to values below 400 ppm **(Fig. 6.3)**.

A similar break in the Sr content of the plagioclase at the level of the Merensky Reef was recorded by Kruger (1982) and by Naldrett **et al.** (1987) from the Rustenburg and Union sections of the Bushveld Complex. The drop in the Sr content of about 100 ppm in these two sections is very similar to that recorded in the Boshoek section **(Fig. 6.4)**.

6.3 Orthopyroxene

Analytical data for cumulus orthopyroxene is given in **Appendix 2.** The composition of the orthopyroxene was calculated in terms of the Mg No. (which is the atomic ratio of Mg/(Mg+Fe)) and plotted against stratigraphic height in **Figure 6.5.** The apparent incompleteness of the plot is caused by the restricted distribution of cumulus orthopyroxene in certain parts of the sequence and the low concentration of cumulus orthopyroxene in leuconorites **(Fig. 4.3)**.

The UG1 unit displays an upward increases in Mg No. while for the UG2 unit the Mg No. is constant. Intermediate sub- units 1 and 2 can be recognized by different trends **(Fig. 6.5)**. Sub-unit

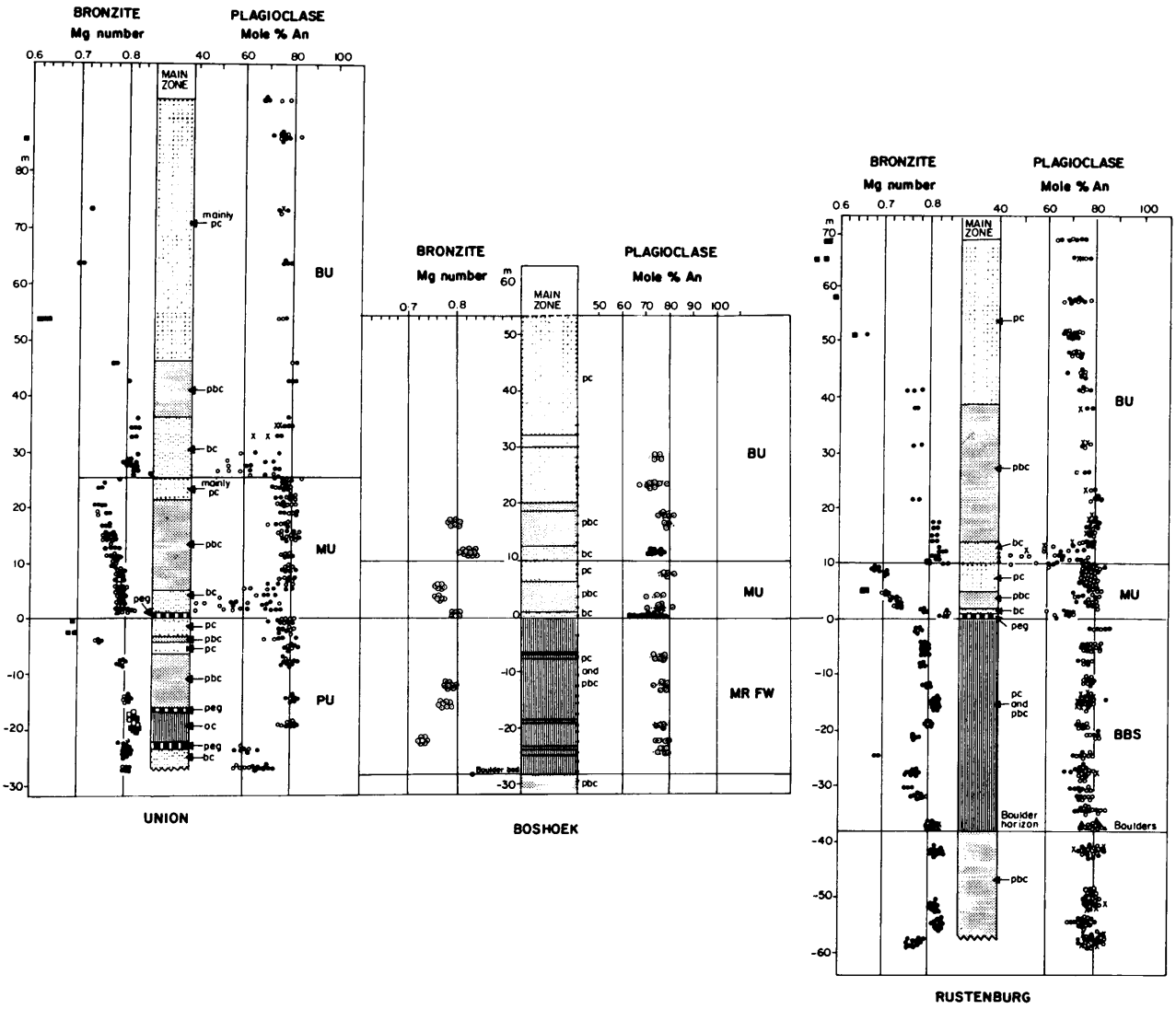

Figure 6.2 Comparison of the variation in Mg No. ((Mg/Mg+Fe) atomic ratio) of bronzite and An content of plagioclase with height in the upper critical zone of the Union, Boshoek and Rustenburg sections. BU = Bastard unit; MU = Merensky unit; PU = Pseudoreef unit; BBS = Boulder Bed Sequence; MRFW = Merensky Footwall unit. Hollow symbols = margins of grains; solid symbols = cores of grains; asterisk = small plagioclase grains enclosed within bronzite; triangles = pyroxene and plagioclase within boulders of the Boulder Bed; closed circles = intercumulus grains; circles = cumulus grains. Data for the Union and Rustenburg sections taken from Naldrett **et al.** (1987).

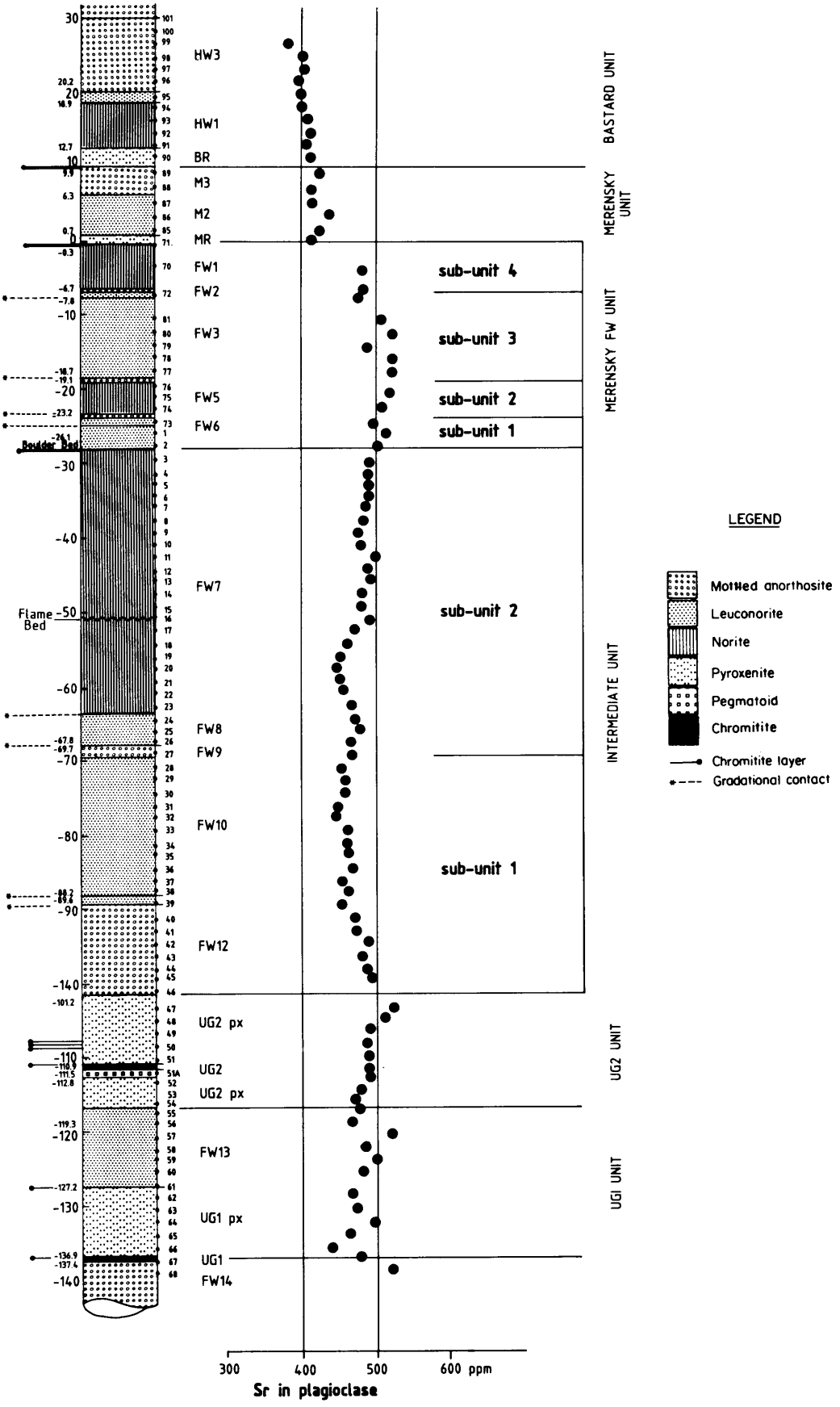

Figure 6.3 Plot of the Sr content of plagioclase against stratigraphic height.

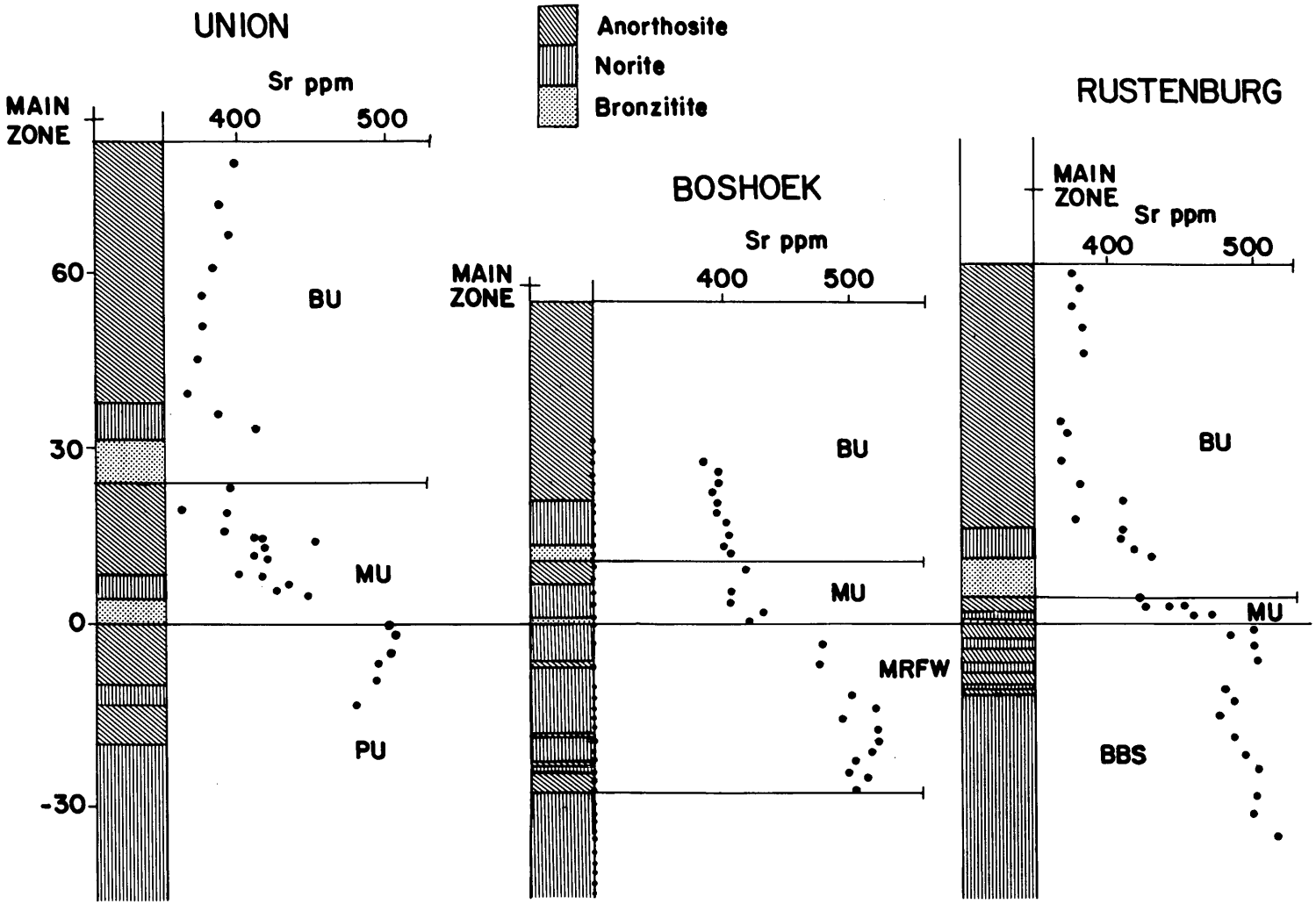

Figure 6.4 Comparison of the change in Sr content of plagioclase across the Merensky unit (MU) in the Union, Boshoek and Rustenburg sections. BU = Bastard unit; MU = Merensky unit; PU = Pseudoreef unit; BBS = Boulder Bed Sequence; MRFW = Merensky Footwall unit. Data for the Union and Rustenburg sections taken from Naldrett **et al.** (1987).

1 displays an upward decrease in Mg No. while the overlying Intermediate sub-unit 2 displays an increase from the base upwards. The very limited data for the Merensky footwall unit suggests a similar increasing trend to that of the Intermediate sub-unit 2. Available data suggests that both the Merensky and Bastard units display an upward decrease in Mg No. **(Fig. 6.5)**.

Comparison with work done by Naldrett **et al.** (1986, 1987) shows similar Mg No. trends for the Union and Rustenburg sections **(Fig. 6.2)** and that equivalent sections of the upper critical zone display prominent decreases in the Mg No. from the base upwards. The only exception is the middle of the Boulder Bed sequence of the Rustenburg section where a sharp increase in the Mg No. results in a reversal of the trend (Kruger, 1982; Naldrett **et al.**, 1986). The reversal can probably be correlated with the reversal in the Merensky footwall unit at Boshoek.

6.4 Chromite

Massive and disseminated chromite was analyzed from the UG1, UG2 and Merensky footwall units. The analytical data, consisting of 250 individual analyses is presented in **Appendix 2.**

The composition of disseminated chromite as well as chromite in thin chromitite stringers deviates considerably from that in the massive UG1 and UG2 chromitite layers **(Figs. 6.6 and 6.7)**. The former have higher $Cr/(Cr+Al)$ and $Fe^{3+}/(Fe^{3+}+Al+Cr)$, but lower $Cr/(Fe^{2+}+Fe^{3+})$ and $Mg/(Mg+Fe^{2+})$ mean ratios than the latter. This difference in composition between massive and disseminated chromite is also evident in the binary-composition variation diagrams **(Figs. 6.8A and 6.8B)**.

Irvine (1975) explained such compositional differences between the chromite of the massive chromitite layers and the disseminated chromite by a process of subsolidus re-equilibration. The disseminated chromite is considered by him to have had essentially the same solidus composition as the chromite of the massive chromitite layers. Subsolidus diffusion between disseminated chromite and surrounding ferromagnesian silicates resulted in an enrichment in Fe in the chromite and concomitant depletion in Mg, essentially because of the large ratio of modal pyroxene to chromite in the rocks.

Another factor which could affect the degree of subsolidus equilibration is the ratio of chromite surface area to volume of silicate surrounding chromite grains i.e. several small chromite grains could equilibrate more readily than a few large grains. In addition, Hatton and Von Gruenewaldt (1985b) suggested that the disseminated chromite and thin chromitite stringers were in contact with a large volume of silicate and the subsolidus diffusion of elements between chromite and surrounding silicates could therefore take place at lower temperatures, compared to massive chromitite layers where the volume of silicates surrounding chromite is low and hence equilibration reactions probably ceased at higher temperatures.

Representative chemical data of the massive chromitite layers UG1, UG2 and the chromitite stringers associated with the base of the Tarentaal layer and the Boulder Bed at the Union and

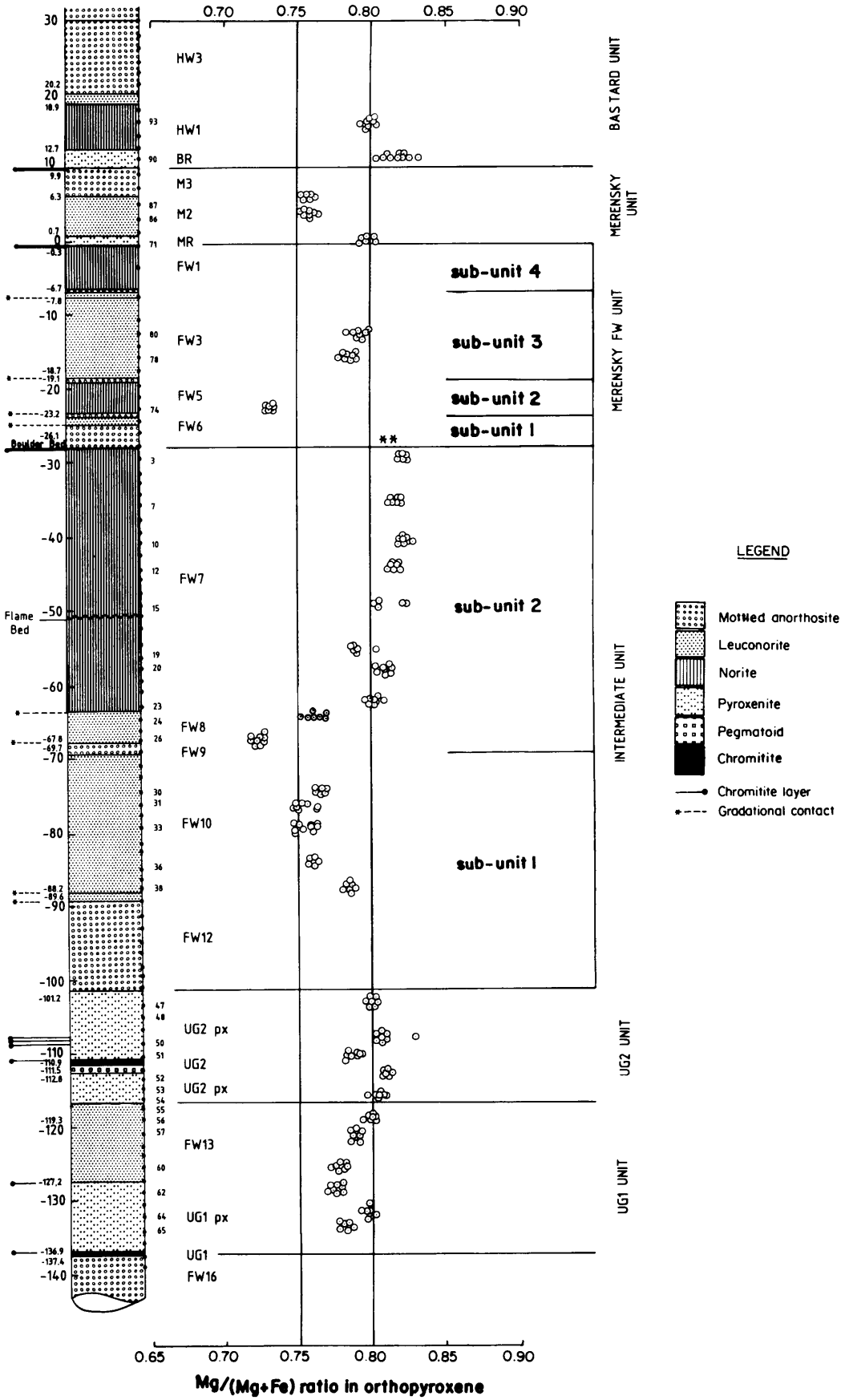

Figure 6.5 Plot of the Mg No. ((Mg/Mg+Fe) atomic ratio) of bronzite against stratigraphic height. The asterisk symbol = Mg No. of the Bronzite held in the boulders of the Boulder Bed (Jones, 1976).

Rustenburg sections respectively, is compared with the data of this study in **Table 6.1.** Distinct differences exist for the UG1 chromitite layer in that the Cr/(Cr+Al) ratio increases while the $Cr/(Fe^{2+}+Fe^{3+})$ and $Fe^{3+}/(Fe^{3+}+Al+Cr)$ ratios decrease from the Union to the Rustenburg sections.

For the chromitite layer at the base of the Tarentaal layer (Union section), the Cr/(Cr+Al) and $Fe^{3+}/(Fe^{3+}+Al+Cr)$ ratios are substantially lower than the values for the chromitite stringer associated with the Boulder Bed in the Boshoek section. This is due to the different thicknesses of the stringers and the associated host rock. The Boulder Bed stringer (3 millimetres thick) and thin Pseudoreef layer (10 millimetres thick) are in contact with mottled anorthosite and feldspathic harzburgite respectively.

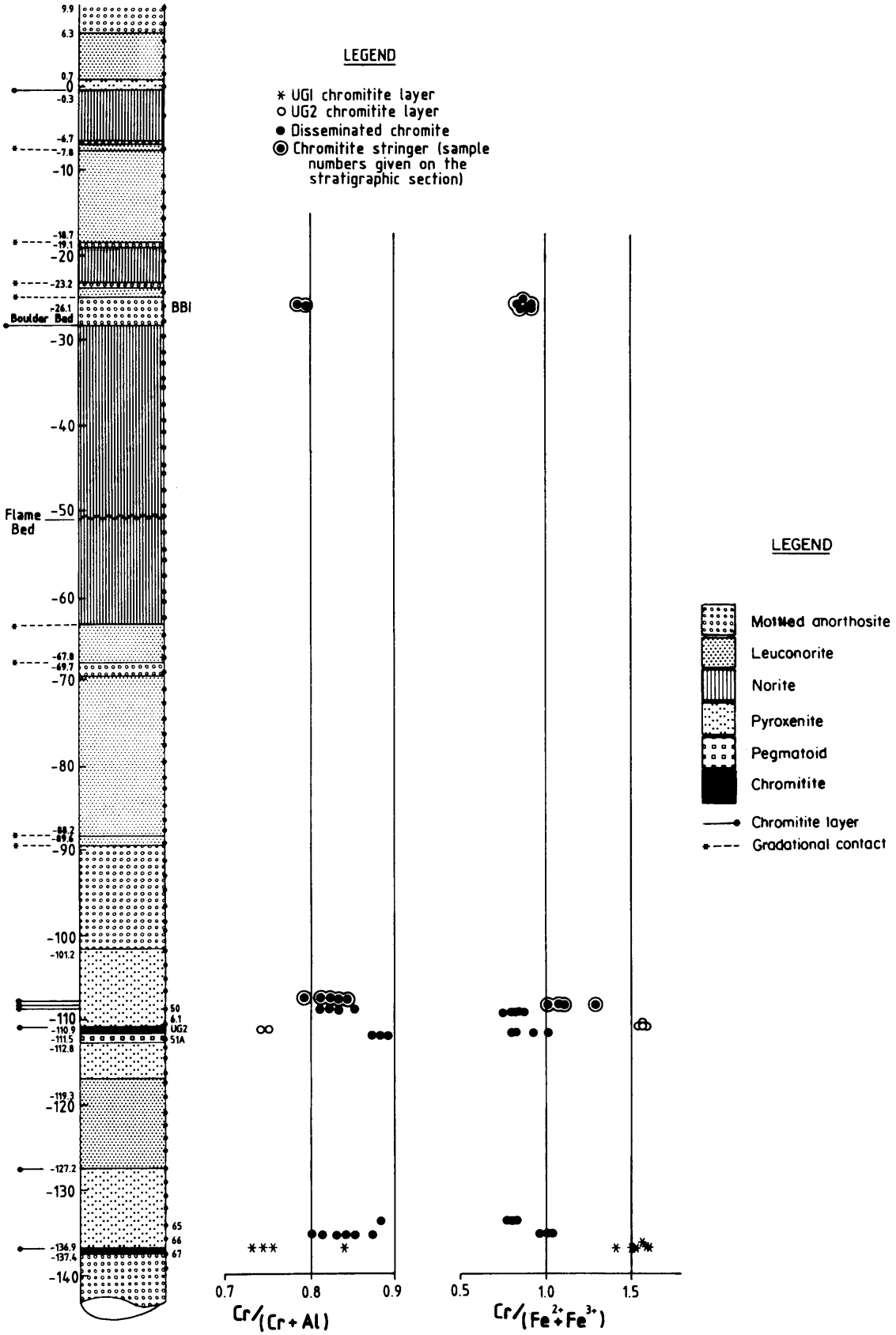

Figure 6.6 Ratios $Cr/(Cr+Al)$ and $Cr/(Fe^{2+}+Fe^{3+})$ plotted against stratigraphic height.

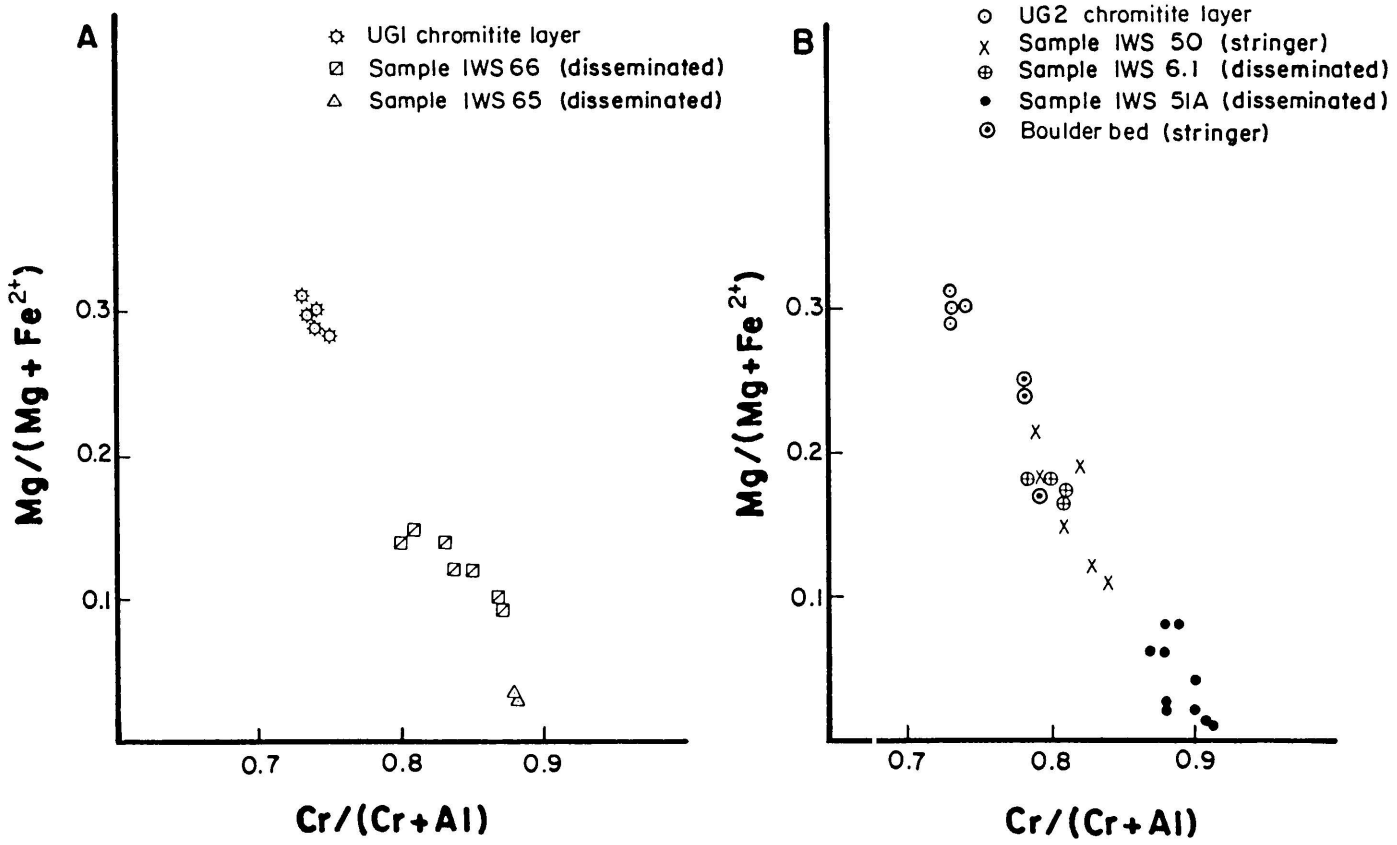

Figure 6.8 Ratio Cr/(Cr+Al) plotted against ratio Mg/(Mg+Fe^{2+}).

Table 6.1 Values of the ratios Cr/(Cr+Al) **[C/CA]**, Cr/(Fe^{2+}+Fe^{3+}) **[C/FF]**, Fe^{3+}/(Fe^{3+}+Al+Cr) **[F/FAC]** and Mg/(Mg+Fe^{3+}) **[M/MF]** for the massive chromitite layers UG1 and UG2 and the Boulder Bed (or Pseudoreef) stringer in the upper critical zone, Union, Boshoek and Rustenburg sections (Data compiled from Eales and Reynolds, 1986[1]; Cousins and Feringa, 1964[2] and this study[3]).

	SECTION	C/CA	C/FF	F/FAC	M/MF
UG1	Union [1]	0.70	1.57	0.11	0.33
	Boshoek [2]	0.73	1.54	0.11	0.29
	Rustenburg [3]	0.77	1.32	0.08	0.20
UG2	Union [1]	0.72	1.53	0.12	0.31
	Boshoek [2]	0.74	1.58	0.11	0.30
	Rustenburg [3]	0.73	1.38	0.05	0.25
Pseudo reef/ Boulder Bed	Union [1]	0.66	0.97	0.17	0.20
	Boshoek [2]	0.79	0.90	0.25	0.17

7. GEOCHEMISTRY

7.1 Introduction

All analyses **(Appendix 1)** are plotted against stratigraphic height to illustrate the chemical differences between layers and units. It is evident from **Figure 7.1** (Folder) that the vertical variation of major elements is largely an indication of the modal composition and the relative thicknesses of the individual rock layers.

7.2 Major elements

Al_2O_3 has a positive correlation with CaO, Na_2O and the trace element Sr, all of which reflects the modal amount of plagioclase. The Al_2O_3 and CaO content reflect the An content of the plagioclase while Na_2O is an indication of the Ab content **(Figs. 7.1A-C; 7.2F)**.

Ti_2O values vary sympathetically with SiO_2 **(Figs. 7.1F-G)**. A decrease in the SiO_2 content is indicative of an increase in the modal amount of plagioclase in the rock. Ti is mainly held in orthopyroxene where it substitutes for Si. The K_2O content is constant against stratigraphic position except for the UG1, UG2, Merensky and Bastard feldspathic pyroxenites where higher values could be closely associated with biotite and small amounts of alkali feldspar, although some may be contained in the orthopyroxene (Cocco **et al.,** 1970). High values were also recorded approximately 87 metres beneath the Merensky Reef and in the mottled anorthosite layer FW9.

The MgO has a negative correlation with Al_2O_3 and reflects the modal percentage of pyroxene in the rocks **(Figs. 7.1A; 7.1D)**. The contacts between the UG1, UG2, Merensky and Bastard feldspathic pyroxenite layers and the under- and overlying more felsic layers display sharp geochemical discontinuities. This reflects the modal composition of the rocks but also stresses the incompleteness of the units both chemically and lithologically.

7.3 Trace elements

All samples were analyzed for 17 trace elements **(Appendix 1)**, but due to the relatively low and inconsistent values obtained for the elements Y, U, Nb, Th and Pb, these were not used in **Figure 7.2** (Folder), a plot of trace elements against stratigraphic height. The distribution of individual trace elements can not be correlated directly with crystallization processes, because their concentration is largely controlled by the modal composition of the rocks.

The distribution of Ni correlates positively with MgO, because Ni tends to partition into olivine and orthopyroxene in the absence of a sulphide liquid **(Figs. 7.1D; 7.2E)**. The higher Ni values in the feldspathic pyroxenite layers (UG1, UG2, Merensky and Bastard) and FW7 norite are not only due to the Ni in the olivine and orthopyroxene, but due to Ni present in the sulphides. In a cyclic unit (e.g. the Merensky or Bastard) the upward depletion of Ni is related to an early separation of sulphides and to the upward increase in the modal amount of plagioclase.

Like Ni, Cr correlates positively with MgO **(Figs. 7.1D; 7.2A)**. Due to the partitioning of Cr into orthopyroxene, the feldspathic pyroxenites have high Cr values, although these high values, can also be ascribed to the abundance of cumulus disseminated chromite in the feldspathic pyroxenite.

Cu does not correlate with any of the major elements. Relatively higher values in the feldspathic pyroxenites (UG1, UG2, Merensky and Bastard), the FW10 leuconorite and at the base of the FW7 norite correlate with high total S values **(Figs. 7.2B; 7.3A)**.

Although elements such as Co and Ni are held mainly in mafic minerals, they are also chalcophile and display a positive correlation with S for the UG1, UG2 and the lower part of the Intermediate unit (sub-unit 1). The increase in sulphur in the upper UG2 feldspathic pyroxenite is very distinct **(Figs. 7.2D-E; 7.3A)**. A general decline in the sulphur content across FW9 mottled anorthosite and FW8 leuconorite up to the middle of FW7 norite (46 metres beneath the Merensky Reef) together with the negative correlation with Co, Ni and Cu, can only be achieved by a change in the sulphide assemblage, e.g. an upward decrease in the amount of pyrrhotite.

Within the Merensky Footwall unit, a positive correlation between MgO, FeO and the trace elements Ni and Co can be observed. Thus, except for the upper part of the Intermediate unit, total sulphur content correlates positively with MgO content and that sulphides tend to predominate in the pyroxenite layers **(Figs. 7.1D-E; 7.2D-E; 7.3A)**.

7.4 Major-element ratio

The whole rock MgO/(MgO+FeO) ratio defines several distinct units and sub-units **(Fig. 7.3B)**. The UG1 and UG2 units combined display an upward increase. The Intermediate sub-unit 1 also displays an increase from the base upwards. This is to be expected due to the intercumulus nature of pyroxene in the FW12 mottled anorthosite. The overlying Intermediate sub-unit 2 displays the same trend, except that the MgO/(MgO+FeO) ratio for the FW7 norite is substantially higher. The Flame Bed (50 metres beneath the Merensky Reef) displays an increase in the MgO/(MgO+FeO) ratio. No reasonable explanation can be given for this phenomenon. The Merensky Footwall unit (subdivided into sub-units 1, 2, 3 and 4) depicts no distinct trend. The MgO/(MgO+FeO) ratio for the Merensky unit displays a prominent decrease, while the Bastard unit displays an increase up to the top of HW2. The MgO/(MgO+FeO) ratio for HW3 displays an increase and a decrease respectively **(Fig. 7.3B)**.

7.5 Major-element - trace-element ratios

In this study, ratios based on selected major and trace elements, which have an affinity for the silicate minerals plagioclase and orthopyroxene, are used in an attempt to define the magma types and then to advance a feasible mechanism for the formation of the layered sequence of the upper critical zone in the Boshoek section.

A cyclic sequence of layers can be defined either with the aid of a parameter that remains constant,

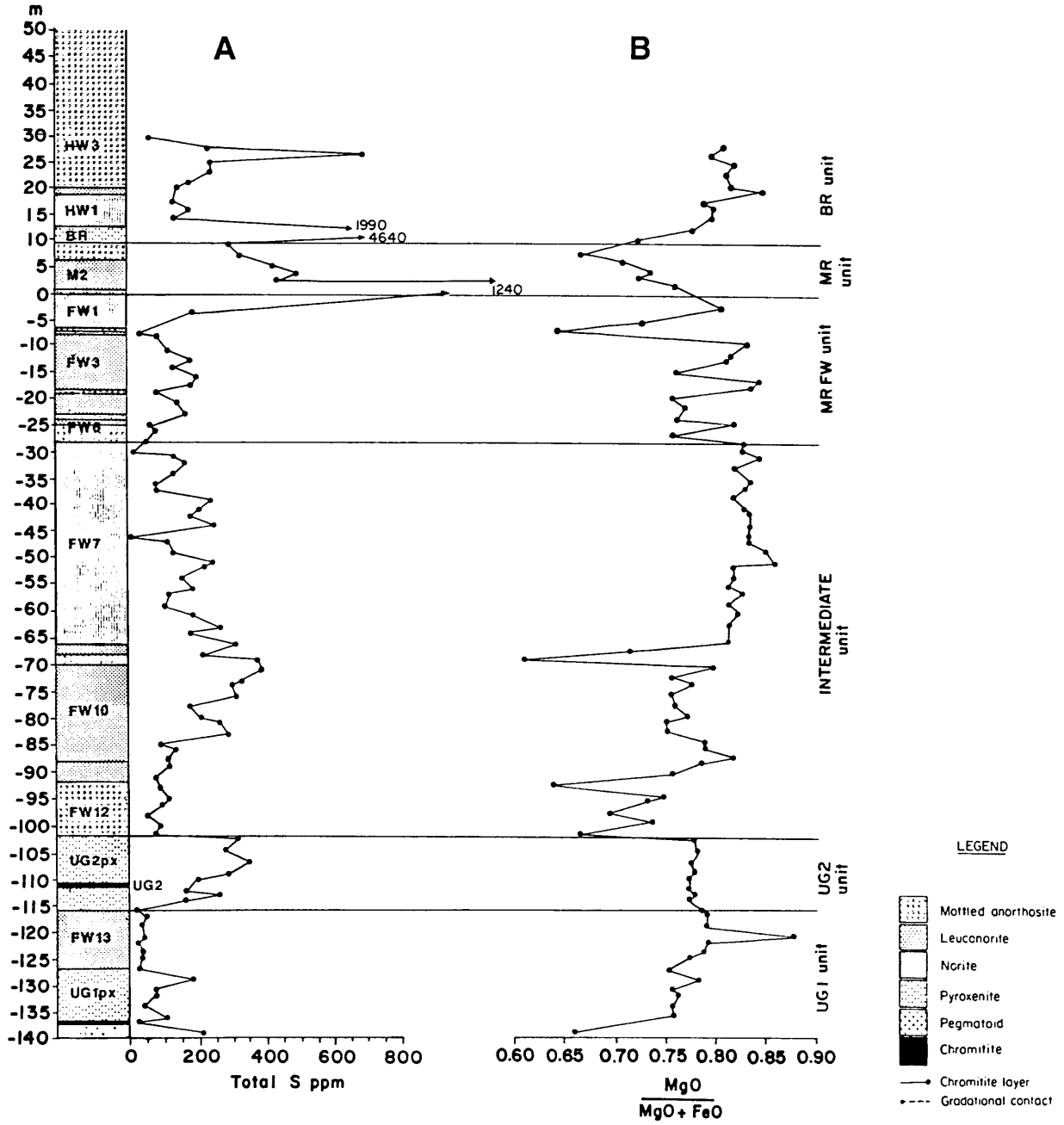

Figure 7.3 Variation of sulphur content and whole rock MgO/(MgO+FeO) ratio with stratigraphic height.

but differs in value for adjacent cycles, or with the aid of a parameter that evolves progressively from a primitive value in each cycle (Eales **et al.**, 1986). Such parameters are useful in identifying the mechanisms that played a role in the formation of a cyclic sequence.

The Sr content of plagioclase (approximated as $Sr/Al_2O_3^*$) as geochemical parameter can be useful in depicting distinct units and thus provide evidence that individual cyclic units were produced by different magma inpulses. This was found to be the case for all the units in the upper critical zone of the Union section (Eales **et al.**, 1986). Although Al is held largely in plagioclase, the correction for the small amount in orthopyroxene (A) must be made.

$$Al_2O_3^* = Al_2O_{3(\text{whole rock})} - A ;$$

where $A = MgO_{(\text{whole rock})}/MgO_{(\text{in opx})} \times Al_2O_{3(\text{in opx})}$.

The calculation is used only for rocks that contain orthopyroxene and plagioclase; rocks that contain large amounts of olivine, chromitite, clinopyroxene and mica are not supposed to be used (Eales **et al.**, 1986).

Other geochemical parameters which relate to plagioclase composition are the Rb/Sr, $Ga/Al_2O_3^*$ and Sr/Na_2O (Eales **et al.**, 1986) ratios. Almost all the Sr is held in the plagioclase while Rb is contained in different phases in different rock types. In the pyroxenites small amounts of biotite and alkali feldspar are the main hosts, while in anorthosite, these elements are held in the plagioclase although some is contained in the accessory alkali feldspar and biotite. The element Ga is largely held in plagioclase where there is a close coherence with Al. In addition to plagioclase, biotite contributes significantly to the Ga content (Barton and Calkin, 1978).

7.5.1 Plagioclase ratios

The $Sr/Al_2O_3^*$ ratio for the upper critical zone displays several distinct segments, as was found to be the case at the Union section (Eales **et al.**, 1986)**(Figs. 7.4).** The UG1 unit together with the lower part of the UG2 unit, the upper part of the UG2 unit, the Intermediate and Merensky Footwall units, the Merensky and Bastard units exhibit different ranges of $Sr/Al_2O_3^*$ ratios.

Distinct increases in the $Sr/Al_2O_3^*$ ratio for the upper part of the upper UG2 feldspathic pyroxenite, and the Flame Bed (50 metres beneath the Merensky unit) are prominent in comparison with the average values of this ratio for the UG1 and lower UG2 feldspathic pyroxenites and the FW7 norite layer. Although the Intermediate and Merensky Footwall units display no distinct difference in $Sr/Al_2O_3^*$ ratio, there is evidence of a variation in the $Sr/Al_2O_3^*$ ratio at the base of the Merensky Footwall unit (above the Boulder Bed), producing subsidiary trends. An additional segment from the base of the Intermediate unit upto the flame bed can be suggested.

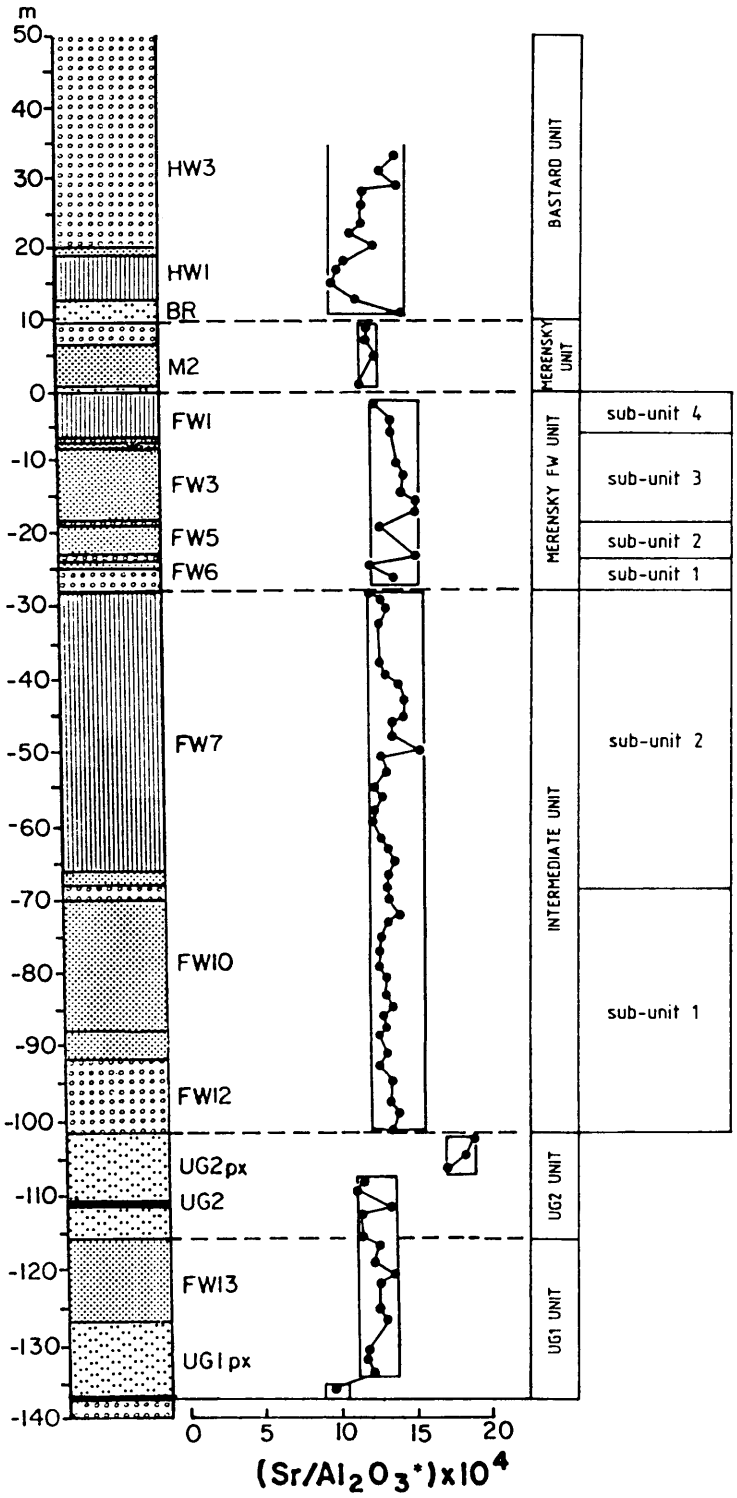

Figure 7.4 Plot of $Sr/Al_2O_3^*x10^4$ ratios against stratigraphic height for the upper critical zone, Boshoek section.

The Merensky feldspathic pyroxenite has a $Sr/Al_2O_3^*$ ratio very similar to that of the UG1 and UG2 feldspathic pyroxenites while the overlying leuconorite and mottled anorthosite display similar $Sr/Al_2O_3^*$ values. The $Sr/Al_2O_3^*$ ratio decreases from the Bastard feldspathic pyroxenite, which has a substantially higher value than the UG1 and UG2 feldspathic pyroxenites, to the overlying HW1 layer, and then increases again with height.

The Rb/Sr ratio is high in the feldspathic pyroxenite layers (UG1, UG2, Boulder Bed, Merensky and Bastard units) **(Fig. 7.5A in folder)**. These high Rb/Sr values that correlate with the high K values can not be explained by the presence of interstitial K-feldspar and biotite in the rock. According to the analytical data, the high Rb/Sr ratio for the pyroxenite is caused by low Sr values i.e. intercumulus plagioclase with a low Sr content compared to the cumulus plagioclase of the more felsic rocks. The upper part of the upper UG2 feldspathic pyroxenite has a distinctly lower ratio. Except for high Rb/Sr values for the Merensky and Bastard feldspathic pyroxenite layers, the more felsic layers of these units display increases in the ratio with height.

$Ga/Al_2O_3^*$ and Sr/Na_2O have similar trends **(Figs. 7.5B-C)**. The UG1 and lower UG2 feldspathic pyroxenites display low values, while the upper part of the upper UG2 feldspathic pyroxenite layer displays a further decrease for $Ga/Al_2O_3^*$ and an increase for Sr/Na_2O. This correlates with the increases in $Sr/Al_2O_3^*$. Furthermore, the Sr/Na_2O ratio decreases erratically, while $Ga/Al_2O_3^*$ in plagioclase-rich lithologies tends to remain constant with increasing stratigraphic height. The Merensky unit displays an increase for the Sr/Na_2O ratio with height. The overlying Bastard unit displays an increase for the ratio $Ga/Al_2O_3^*$ from the base of the unit to approximately 30 metres above the Merensky Reef, compared to the Sr/Na_2O ratio which increases from the Bastard feldspathic pyroxenite up to the HW2 leuconorite layer from where the trend decreases with height.

7.6 Trace element ratios

Eales **et al.** (1986) showed that, with certain element ratios as parameters, the units in the upper critical zone in the Union section evolved progressively from primitive values within each cycle. The use of these ratios could make it possible to recognize the different units, the presence of different magma types and the possibility of a mixing process between these magmas to produce intermediate values for these ratios.

The mafic minerals of the rocks are hosts for Ni, Co, Cr, V, Sc and Ti, and for this reason the concentrations of these elements are high in the mafic rocks. However, ratios of elements can be selected on the basis of their presence in one mineral (orthopyroxene) and the exclusion from an associated second or third mineral (plagioclase), and should be independent of the modal proportions of the minerals concerned (Eales **et al.**, 1986). Ratios such as Cr/Sc, Cr/V, Ni/Sc and Co/V should therefore be usefull to detect progressive change throughout a unit, or to accentuate geochemical discontinuities. The trends, however, have been produced by less data points due to the omission of values which fall beneath the analytical detection limit.

7.6.1 Orthopyroxene ratios

The UG1 and UG2 feldspathic pyroxenite layers display high Cr/Sc, Ni/Sc and Cr/V ratios (**Figs. 7.5E-G**). The norite and leuconorite in the overlying Intermediate unit have low to intermediate ratios, and although values fluctuate considerably they tend to increase with stratigraphic height. The Co/V ratio displays an increase in range and ratio with an increase in height (**Fig. 7.5H**). A distinct upward decrease in range and a slight decrease in value is displayed by the Cr/V and Co/V ratios from between the Intermediate sub-unit 2 and the overlying Merensky Footwall unit.

Ratios Cr/Sc and Ni/Sc display decreasing trends for the Merensky and Bastard units from the base upwards, while for the Bastard unit, the Cr/V ratio values also decrease. An exception, according to the cyclic trends depicted by Eales **et al.** (1986), is the indistinct nature of the Cr/V and Co/V ratios in the Merensky unit (**Figs. 7.5G-H**). The Cr/V and Co/V ratios display upward increases from the base of the unit to the top, except for an abrupt decrease in the M3 mottled anorthosite. The Co/V ratio displays a further increase towards the Bastard feldspathic pyroxenite layer.

The Merensky and Bastard units in the Boshoek section can thus be considered to have been produced by crystallization from several liquid layers, as indicated by the chosen parameters that progressively evolved from a primitive initial state. The underlying UG1, UG2, Intermediate and Merensky Footwall units do not show any trends of this type. The major element-trace element ratios suggest that a mixing process involving distinct magma types produced these units.

8. DISCUSSION AND INTERPRETATION

8.1 Regional correlation of the geological sections

As was shown in **Chapter 2**, the lower part of the Rustenburg Layered Suite in the southwestern Bushveld Complex is confined to a number of basins, also referred to as troughs by Cameron (1964), separated from one another by anticlinal folds. The thickness of the different zones within these basins differs considerably. The combined lower and lower critical zones in the Rustenburg section is approximately three times thicker than the lower critical zone in the Boshoek section where lower zone rocks are not developed according to Coertze (1974). It is of interest in this regard to note that the LG1 - LG6 interval of the lower critical zone in the Boshoek section is twice as thick as the corresponding interval in the Rustenburg section (Cousins and Feringa, 1964).

The subdivision of the lower part of the Rustenburg Layered Suite into the lower and critical zones is based on the appearance of abundant cumulus chromite together with the presence of the first chromitite layer (Coertze, 1974). In the Boshoek area the first chromitite layer, LG1 is situated 104 metres above the floor (Fourie, 1959) and thus confirms that the lower zone is underdeveloped or absent in this area. The difference in thickness for the lower critical zone in the two sections could be explained by the presence of the prominent Kookfontein upfold.

Variations in thickness of the different rock units are also evident in the upper critical zone of the Boshoek and Rustenburg sections **(Fig. 8.1)**. Borehole E in the Boshoek section situated above the Kookfontein anticline, intersected a substantially thinner upper critical zone sequence compared especially to the sequence southeast of the upfold **(Figs. 2.2 and 8.1)**. No chromitite layers are developed here and the UG1 and UG2 feldspathic pyroxenite layers are separated by leuconorite. The sublayers of the Intermediate and Merensky units are thinner while the Bastard unit correlates well with other boreholes. This is due to the fact that the Kookfontein anticline, which physically divides the Boshoek and Rustenburg sections on the surface, has a fold axis which strikes north-south with a plunge direction to the north **(Fig. 8.1)**.

Southeast of the Kookfontein upfold (boreholes G,H,I) **(Figs. 2.2 and 8.1)** the succession is normal in the sense that the UG1 and UG2 chromitite layers and their associated feldspathic pyroxenite layers are present. The UG1, UG2, Intermediate, Merensky Footwall and Merensky units thicken to the southeast while the Bastard unit becomes thinner. The thickness between the Merensky Reef and the base of the UG1 unit is 136, 70 and 79 metres for boreholes I, E and B respectively.

The Boulder Bed - Merensky unit interval in the Rustenburg section is illustrated in **Figure 8.1**. From this it is evident that there is a thickening of this interval in the central part and a decreases in thickness to the west and east and is related to the basin-shaped nature of the floor (Viljoen and Hieber, 1986).

The separation of the mafic sequence into discrete subchambers by the Spruit- and Kookfontein upfolds are important features which, although they do not deform the critical zone, could be assosiated with important lateral differences in the lithology of the critical zone.

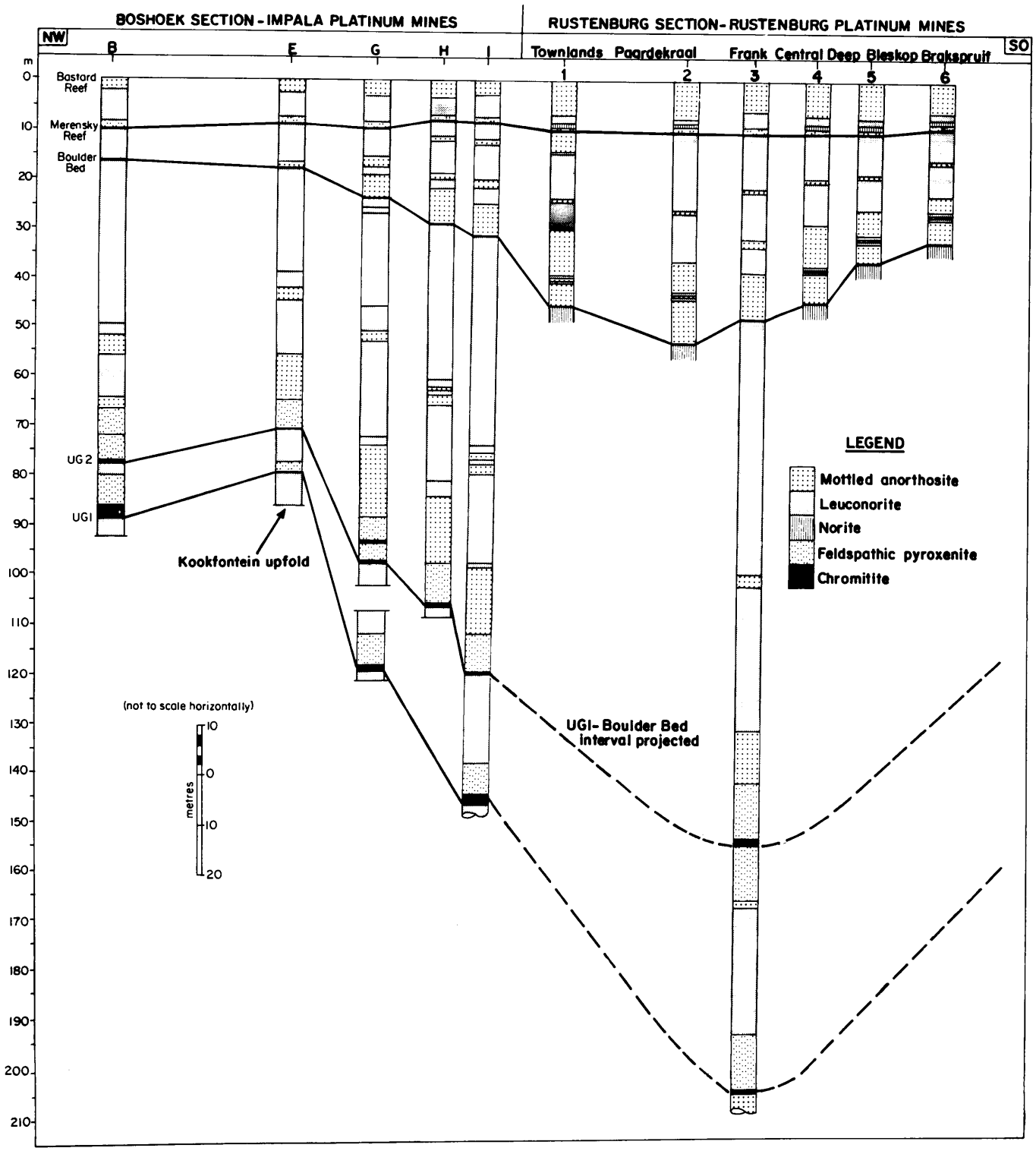

Figure 8.1 Reconstructed cross-section of the Boshoek and Rustenburg sections showing the lithology of the respective upper critical zones. Data for the Boshoek and Rustenburg sections taken from Leeb du Toit (1986) and Viljoen and Hieber (1986) resectively.

Well-defined cyclic units make up the upper critical zone stratigraphy at the Rustenburg, Boshoek and Union sections. The correlation of these lithologies will be attempted on the basis of work by De Klerk (1982); Kruger (1982); Leeb du Toit (1986); Viljoen and Hieber (1986a); Viljoen **et al.** (1986b) and Naldrett **et al.** (1987).

The UG1 unit in the Rustenburg and Boshoek sections consists of a basal chromitite layer with thicknesses of 0,70 and 0,96 metres respectively, and is overlain by feldspathic pyroxenite and leuconorite. The UG1 unit in the Union section, however, consists of two main chromitite layers, separated by a 0,32 metre thick medium grained pyroxenite, while the overlying leuconorite is absent. According to Naldrett **et al.** (1987), the UG1 unit in the northeastern part of the Union section contains additional felsic rock layers such as norite. In the Rustenburg section the UG1 unit contains, in addition to the leuconorite, a mottled anorthosite layer at the top.

The contact between the UG1 feldspathic pyroxenite and the overlying leuconorite at the Boshoek section is usually marked by a 1 to 10 centimetre thick chromitite layer, while at the Union section two thin chromitite layers are present in the UG1 feldspathic pyroxenite.

At the Union and Rustenburg sections, like in the Boshoek area, the UG2 chromitite layer is associated with a pegmatoidal, feldspathic pyroxenite footwall and is situated in the middle of a thick feldspathic pyroxenite (**Fig. 8.2**). The immediate hanging wall of the UG2 chromitite layer at the Union section, however, consists of harzburgite which has a gradational contact with the overlying pyroxenite.

In the northwestern Bushveld the UG2 unit is overlain by the Pseudoreef unit. This unit is correlated with the Boulder Bed Sequence or Merensky Footwall unit (Naldrett **et al.**, 1986) and consists of a lower coarse-grained, pegmatoidal, feldspathic harzburgite, approximately 1,50 metres thick, with an undulating lower contact, and an upper medium to coarse-grained, feldspathic harzburgite, termed the "Tarentaal". The upper harzburgite is separated from the lower portion by a 5 to 10 millimetre thick irregular chromitite layer (De Klerk, 1982; Viljoen **et al.**, 1986a). The Pseudoreef Marker, a pegmatoidal feldspathic pyroxenite, overlies the Pseudoreef unit and passes upwards into a feldspathic pyroxenite and melanorite. At the top, the Pseudoreef Marker is defined by a thin mottled anorthosite layer, known as the Pothole Marker. Overlying the Pothole Marker is a 7 metre thick leuconorite layer. Above the leuconorite is a 8 metre thick mottled anorthosite layer, which forms the footwall of the Merensky Reef (**Fig. 8.2**).

De Klerk (1982) noted that only the basal parts of the UG1, UG2 and Pseudoreef units are present in the Union section and provides stratigraphical and geochemical evidence supporting the incompleteness of these units. He suggested that the missing sequences were either removed or that further crystallization never occurred.

The Intermediate unit in the Boshoek section and the interval between the upper UG2 feldspathic pyroxenite layer and the Boulder Bed in the Rustenburg section are very similar. Notable differences are that the "flame bed" in the Rustenburg section is situated approximately 90 metres beneath the

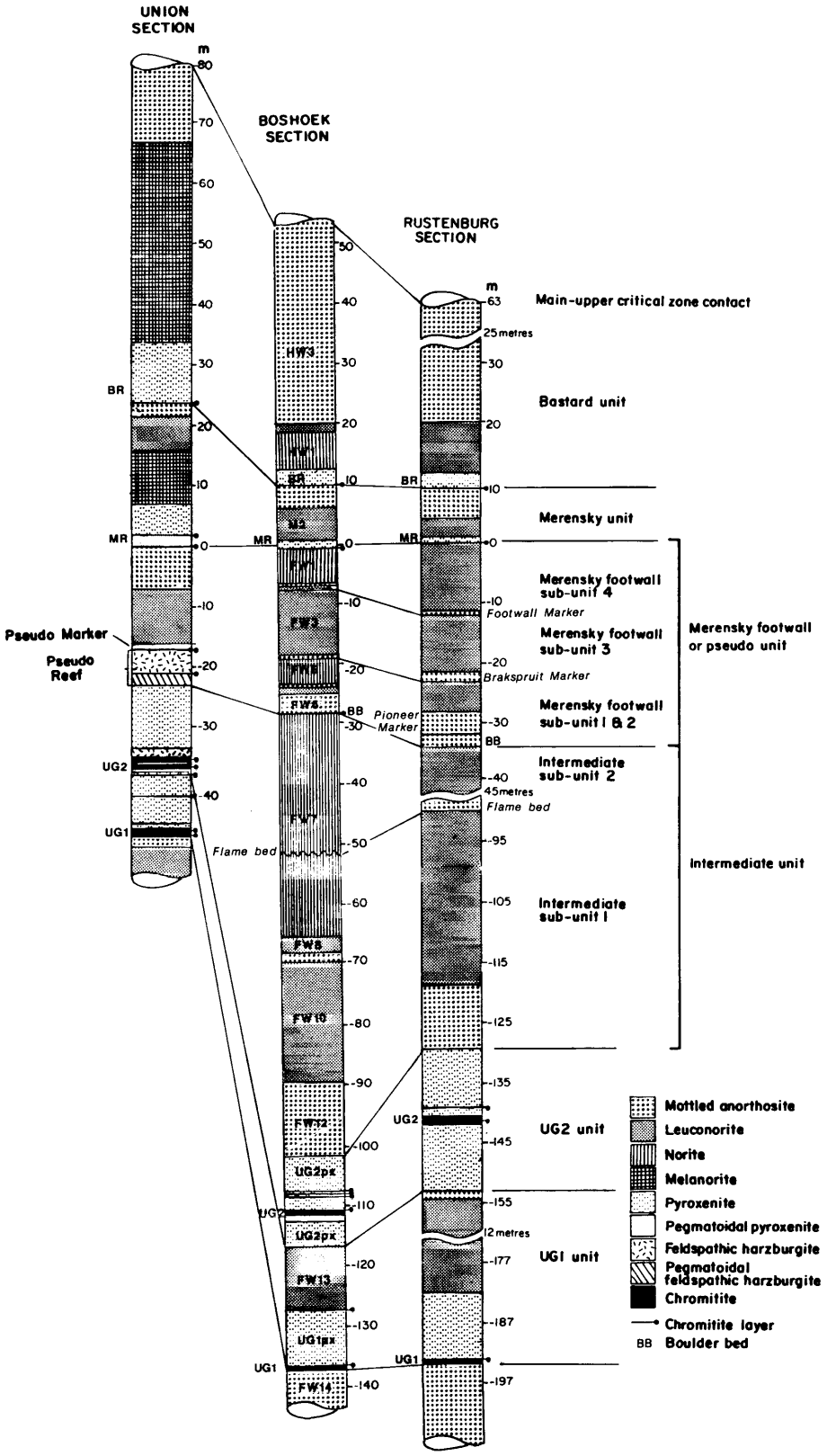

Figure 8.2 Correlation of the upper critical zone in the Union, Boshoek and Rustenburg sections. Data taken from Viljoen **et al.** (1986), Leeb du Toit (1986) and Viljoen and Hieber (1986) respectively.

Merensky Reef, whereas the same horizon in the Boshoek section is situated in FW7 norite, 52 metres below the Merensky Reef, and that the mottled anorthosite at the base of the Intermediate sub-unit 2 in the Boshoek section does not seem to be developed in the Rustenburg sequence **(Fig. 8.2)**.

The Merensky Footwall unit (Boulder Bed Sequence) overlies the UG2 unit in the Rustenburg section (Naldrett **et al.**, 1987) and is correlated with the Pseudoreef unit in the Union section. The interval above the Boulder Bed in the Rustenburg section (Boulder Bed Sequence) consists of several anorthosite markers (Footwall, Brakspruit and Pioneer) and associated leuconorite layers **(Fig. 8.2)**. The Pioneer Marker is correlated with the upper part of FW6 at the Boshoek section, which consists of leuconorite and overlying anorthosite layers. Two fine-grained pyroxenite layers, 2 to 3 centimetres thick, define the upper and lower contacts of the leuconorite layer. The Pioneer marker, in turn, consists of alternating mottled anorthosite and leuconorite layers, with two thin, closely spaced pyroxene-rich layers known as the "tram tracks" (Viljoen and Hieber, 1986), at the base of the uppermost mottled anorthosite layer **(Fig. 8.2)**.

The Brakspruit Marker consists of a 1,50 metre thick mottled anorthosite layer with thin interlayered leuconorite and norite layers (Viljoen and Hieber, 1986). This layer is correlated with the FW4 mottled anorthosite layer in the Boshoek section, which is approximately 2 metres thick with alternating mottled anorthosite being interlayered with leuconorite sublayers (Leeb du Toit, 1986).

The Footwall Marker consists of a well defined mottled anorthosite layer, 40 to 100 centimetre thick with a 5 to 15 centimetre thick leuconorite layer in the middle. This marker is correlated with the FW2 leuconorite (FW2(b)) and overlying mottled anorthosite (FW2(a)) layers **(Fig. 8.2)**. Where FW2 attains a maximum thickness of 2 metres, however, a 1 to 2 centimetre thick pyroxenite or pegmatitic pyroxenite (FW2(c)) is developed at the base. In the studied profile FW2(c) is absent.

Unlike the Merensky unit in the Boshoek section, where the basal part of the unit consists of feldspathic pyroxenite, the basal part of the Merensky unit in the Union and Rustenburg sections consists of a coarse, pegmatoidal, feldspathic pyroxenite, bounded by thin chromitite at the top and bottom. A medium-grained feldspathic pyroxenite occurs above the pegmatoid and is approximately 6 metres thick. The Merensky-Bastard Reef interval, however, is slightly thicker than the Rustenburg and Boshoek sections.

In all three areas the Bastard unit commences with a feldspathic pyroxenite which has a thin chromitite layer developed at the sharp basal contact **(Fig. 8.2)**. The feldspathic pyroxenite passes upward into melanorite, leuconorite and mottled anorthosite ("Giant mottled anorthosite").

8.2 Composition of the Bushveld Complex magmas

The composition of the potential parental magmas to the lower and critical zones of the Bushveld Complex is provided by the marginal rocks and syn-Bushveld sills in the floor rocks of the Complex (Davies **et al.**, 1980; Cawthorn **et al.**, 1983 and Sharpe, 1981, 1984, 1985). Two suites of sills have

been recognized in the floor, of which the older, pre-Bushveld suite is extensively altered to amphibolitic rock-types and is truncated by the younger syn-Bushveld sills and marginal rocks. Syn-Bushveld sills are further subdivided into the B1, B2 and B3 marginal groups on the grounds of composition (**Table 8.1**) and their stratigraphic relation to the Rustenburg Layered Suite.

Harmer and Sharpe (1985) and Sharpe (1985) showed, by using Sr isotope, whole rock major- and trace element geochemistry, that distinct marginal rock groups can be related to the lower and critical zones. The B1 magma, a magnesian basalt, is assumed to be parental to the lower zone, while the B2 and B3 magmas, which are tholeiitic in composition, together with residual B1 liquid, were responsible for the critical zone (Hatton, 1989).

Hatton (1987) found that the LREE La, Ce and Sm concentrations in upper critical zone samples from the western sector of the eastern Bushveld Complex are lower than in the underlying lower critical zone. The increase in the proportion of plagioclase in the upper critical zone should, according to Hatton (1987), cause an increase in the LREE concentration due to the strong preference of these elements for plagioclase. The observed decrease in LREE content was related by him to the addition of a new, low LREE B3 parental magma prior to the formation of the upper critical zone.

It is furthermore of interest that the initial Sr isotope ratios of the different marginal rock groups can be correlated with distinctive sequences within the Layered Suite (Harmer and Sharpe, 1985; Sharpe, 1985). The B1 group has a lower average value (0,7044) than the B2 and B3 groups (averages of 0,7068 and 0,7065 respectively). The critical zone rocks have average initial Sr isotope ratios (between 0,7051 and 0,7062) intermediate to the values of the B1 and the B2/B3 groups (Harmer and Sharpe, 1985; Hatton, 1987) which suggests that these rocks crystallized from mixtures of B1 and a combination of B2/B3 magmas. The initial Sr isotope ratio of most of the main zone cumulates is 0,7086 (Kruger and Marsh, 1982; Sharpe, 1985), which is higher than any of the marginal rock groups. This led Sharpe (1985) and Hatton (1989) to suggest the presence of a fourth parental Bushveld magma, referred to as B4, and considered by Hatton to be an aluminous tholeiite on the basis of the bulk composition of the main zone cumulates.

A significant change in the initial Sr isotope ratio takes place across the Merensky unit (Kruger and Marsh, 1982) with the highest initial Sr isotope ratio some distance above the Merensky Reef. This is taken as the strongest evidence that the Merensky unit formed in response to a mixing event between the B4 magma from which the main zone cumulates crystallized and residual B1 and B2/B3 magmas in the magma chamber (Hatton, 1989).

Sharpe and Irvine (1983), who determined the melting properties of the chilled marginal rocks, showed that the U (or B1) magma had a higher liquidus temperature (1280 - 1290 °C), compared to 1190 °C for the A (or B2/B3) type magma. The general crystallization order for the B1 magma was determined to be olivine plus minor chromite, orthopyroxene and plagioclase, compared to plagioclase plus chromite, olivine, orthopyroxene and clinopyroxene for the B2/B3 magmas. They (Sharpe and Irvine, 1983; Irvine and Sharpe, 1986) also showed that the mixing between these two

Table 8.1 Estimated composition of the B1, B2 and B3 parental magmas based on marginal and syn-Bushveld sill compositions. Taken from Harmer and Sharpe (1985).

	B1	s	B2	s	B3	s
SiO_2	55.72	1.49	49.92	1.90	50.79	1.55
TiO_2	0.32	0.05	0.68	0.23	0.39	0.18
Al_2O_3	11.33	1.05	16.21	0.37	16.05	0.58
FeO	9.30	0.28	12.17	1.90	9.09	1.31
MnO	0.17	0.01	0.20	0.04	0.16	0.01
MgO	13.00	2.29	6.94	0.75	8.26	0.88
CaO	6.37	0.37	11.57	0.33	11.48	1.00
Na_2O	1.72	0.21	2.15	0.33	2.31	0.05
K_2O	0.88	0.18	0.15	0.02	0.19	0.04
P_2O_5	0.07	0.02	0.14	0.08	0.03	0.03
Co	92	13	89	6	85	7
Cr	1104	337	197	120	430	228
V	162	7	232	46	150	42
Zn	101	56	39	22	23	9
Y	16	7	21	7	12	2
Sr	182	26	347	18	330	36
Rb	33	7	2	1	3	1
SrRo	0.703-0.705		0.7065-0.7075		0.7065	

magma types leads to the crystallization of chromite, a mechanism which is now widely favoured for the origin of chromitite layers in the Rustenburg Layered Suite of the Bushveld Complex (Hatton and Von Gruenewaldt, 1987; Von Gruenewaldt **et al.,** 1986).

Concerning the formation of sulphides, Campbell **et al.** (1983) suggested that the magmas present in the magma chamber were close to saturation in sulphide. Mixing of two types of magmas referred to above would result in oversaturation of sulphur and to the formation of immiscible sulphide droplets. The variation in temperature caused by cooling and or by mixing of a primitive magma (B1) and differentiated liquid (B2/B3), will have a greater influence on the sulphide solubility than variations in the FeO content for approximately 50% crystallization (Naldrett and Von Gruenewaldt, 1988). Experimental considerations therefore suggest that magma mixing processes can result in the formation of chromitite layers and also the separation of immiscibile sulphides associated with the chromitite layers in the critical zone.

Investigation into the density and viscosity characteristics of the different melts were conducted by Sharpe **et al.** (1983) and by Hatton (1989) with the aid of the algorithms of Bottinga **et al.** (1982). The results, summarized by Hatton and reproduced here as **Figure 8.3,** shows that the B1 magma has a lower density than the B2 and B3 magmas.

8.3 Interpretation

With the above information on the parental magmas of the Bushveld Complex it will be attempted to reconstruct the crystallization history of the sequence under investigation.

The lower critical zone of the Boshoek section consists of pyroxenitic rocks (Cousins and Feringa, 1964) which are generally accepted to have crystallized from B1 magma (Sharpe, 1985). The overlying upper critical zone, which consists mainly of plagioclase-rich rocks with minor associated pyroxenite layers, is assumed to have crystallized from magma in which the B2/B3 component predominated as deduced from the increase in the Sr isotopic ratio across the lower - upper critical zone transition (Sharpe, 1985; Kruger **et al.,** 1987).

It is suggested that, prior to the formation of the UG1 unit, B2/B3 magma was emplaced into the magma chamber which contained B1-dominant magma. It has been shown by Campbell (1983); Sharpe **et al.** (1983) and Hatton (1989) that an input of fresh primitive B2/B3 magma which is more dense than the resident, B1-dominant magma, will be emplaced into the magma chamber as a turbulent fountain due to the initial momentum of emplacement. Mixing between the B2/B3 magma and the resident B1 magma (higher temperature and lower density) could take place within the plume to produce chromite (Campbell **et al.,** 1983). The magma chamber then stratified with the B1-dominant magma elevated above the newly intruded B2/B3 magma, while the crystallized chromite settled to the floor, producing a chromitite layer like the UG1. A hybrid layer Bh_{aci} (B1 and B2/B3 mixture) produced during the emplacement of the B2/B3 magma will spread out at its own density level between the elevated B1 and the floor.

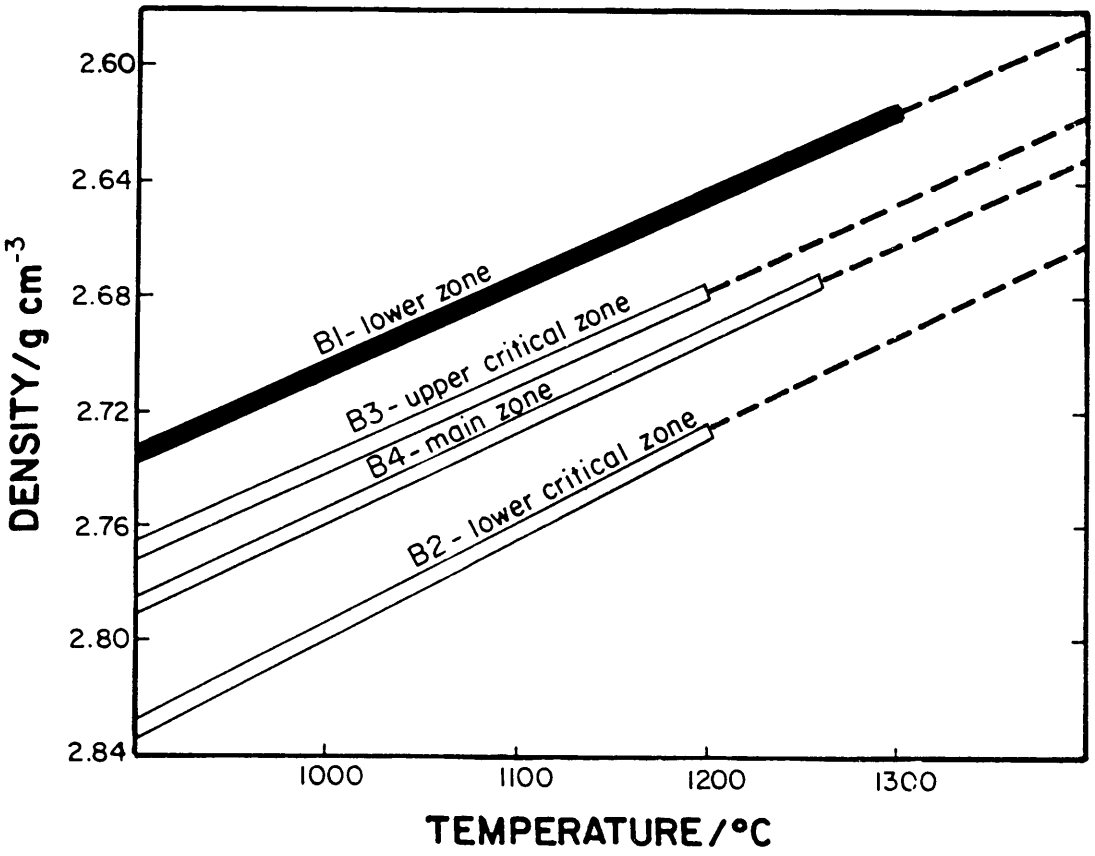

Figure 8.3 Density relations of the B1, B2, B3 and assumed B4 parental magmas according to Hatton (1989).

As a result of the difference between the liquidus temperatures of the B1 and B2/B3 magmas, the elevated B1 magma will be cooled by the underlying B2/B3-dominant hybrid magma and crystallize orthopyroxene. Due to the density of orthopyroxene crystals which is substantially higher than the density of the Bushveld magmas, it has been calculated that crystallization of approximately 5% of orthopyroxene crystals in the basal portion of the B1 magma will raise the bulk density to that of the B2/B3-dominant hybrid magma (Hatton, 1989). A crystal-liquid mass can therefore slump down through the hybrid magma to the chamber floor (Huppert **et al.**, 1984) where it will form a layer of cumulus orthopyroxene grains with intercumulus plagioclase.

Due to the higher liquidus temperature of the elevated B1 magma, convection in the B2/B3-dominant hybrid magma layer will cease since it is driven by the upward loss of heat (Hatton, 1989). Crystallization from the B2/B3-dominant hybrid magma, in response to heat loss through the floor of the chamber, will depend on the viscosity of the magma and the rate of cooling. According to Martin (1990), both crystal settling and in situ crystallization may occur in the same magma chamber. In situ crystallization will occur if supercooling is maintained below the temperature required for homogeneous nucleation, whereas, if supercooling does occur, crystals will form in suspension and later settle to the floor (Martin, 1990). As stated in **Paragraph 8.1.1**, the B2/B3-dominant magma will primarily have plagioclase on the liquidus (producing anorthosite) and will be followed, as the temperature decreases, by plagioclase and orthopyroxene (producing leuconorite).

8.3.1 Units in the Merensky footwall

For modeling purposes, the B1-type, the B2/B3-type and B4-type magmas are referred to as Ba, Bc and Bx respectively, while any hybrid liquid which is produced by the mixing of B1 with B2/B3 and B4 magmas will be referred to as Bh_{aci} (Bh_{ac1}, Bh_{ac2}, ect.) and Bh_{axi} (Bh_{ax1}, Bh_{ax2}, ect.) respectively.

It is envisaged that a Bc type magma layer was situated at the bottom of the stratified magma chamber and that the FW14 anorthosite crystallized from this layer. Formation of the UG1 unit was initiated by mixing between Ba and Bc magmas during further emplacement of Bc magma, causing a sufficient amount of chromite to crystallize in order to produce the UG1 chromitite layer **(Fig. 8.4A)**. Mixing between the Ba and Bc magmas during the emplacement, however, was sufficient to produce a hybrid layer Bh_{ac1}. The slumping (stage 1) of a layer of Ba crystal-liquid mass through the underlying Bhac1 magma layer to the floor (FW14) of the chamber **(Fig. 8.4B)** crystallized orthopyroxene with intercumulus plagioclase while the overlying leuconorite (FW13) was produced by plagioclase and orthopyroxene crystallizing from the Bh_{ac1} magma **(Fig. 8.4C)**.

The UG2 lower feldspathic pyroxenite layer formed by the next slumping process (stage 2) **(Fig. 8.4D)**, whilst the UG2 chromitite layer was produced by a new influx of Bc magma into the chamber, resulting in extensive mixing between the Ba, Bh_{ac1} and Bc magma layers **(Fig. 8.4E)**.

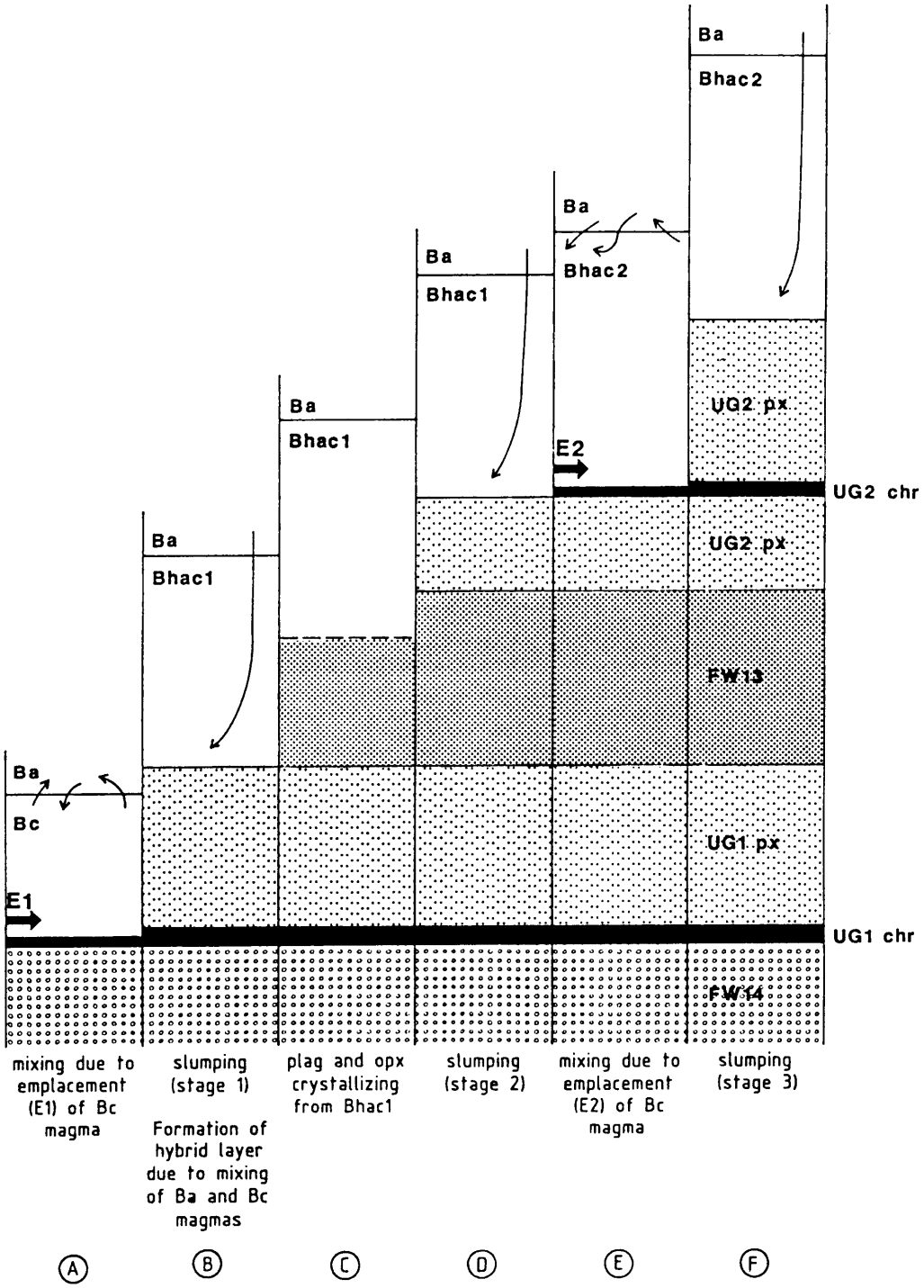

Figure 8.4 Schematic representation of the postulated sequence of events responsible for the formation of the UG1 and UG2 units.

The upper feldspathic pyroxenite, which hosts the "Leader triplets", is produced by the third slumping process (stage 3) during which limited mixing of slumped material and the newly formed Bh_{ac2} hybrid magma could have produced the thin chromitite layers **(Fig. 8.4F).**

The mineral chemistry of the plagioclase and orthopyroxene in the UG1 and UG2 units is depicted in **Figures 6.1, 6.3 and 6.5.** Intercumulus plagioclase of the UG1 and UG2 feldspathic pyroxenite layers has a lower An content than the cumulus plagioclase crystals of the associated leuconorite and mottled anorthosite layers. According to Hatton (1989), the derivation of the pyroxenites from the Ba (or B1) magma and the norites and anorthosites from tholeiitic Bc-dominant (or B2/B3) magmas could account for this. The relatively high An content at the base of the UG2 lower feldspathic pyroxenite layer is considered to be due to the infiltration of liquid residua from the top of the UG1 unit (FW13 leuconorite) into the intercumulus space of the base of the succeeding layer or UG2 unit (Eales **et al.,** 1986). No evidence for the infiltration of liquid from the UG2 upper feldspathic pyroxenite to the overlying FW12 mottled anorthosite is present. It is expected that a small quantity of late liquid from the UG2 feldspathic pyroxenite will have very little effect on the overlying plagioclase-dominant rock, whereas, small quantities of late liquid from a plagioclase-dominant rock (FW13) will have a big effect on small amounts of interstitial plagioclase in the overlying UG2 feldspathic pyroxenite.

Distinct increases in the $Sr/Al_2O_3^*$ and Sr/Na_2O ratios and a decrease in Rb/Sr for the upper parts of the UG1 and upper UG2 feldspathic pyroxenites **(Figs. 7.4A-H),** can be explained by limited mixing between the Ba crystal-liquid mass (or B1) and some Bh_{ac2} (or B2/B3-dominated hybrid) magmas during the slumping process.

The Intermediate and Merensky Footwall units which consist of two and four sub-units respectively are characterized by an increase in the modal amount of orthopyroxene with height **(Figs. 3.1 and 4.4).** Periodic influxes of primary Bc magma at the base of the stratified liquid column, is considered a suitable mechanism, as this could result in the crystallization of plagioclase only to form anorthosite (FW12)**(Fig. 8.5A and 8.5B).** As the temperature of the newly emplaced Bc magma decreases, the plagioclase was joined by bronzite on the liquidus to produce the FW11 and FW10 leuconorite **(Fig. 8.5C).**

A second influx of primary Bc magma could have resulted in a sufficient increase in the temperature of the Bc magma already present above the floor, causing the composition of the liquid to move away from the plagioclase - bronzite cotectic, into the primary phase volume of plagioclase. Crystallization of plagioclase alone would then produce the FW9 anorthosite **(Fig. 8.5D).** Crystallization of plagioclase alone will cause the composition of the hybrid Bc magma to change and to produce the FW8 leuconorite **(Fig. 8.5D).** The FW7 norite **(Fig. 8.5E),** however, does require an additional orthopyroxene component. It is envisaged that, in response to gradual cooling, the overlying Bh_{ac2} magma, with orthopyroxene on the liquidus, commenced to crystallize.

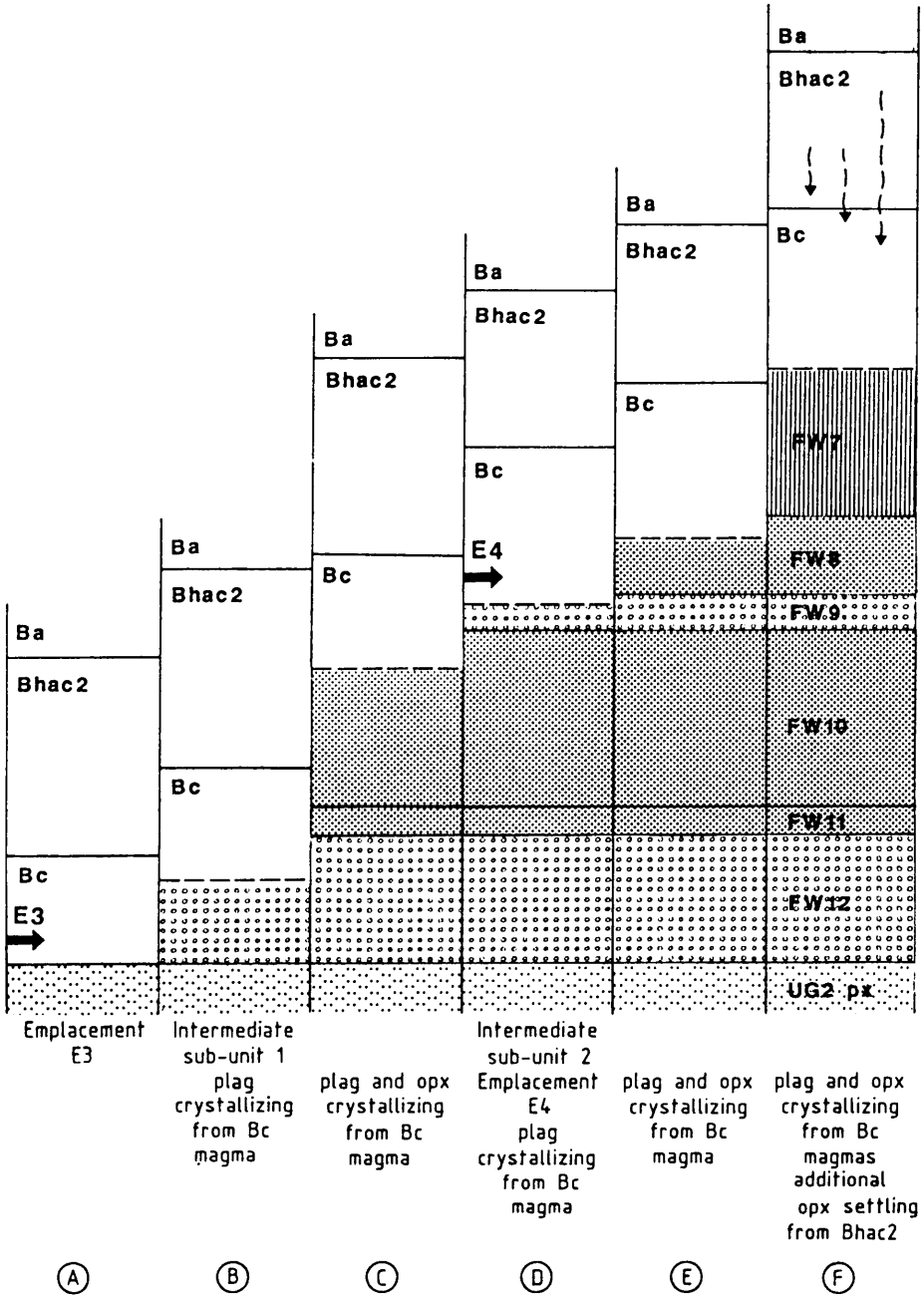

Figure 8.5 Schematic representation of the postulated sequence of events responsible for the formation of the Intermediate unit.

The orthopyroxene settled through the crystallizing Bc layer to the floor, to yield the required additional orthopyroxene component for the FW7 norite.

Sub-units in the Merensky Footwall unit are considered to have formed by the same process where the liquidus temperature of the Bc magma was increased by periodic, but gentle influxes of primary Bc magma above the floor of the chamber **(Figs. 8.6A-H)**. Although the mottled anorthosite layers FW9, FW6(a), FW4 and FW2 are relatively thin (290, 110, 40 and 33 centimetres respectively), only slight changes in composition away from the plagioclase-orthopyroxene cotectic to produce plagioclase alone is required for the formation of these layers.

The 3 metre thick FW6(d) mottled anorthosite, however, is associated with the pyroxenitic nodules of the "Boulder Bed". According to Jones (1976), the mafic spheroids represent a disrupted pyroxenite layer, while Leeb du Toit (1986) noted that the "boulders" formed as a result of the break-up of an unstable pyroxenite layer. In this study, however, it is concluded that the Boulder Bed was formed by crystal-liquid slumping (stage 4) from the Ba magma. The slumped crystal-liquid is considered to have broken up into nodules due to the small volume of slumped material involved **(Fig. 8.6A)**.

Closely associated with the thin anorthosite layers and the mechanism which produced the sub-units, are the non-cotectic FW5 and FW1 norites. The formation of these norites do require an additional orthopyroxene component and the most likely source would be crystal settling from the Bh_{ac2} magma layer through the Bc magma **(Figs. 8.5F, 8.6D and 8.6H)**. The difference between invoking slumping of a crystal-liquid layer from the Ba magma layer and in the other instance crystal settling from the Bh_{ac2} hybrid magma, could possibly be related to the volume of primary Bc magma emplaced. A large volume of Bc magma would have the effect of more effective cooling of the elevated Ba magma and consequently cause crystal-liquid slumping. In comparison, small, gentle influxes and comparatively slow cooling may allow orthopyroxene crystals to settle from the Bh_{ac2} hybrid magma through the underlying Bc magma to produce non-cotectic norite.

The composition of the cumulus plagioclase in the sub-units 1 and 2 of the Intermediate unit displays ill defined increases in An content with height, while an upward increase in the An content is also evident from the Boulder Bed at the base of the Merensky Footwall unit to the top of FW5 **(Fig. 6.1)**. The upper part of the Merensky Footwall unit suggest an upward decrease in An content. Such an upward increase in An content in certain units is not unusual and has been documented by several workers (Van Zyl, 1960, 1970; Meyer, 1969; Vermaak, 1976; Cameron, 1980; De Klerk, 1982; Kruger, 1982; Kruger and Marsh, 1985; Eales **et al.**, 1986; Naldrett **et al.**, 1987 and Hatton, 1989).

A process to explain the upward increases in An content, is related to the nature of emplacement of the Bc magma influxes.

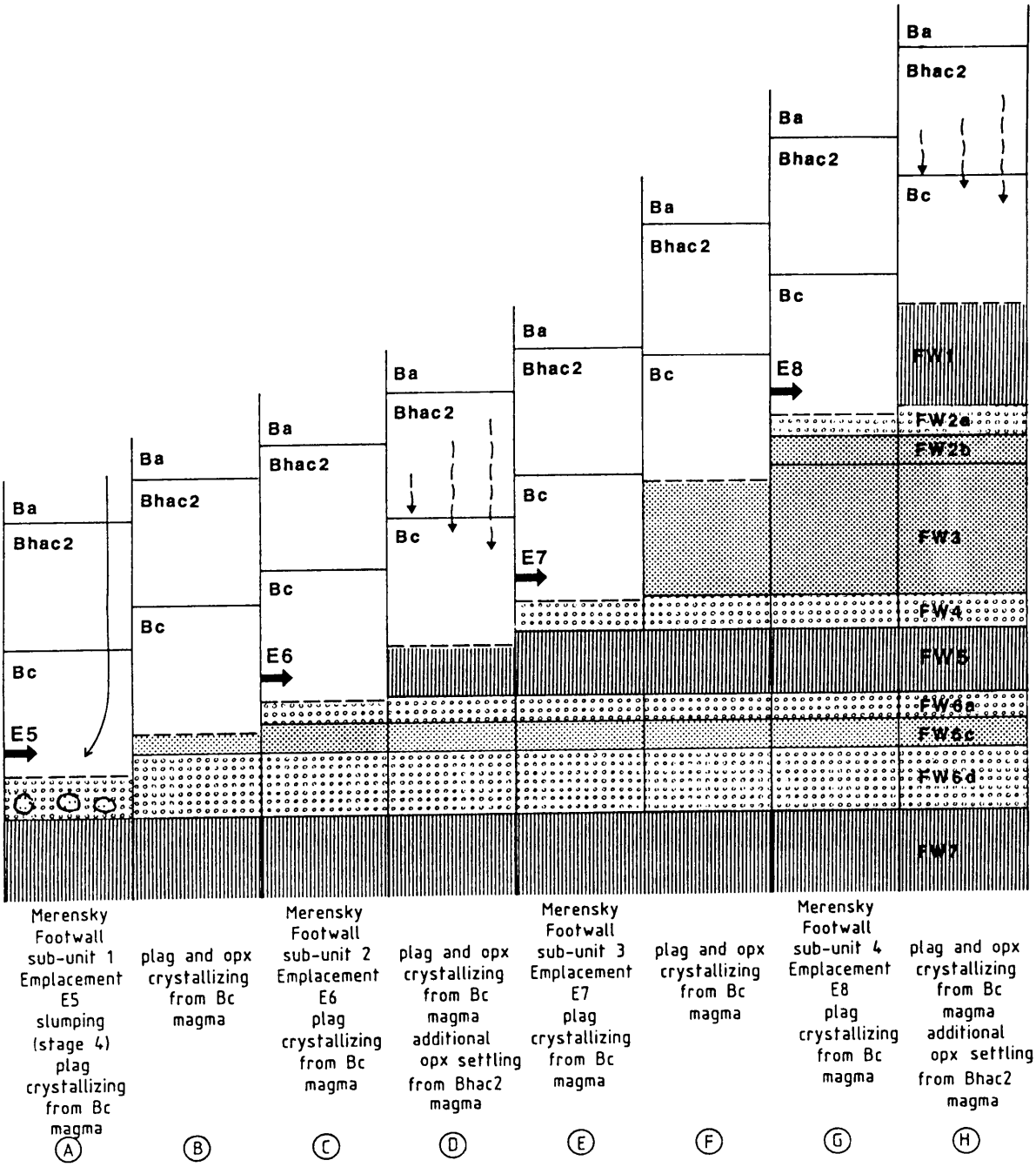

Figure 8.6 Schematic representation of the postulated sequence of events responsible for the formation of the Merensky Footwall unit.

For the formation of the UG1 and UG2 chromitite layers and associated pyroxenite comparatively large influxes are proposed which resulted in mixing events and the subsequent formation of Bh_{ac1} hybrid magmas. After formation of the UG2 upper feldspathic pyroxenite, Bc influxes are considered to be small and less turbulent so that mixing was restricted initially to residual Bh_{ac2} magma at the base of the magma chamber. Each additional small pulse of primary Bc magma could therefore result in a gradual increase in the primary Bc component of the Bc magma layer at the base of the stratified magma chamber. Consequently the plagioclase crystallizing from this layer could display irregular upward increases in the An content.

In the upper part of the Merensky Footwall unit, from the FW4, the influxes of primitive Bc magma were probably sufficient to shift the magma composition at the bottom of the chamber into the primary phase volume of plagioclase, but insufficient to change the composition of the crystallizing plagioclase to higher An values, so that a normal trend of decreasing An values is observed from this level upward in the succession.

An upward decrease in Mg No. of the orthopyroxene in sub-unit 1 of the Intermediate unit is due to normal fractional crystallization from the Bc magma. The upward increase in Mg No. for sub-unit 2 of the Intermediate unit and the Merensky Footwall unit with height however, suggests a reversal of the normal differentiation trend (**Fig. 6.5**). This was also found to be the case for the Pseudoreef Marker at the Union section (De Klerk, 1982) and approximately 25 metres above the Boulder Bed at the Rustenburg section (Kruger, 1982; Kruger and Marsh, 1985; Naldrett **et al.**, 1986). An explanation for the reversals of the normal differentiation, could be the settling of more primitive orthopyroxene crystals from the Bh_{ac2} hybrid magma to the FW7 norite.

8.3.2 Merensky and Bastard units

Before establishing a hypothesis for the origin for the Merensky and Bastard units, several features concerning these unit must be emphasized:

1. the undulating Merensky Reef/ FW1 contact. The origin of this feature is, according to Leeb du Toit (1986), due to erosion and resorption of the floor.

2. the decrease in Sr content in plagioclase and the increase in initial Sr-isotope ratio upwards through the sequence (Kruger, 1982; Kruger and Marsh, 1982; Sharpe, 1985; Naldrett **et al.**, 1987).

3. the geochemical trends of the Merensky and Bastard units which cannot be explained by normal fractional crystallization.

4. the cyclic sequence of pyroxenite-leuconorite-mottled anorthosite for the Merensky and Bastard units.

Other constraints on a genetic model for the Merensky unit according to Naldrett **et al.** (1987) are:

1. the presence of thin chromitite layers or stringers at the base and top of the Merensky Reef.

2. the high proportion of sulphides of the Merensky Reef in comparison with the other units.

The origin of the Merensky unit is related to the emplacement of the main zone magma Bx (or B4) which has plagioclase on the liquidus, a low Sr content, a high initial Sr isotope ratio, a lower temperature (1260 °C) than the Ba magma, and a higher temperature and density than the Bc and hybrid Bh_{ac2} already contained in the chamber **(Fig. 8.3)** (Hatton, 1989). Thermal equilibration between the hot Bx magma and the floor will lead to thermal erosion and resorption of the FW1 norite, while in terms of the elevated, colder hybrid Bh_{ac2} and Bc magma layers, thermal equilibration will be rapid due to convection **(Fig. 8.7A)**. Sulphide separation and crystallization of orthopyroxene in the still elevated Ba magma layer will be enhanced by the cooling effect of the Bx magma, causing the bulk density of the crystal-rich portion of the Ba magma layer to increase and to slump (stage 5) to the floor of the chamber. It must be noted, that the cooling effects of earlier Bc emplacements on overlying Ba did not result in the Ba liquid attaining sulphur saturation. Limited mixing between the Bx magma and the Ba crystal-liquid could result in limited amount of chromite to crystallize. The chromite would settle out to form the thin chromitite stringer at the base of the Merensky pyroxenite, followed by the settling of orthopyroxene and sulphide droplets. Settling of orthopyroxene and sulphide droplets from the slumped Ba magma layer would cause the density of the slumped Ba magma to decrease. Consequently, the slumped Ba magma would rise and mix with the overlying Bx magma. This could result in further chromite crystallization to produce the chromitite layer on the top of the Merensky pyroxenite, and the formation of an overlying hybrid magma Bh_{ax1} **(Fig. 8.7B)**. From this hybrid magma orthopyroxene and plagioclase would crystallize to produce the M2 leuconorite, while, the M3 mottled anorthosite will be produced by the crystallization of plagioclase alone. **(Fig. 8.7C and D)**. Although the Merensky pegmatoid is not developed in the study area, it is considered to have formed subsequently in response to either postcumulus replacement (Irvine **et al.,** 1983) or recrystallization of the pyroxenite between the chromitite stringers in the presence of volatiles (Campbell **et al.,** 1983; Naldrett **et al.,** 1987).

According to Hatton (1989), plagioclase crystallizing from the Ba magma would have a lower An content than plagioclase crystallizing from a tholeiitic magma like Bx. This could produce the observed compositional trends in **Figure 6.1** where it is shown that the An content of plagioclase in the Merensky feldspathic pyroxenite is lower than the An content of the plagioclase of the leuconorite and mottled anorthosite.

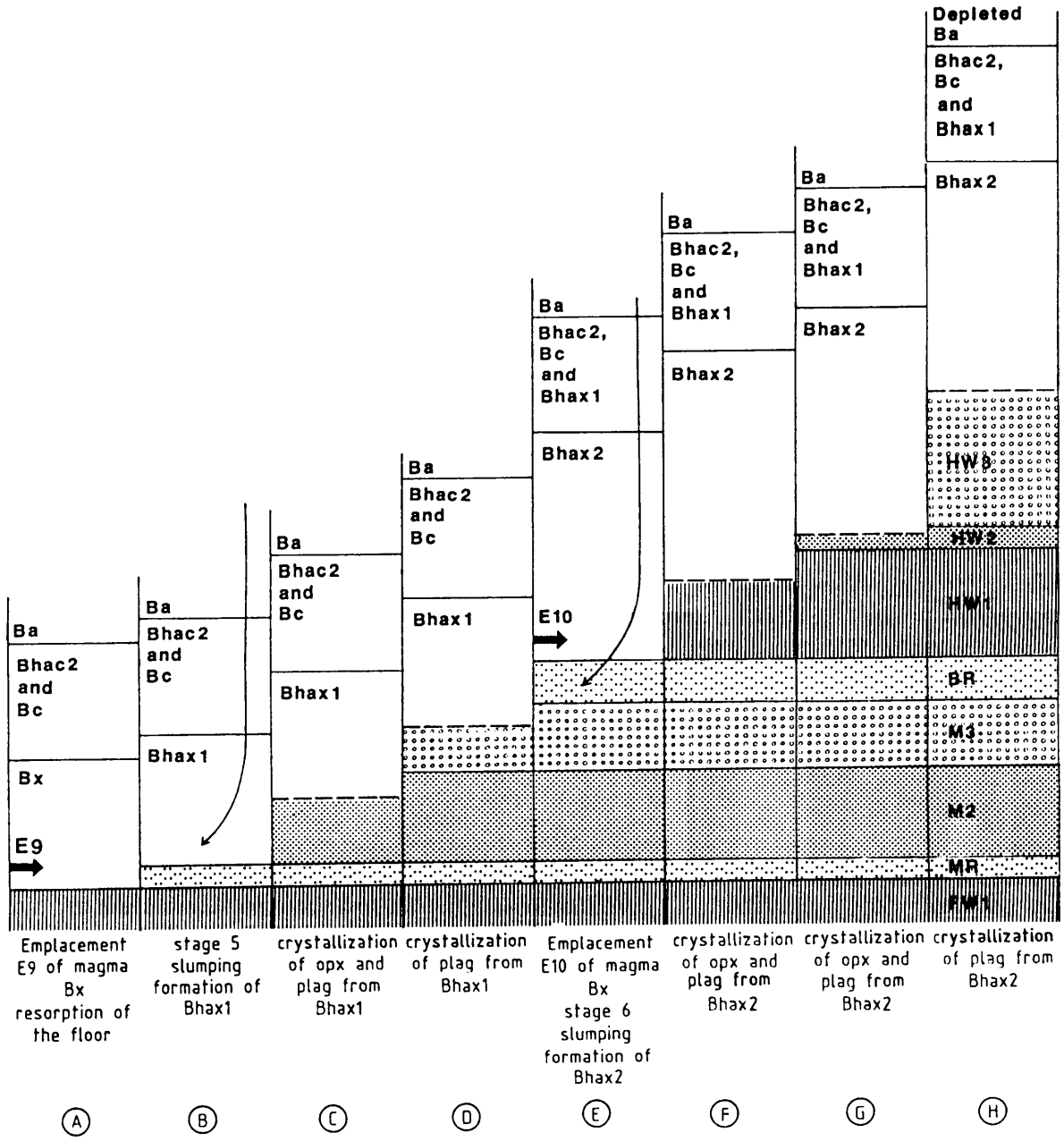

Figure 8.7 Schematic representation of the postulated sequence of events responsible for the formation of the Merensky and Bastard units.

The Bastard unit is produced by a further episode of slumping (stage 6) **(Fig. 8.7E)**, prior to the second emplacement of Bx magma along the chamber floor. Orthopyroxene settling from the slumped Ba magma layer could have produced the Bastard feldspathic pyroxenite, causing the density of the slumped Ba magma to decrease. Consequently, the slumped Ba magma would rise and mix with the overlying Bx magma, resulting in the formation of an overlying hybrid magma Bh_{ax2} **(Fig. 8.7E)**. Orthopyroxene and plagioclase would crystallize to produce the HW1 norite and HW2 leuconorite while, the overlying HW3 mottled anorthosite was produced by the crystallization of plagioclase alone **(Figs. 8.7F, 8.7G and 8.7H)**.

9. CONCLUSIONS

The investigation of the Boshoek section as a representative lithological section through the upper critical zone in the southwestern Bushveld Complex, has shed some light on the following:

The structure of the adjacent floor rocks west and southwest of the Impala lease area is dominated by two different stages of folding. The first stage of folding is confined to the Magaliesberg Quartzite Formation with fold-axes parallel to the Layered Suite/floor contact. The second stage of large-scale folding resulted in the undulating contact between the floor and the Rustenburg Layered Suite with fold-axes at approximately right angles to the stage 1 folding event. As a result of this second event, the lower zone in the south western Bushveld Complex is confined to a number of basins, separated from one another by anticlinal folds. This explains the lithologically different lower zone sequences in the Rustenburg and Marikana sections, and the subsequent transgression northwards towards the Boshoek section in response to the addition of fresh magma into the magma chamber. Variations in thickness of the different rock units are also evident in the upper critical zone of the Boshoek and Rustenburg sections and could be explained by the presence of the prominent Kookfontein upfold.

For purposes of this study the upper critical zone is divided into six units on the basis of lithological features and geochemical trends. They are the UG1, UG2, Intermediate, Merensky Footwall, Merensky and Bastard units. The Intermediate and Merensky Footwall units are further subdivided into sub-units on the basis of modal-mineral proportions and whole rock geochemical trends.

An attempt to reconstruct the crystallization history of the sequence under investigation is based on mineralogical and geochemical trends, together with the characteristics of the potential parental magmas to the lower and critical zones of the Bushveld Complex. The addition of pulses of B2/B3 magma into a magma chamber which contains B1-dominant magma is suggested. The B1-dominant magma has a higher liquidus temperature but lower density and consequently will be elevated, where it will cool and crystallize orthopyroxene. As a result of an increase in the bulk density, the orthopyroxene laden bottom portion of the B1 layer will slump and sink through the B2/B3 magma to the floor. This slumping mechanism is assumed to have produced the feldspathic pyroxenite layers of the UG1, UG2, Merensky, Bastard units and the Boulder Bed.

Periodic increases in the temperature of the B2/B3 magma and thus the return to plagioclase as the only mineral phase on the liquidus can be due to periodic, gentle influxes of primary B2/B3 magma and its gradual mixing with the hybridized magma (Bh_{aci}) at the base of the stratified liquid colunm. This could produce the sub-units which have been identified in the Intermediate (sub-units 1 and 2) and Merensky Footwall (sub-units 1, 2, 3 and 4) units.

The emplacement of the main zone magma B4 and slumping of an orthopyroxene-enriched B1 magma layer is also called for to produce the Merensky and Bastard units. The Merensky pyroxenite is formed by settling orthopyroxene and sulphides from the slumped B1 layer, while a hybrid layer Bh_{axi} is produced by the decrease in the bulk density of the slumped layer and its mixing with limited amounts of B4 magma. The more felsic layers (norite and leuconorite, mottled anorthosite) are produced by crystallization of first the

hybrid Bh_{axi} (B1 and B4) and subsequently the B4 magmas.

ACKNOWLEDGEMENTS

I wish to thank the following persons and institutions:

- CISR, as this project was financed from a grant by the national Geosciences Programme of the Foundation for Research Development.

- the Institute for Geological Research on the Bushveld Complex, for the support during this study. Special thanks to Professor G. Von Gruenewaldt for his patients, support and guidance, and to Dr. C. Hatton for his inspiration. The assistance of Drs. M. Sharpe and H. Horst of the XRF and microprobe laboratories are gratefully acknowledged.

- the management of General Mining, for affording me the opportunity of undertaking the project; the geologists and management of Wildebeestfontein South Mine (Impala Platinum Ltd) for their co-operation, interest and help.

- staff members of the Geological Survey of the Department of Mineral and Energy Affairs, for their continued interest and help. The assistance of Mr. J. Trojak while using the LECO CS244 infrared absorption spectrometer is gratefully acknowledged.

I wish to express my sincere appreciation to my wife and parents for their support and encouragement during this study.

REFERENCES

Barnard, K.J. and Hopkins, D.A.S. 1980. Review of geology and potential of Boshoek chrome belt, Western Transvaal, South Africa. Applied Earth Science, 84(B), pp 137-143.

Barton, J.D. and Calkin, F. 1978. Crystal chemistry of gallium. In: Wedepohl, K.H. (Ed.) Handbook of Geochemistry. Vol. II. Springer-Verlag Berlin, pp 31-A-1 - 31-A-2.

Bottinga, Y., Weill, D. and Richet, P. 1982. Density calculations for silicate liquids. I. Revised method for aluminosilicate compositions. Geochim. Cosmochim. Acta., 46, pp 909-919.

Buchanan, D.C., Nolan, J., Wilkinson, N., De Villiers, J.R.P. 1983. An experimental investigation of sulfur solubility as a function of temperature in synthetic silicate melts. Spec. Publ. Geol. Soc. S.Afr., pp 383-391.

Butcher, A.R. and Merkle, R.K.W. 1986. postcumulus modification of magnetite grains in the upper zone of the Bushveld Complex, South Africa. Lithos, 20, pp 247-260.

Cameron, E.N. 1964. Chromite deposits of the eastern part of the Bushveld Complex, In Houghton, S.H. (Ed.) The geology of some ore deposits in South Africa. Vol. II. Geol. Soc. S.Afr., pp 131-168.

Cameron, E.N. 1980. Evolution of the lower critical zone, central sector, eastern Bushveld Complex, and its chromite deposits. Econ. Geol., 75, pp 845-871.

Campbell, I.H., Roeder, P.L. and Dixon, J.M. 1978. Crystal buoyancy in basaltic liquids and other experiments with a centrifuge furnace. Contrib. Mineral. Petrol., 67, pp 369-377.

Campbell, I.H., Naldrett, A.J. and Barnes, S.J. 1983. A model of the origin of the platinum rich sulfide horizons in the Bushveld and Stillwater Complexes. Journal of Petrology, 24(2), pp 133-165.

Cawthorn, R.G. and Davies, G. 1983. Experimental data at 3 Kbars pressure on parental magma to the Bushveld Complex. Contrib. Mineral. Petrol., 83, pp 128-135.

Cocco, G., Fanfani, C. and Zanazzi, P.F. 1970. Crystal chemistry of potassium. In: Wedepohl, K.H. (Ed.) Handbook of Geochemistry. Vol. II. Springer-Verlag Berlin, pp 19-A-1 - 19-A-9.

Coertze, F.J. 1961. The Rustenburg fault as a controlling factor of ore - deposition southwest of Pilanesberg. Trans. Geol. Soc. S.Afr., 65, pp 253-262.

Coertze, F.J. 1974. The geology of the basic portion of the Western Bushveld igneous complex. Geol. Surv. S.Afr., Memoir 66, p 148.

Cousins, C.A. and Feringa, G. 1964. The chromite deposits of the Western Belt of the Bushveld Complex. In: Houghton, S.H. (Ed.) The geology of some ore deposits in South Africa. Vol. II. Geol. Soc. S.Afr., pp 183-202.

Cox, K.G., Bell, J.D. and Pankhurst, R.J. 1979. The interpretation of igneous rocks. George Allen and Unwin, London, p 450.

Davies, G., Cawthorn, R.G., Barton, J.M. and Morton, M. 1980. Parental magma to the Bushveld Complex. Nature, 287, pp 33-35.

Du Plessis, C.P. and Walraven, F. 1990. The tectonic setting of the Bushveld Complex in Southern Africa, Part 1. Structural deformation and distribution. Tectonophysics, 179, pp 305-319.

De Klerk, W.J. 1982. The geology, geochemistry and silicate mineralogy of the upper critical zone of the northwestern Bushveld Complex at Rustenburg Platinum mines, Union section. Unpubl. M.Sc thesis, Rhodes University, p 210.

Eales, H.V., Marsh, J.S., Mitchell, A.A., De Klerk, W.J., Kruger, F.J. and Field, M. 1986. Some geochemical constraints upon models for the crystallization of the upper critical zone - main zone interval, northwestern Bushveld Complex. Mineral Magazine, 50, pp 567-582.

Eales, H.V. and Reynolds, I. M. 1986. Cryptic variations within chromitites of the upper critical zone, northwestern Bushveld Complex. Econ. Geol., 81, pp 1056-1066.

Fourie, G.P. 1959. The chromite deposits in the Rustenburg area. Geol. Surv. S.Afr., Bull., 27, p 45.

Gain, S.B. 1985. Geologic setting of the platiniferous UG2 chromitite layer on the farm Maandagshoek, eastern Bushveld Complex. Econ. Geol., 80, pp 925-943.

Hall, A.L. 1932. The Bushveld Igneous Complex of the central Transvaal. Geol. Surv. S.Afr., Memoir, 28, p 560.

Harmer, R.E. and Sharpe, M.R. 1985. Field relations and strontium isotope systematics of the marginal rocks of the eastern Bushveld Complex. Econ. Geol., 80, pp 813-837.

Hatton, C.J. and Von Gruenewaldt, G. 1985. Chromite from the Swartkop chrome mine - an estimate of the effects of subsolidus re-equilibration. Econ. Geol., 80, pp 911-924.

Hatton, C.J. and Von Gruenewaldt, G. 1987. The geological setting and petrogenesis of the Bushveld chromitite layers. In: Stowe, C.W. (Ed). Evolution of Chromium ore fields. Van Nostrand Reinhold, New York, pp 109-143.

Hatton, C.J. 1987. Parental magmas of the Bushveld Complex and their PGE content. In: Platinum-group element deposits. Course notes, pp 4.1-4.12.

Hatton, C.J. 1989. Densities and liquidus temperatures of Bushveld parental magmas as constraints on the formation of the Merensky Reef. In: Prendergast, M.D. and Jones, M.J. (Eds). Magmatic sulfides - the Zimbabwe Volume. IMM, London, pp 87-93.

Hill, R. and Roeder, P. 1974. The crystallization of spinel from basaltic liquid as a function of oxygen fugacity. Journal of Geology, 82, pp 709-729.

Houghton. D.R., Roeder, P.L. and Skinner, B.J. 1974. Solubility of sulfur in mafic magmas. Econ. Geol., 69, pp 451-462.

Huppert, H.E. and Sparks, R.S.J. 1980. The fluid dynamics of a basaltic magma chamber replenished by influx of hot, dense ultrabasic magma. Contrib. Mineral. Petrol., 75, pp 279-289.

Huppert, H.E., Sparks, R.S.J. and Turner, J.S. 1984. Some effects of viscosity on the dynamics of replenished magma chambers. Journal of Geophysical Research., 89, pp 294-303.

Irvine, T.N. 1975. Crystallization sequences in the Muskox intrusion and other layered intrusions - II. Origin of chromitite layers and similar deposits of other magmatic ores. Geochim. Cosmochim. Acta., 39, pp 991-1020.

Irvine, T.N. 1980. Origin of chromitite layers in the Muskox intrusion and other stratiform intrusions: A new interpretation. Geology, 5, pp 273-277.

Irvine, T.N. and Sharpe, M.R. 1981. Source-rock compositions and depths of origin of Bushveld and Stillwater magmas. Carnegie Inst. Washington Yearbook, 81, pp 294-303.

Irvine, T.N. and Sharpe, M.R. 1986. Magma mixing and the origin of stratiform oxide ore zones in the Bushveld and Stillwater Complexes. In: Gallagher, M.J., Ixer, R.A., Neary, C.R. and Prichard, H.M. (Eds). Metallogeny of basic and ultrabasic rocks. Inst. Min. Met., London, pp 183-198.

Irvine, T.N., Keith, D.W. and Todd, S.G. 1983. The J-M platinum-palladium reef of the Stillwater Complex, Montana II. Origin by double-diffusive convective magma mixing and implications for the Bushveld Complex. Econ. Geol., 78, pp 1287-1334.

Jones, J.P. 1976. Pegmatoidal nodules in the layered rocks of the Bafokeng leasehold area. Trans. Geol. Soc. S.Afr., 79, pp 312-320.

Kruger, F.J. 1982. The petrology of the Merensky cyclic unit and associated rocks and their significance in the evolution of the Western Bushveld Complex. Unpubl. Ph.D. Thesis, Witwatersrand University.

Kruger, F.J. and Marsh, J.S. 1982. Significance of $^{87}Sr/^{86}Sr$ ratios in the Merensky cyclic unit of the Bushveld Complex. Nature, 298, pp 53-55.

Kruger, F.J. and Marsh, J.S. 1985. The mineralogy, petrology and origin of the Merensky cyclic unit in the western Bushveld complex. Econ. Geol., 80, pp 958-974.

Kruger, F.J., Cawthorn, R.G. and Walch, K.L. 1987. Strontium isotope evidence against magma addition in the upper zone of the Bushveld Complex. Earth Planet. Sci. Lett., 84, pp 51-58.

Lee, C.A. and Sharpe, M.R. 1979. Spheroidal pyroxenite aggregates in the Bushveld Complex - a special case of silicate liquid immisibility. Earth planet. Sci. Lett., 44, pp 295-310.

Lee, A.C. and Sharpe, M.R. 1980. The "Boulder Bed" and Merensky Reef - further examples of silicate liquid immiscibility and spherical aggrergation in the Bushveld Complex.
Earth Planet. Sci. Lett., 18, pp 141-147.

Leeb du Toit, A. 1986. The Impala Platinum Mines. In: Anhaeusser, C.R. and Maske, S. (Eds). Mineral deposits of Southern Africa. Geol. Soc. S.Afr., I, II, pp 1091-1106.

Martin, D. 1990. crytal settling and in situ crystallization in aqueous solutions and magma chambers. Earth Planet. Sci. Lett., 96, pp 336-348.

Meyer, G. 1969. Some petrological aspects of the mafic rocks from four borehole sections between the Merensky Reef and the main-zone gabbro in the western and eastern Bushveld Complex.Unpubl. M.Sc thesis, Univ. Potchefstroom for Christian Higher Education, p 91.

McLaren, C.H. and De Villiers, J.P.R. 1982. The platinum-group chemistry and mineralogy of the UG2 chromitite layer of the Bushveld Complex. Econ. Geol., 77, pp 1348-1366.

Mostert, A.B., Hofmeyr, P.K. and Potgieter, G.A. 1982. The platinum-group mineralogy of the Merensky Reef at the Impala Platinum Mines, Bophuthatswana. Econ. Geol., 77, pp 1385-1394.

Naldrett, A.J., Gasparrini, E.C., Barnes, S.J., Von Gruenewaldt, G. and Sharpe, M.R. 1986. The upper critical zone of the Bushveld Complex and the origin of Merensky-type ores. Econ. Geol., 81, pp 1105-1117.

Naldrett, A.J., Cameron, G., Von Gruenewaldt, G. and Sharpe, M.R. 1987. The formation of stratiform platinum-group element deposits in layered intrusions. In: Parsons, I. (Ed). Origin of Igneous Layering, Nato AS1 series. D. Reidel Publishing Co., Dordrecht.

Naldrett, A.J. and Von Gruenewaldt, G. 1989. The association of PGE with chromitite in layered intrusions and ophiolite complexes. Econ. Geol., 84, p 180.

Roeder, P.L. and Campbell, I.H. 1985. The effect of postcumulus reactions on composition of chrome-spinels from the Jimberlana intrusion. Journal of Petrology, 36, pp 763-786.

Shand, S.J. 1943. Eruptive rocks. Murby and Co., London. p 488.

Sharpe, M.R. and Snyman, J.A. 1978. A model for the emplacement of the eastern compartment of the Bushveld Complex. Tectonophysics, 65, pp 85-110.

Sharpe, M.R. 1981. The chronology of magma influxes to the eastern compartment of the Bushveld Complex as exemplified by its marginal border groups. Journal Geol. Soc. London, 138, pp 307-326.

Sharpe, M.R. and Chadwick, B. 1982. The geometry and origin of structures in certain Transvaal sequence rocks within and adjacent to the eastern compartment of the Bushveld Complex. Trans. Geol. Soc. S.Afr. 85, pp 29-41.

Sharpe, M.R. and Irvine, T.N. 1983. Melting relations of two Bushveld chilled margin rocks and implications for the origin of chromite. Carnegie Inst. Washington, Ybk., 82, pp 295-300.

Sharpe, M.R., Irvine, T.N., Mysen, B.O. and Hazen, R.M. 1983. Density and viscosity characteristics of melts of Bushveld chilled margin rocks. Carnegie Inst. Washington, Yearbook, 82, pp 300-305.

Sharpe, M.R. 1984. Petrography, classification and chronology of mafic sill intrusions beneath the eastern Bushveld Complex. Geol. Surv. S.Afr., Bull. 77.

Sharpe, M.R. 1985. Strontium isotope evidence for preserved density stratification in the main zone of the Bushveld Complex, South Africa. Nature, 316, pp 119-126.

Sharpe, M.R. and Hulbert, L.J. 1985. Ultramafic sills beneath the eastern Bushveld Complex: mobilized suspensions of early lower zone cumulates in a parental magma with boninitic affinities. Econ. Geol., 80, pp 849-871.

South African Committee for Stratigraphic (SACS). 1980. Stratigraphy of South Africa. Part 1 (Comp. L.E.Kent). Lithostratigraphy of the Republic of South Africa, South West Africa/Namibia and the Republics of Bophuthatswana, Transkei and Venda. Handb. Geol. Surv. S.Afr., 8.

Sparks, R.S.J. and Huppert, H.E. 1984. Density changes during the fractional crystallization of basaltic magmas: fluid dynamic implications. Contrib. Mineral. Petrol., 85, pp 300-309.

Sparks, R.S.J., Huppert, H.E. and Turner, J.S. 1984. The fluid dynamics of evolving magma chambers. Trans. R. Soc. London, A310, pp 511-534.

Streckeisen, A. 1976. To each plutonic rock its proper name. Earth. Sci. Reviews, 12, pp 1-33.

Truter, F.C. 1955. Modern concepts of the Bushveld Igneous Complex. Southern Reg. Com. Geol. Salisbury, Pamphlet 850, pp 77-91.

Van Zyl, J.P. 1960. Die petrologie van die Merenskyrif en geassosieerde gesteentes in 'n aantal boorgate en mynprofiel op Swartklip 988, Rustenburg. Unpubl. M.Sc thesis, Univ. Potchefstroom for Christian Higher Education.

Van Zyl, J.P. 1970. The petrology of the Merensky Reef and the associated rocks on Swartklip 988, Rustenburg district. In: Visser, D.J.L. and Von Gruenewaldt, G. (Eds). Symposium on the Bushveld Igneous Complex and other layered intrusions., Geol. Soc. S.Afr., Spec. Pub., 1, pp 242-265.

Vermaak, C.F. 1976. The Merensky reef - thoughts on its environment and genesis.
Econ. Geol., 71, pp 1270-1295.

Vermaak, C.F. and Von Gruenewaldt, G. 1981. Third International Platinum Symposium. Pretoria.

Viljoen, M.J., De Klerk, W.J., Coetzer, P.M., Hatch, N.P., Kinloch, E. and Peyerl, W. 1986a. The Union section of Rustenburg platinum mines limited, with reference to the Merensky reef. In: Anhaeusser, C.R. and Maske, S. (Eds). Mineral deposits of Southern Africa., Geol. Soc. S.Afr., I, II, pp 1061-1090.

Viljoen, M.J. and Hieber, R. 1986b. The Rustenburg section of Rustenburg platinum mines limited, with reference to the Merensky reef. In: Anhaeusser, C.R. and Maske, S. (Eds). Mineral deposits of Southern Africa., Geol. Soc. S.Afr., I, II, pp 1107-1134.

Von Gruenewaldt, G. 1979. A review of some recent concepts of the Bushveld complex, with particular reference to sulfide mineralization. Canadian Mineralogist, 17, pp 233-256.

Von Gruenewaldt, G., Hatton, C.J., Merkle, R.K.W. and Gain, S.B. 1986. Platinum-group element - chromitite associations in the Bushveld complex. Econ. Geol., 81, pp 1067-1079.

APPENDIX 1

Whole rock analyses

Rock-type codes for all the rocks analysed

ma	-	mottled anorthosite
ln	-	leuconorite
n	-	norite
fpx	-	feldspathic pyroxenite
peg	-	pegmatoid
chr	-	chromite

Sample: IWS	1	2	3	4	5	6	7	8	9	10	11	12	13	14	15	16	17
Height*:	-26.0	-27.8	-29.5	-31.1	-32.4	-34.1	-35.7	-37.4	-39.1	-40.8	-42.4	-44.1	-45.7	-47.4	-49.2	-50.7	-52.4
Rock type:	ma	ma	n	n	n	n	n	n	n	n	n	n	n	n	n	n	n
SiO2	49.46	49.48	49.91	48.89	49.24	48.29	48.86	48.82	47.97	47.28	46.33	46.11	46.08	48.12	47.31	47.65	47.23
TiO2	0.07	0.06	0.07	0.07	0.07	0.06	0.07	0.07	0.06	0.05	0.05	0.05	0.06	0.06	0.06	0.07	0.05
Al2O3	26.11	31.22	25.37	23.76	22.38	23.98	22.99	23.14	23.18	25.99	23.27	22.35	22.35	23.91	20.92	19.53	24.27
FeO	4.17	2.45	4.12	4.36	4.33	4.41	4.57	4.63	4.63	3.94	5.24	5.11	5.12	4.28	4.93	4.74	5.06
MnO	0.10	0.04	0.10	0.10	0.09	0.10	0.11	0.10	0.11	0.09	0.11	0.11	0.11	0.10	0.10	0.09	0.11
MgO	9.90	4.00	10.41	10.92	12.20	10.39	11.81	11.54	10.86	9.92	13.60	13.18	13.28	11.23	14.76	14.84	11.72
CaO	12.25	13.44	11.23	10.80	10.71	10.75	10.63	10.41	10.57	11.36	10.61	10.43	10.51	10.84	10.12	9.98	10.59
Na2O	1.63	1.97	1.58	1.58	1.54	1.78	1.58	1.59	1.48	1.70	1.38	1.56	1.48	1.49	1.50	1.76	1.52
K2O	0.21	0.20	0.17	0.14	0.13	0.14	0.13	0.15	0.13	0.16	0.15	0.17	0.17	0.16	0.16	0.16	0.15
P2O5	0.00	0.00	0.00	0.00	0.01	0.00	0.00	0.00	0.00	0.00	0.00	0.00	0.00	0.01	0.00	0.00	0.01
TOTAL	103.90	102.86	102.96	100.62	100.70	99.90	100.75	100.45	98.98	100.49	100.74	99.07	99.16	100.19	99.86	98.82	100.71
Zn	34	17	34	33	32	34	37	38	34	32	41	44	45	33	36	31	40
Cu	11	13	10	10	10	10	8	10	12	10	11	13	12	12	13	7	18
Ni	184	38	204	210	215	214	243	242	231	284	498	405	404	260	379	317	375
Co	27	8	24	27	29	27	33	30	28	30	40	37	41	30	35	34	36
Ga	16	19	14	13	11	14	14	10	12	14	14	17	13	16	13	15	15
Nb	0	0	0	0	0	0	0	0	0	0	0	0	0	0	0	0	0
Zr	18	24	21	18	21	17	19	19	16	20	19	20	19	18	18	18	18
Y	0	3	0	0	0	0	0	0	0	0	0	3	0	0	0	0	0
Sr	315	422	303	297	288	303	296	292	297	341	320	315	318	323	281	300	307
Rb	4	3	4	0	0	0	0	3	0	4	3	4	0	3	3	4	5
U	0	0	0	0	0	0	0	0	0	0	0	0	0	0	0	0	0
Th	0	0	0	0	0	0	0	0	0	0	0	0	0	0	0	0	0
Pb	0	0	0	0	0	0	0	0	0	0	0	0	0	0	0	0	3
Cr	953	172	988	1023	1013	1074	1110	1088	1103	938	997	773	755	1026	893	980	826
V	80	28	70	19	56	74	25	69	90	24	75	45	61	72	27	44	64
Ba	47	48	20	61	48	50	43	16	36	66	28	64	36	33	29	21	36
Sc	13	12	31	17	10	27	12	0	20	26	0	0	0	54	19	0	11
S	80	50	10	120	160	120	80	80	240	200	170	250	0	110	120	240	210

Sample: IWS	18	19	20	21	22	23	24	25	26	27	28	29	30	31	32	33
Height*:	-54.1	-55.8	-57.4	-59.1	-60.8	-62.6	-64.2	-65.9	-67.6	-69.3	-71.0	-72.7	-74.4	-76.2	-77.8	-79.5
Rock type:	n	n	n	n	n	n	ln	ln	ln	ma	ln	ln	ln	ln	ln	ln
SiO2	47.38	47.45	48.04	47.85	47.69	48.37	47.31	47.34	47.42	48.06	47.68	46.38	47.64	48.25	48.04	48.28
TiO2	0.06	0.05	0.08	0.06	0.08	0.07	0.03	0.03	0.04	0.07	0.07	0.06	0.06	0.05	0.05	0.04
Al2O3	23.21	25.79	21.54	24.08	22.00	22.45	33.66	32.27	32.74	32.41	27.19	27.81	30.30	31.32	31.55	31.64
FeO	4.95	4.32	5.38	4.86	5.54	5.07	1.11	1.34	1.61	1.70	3.31	2.93	2.25	2.29	2.10	2.02
MnO	0.11	0.09	0.12	0.11	0.12	0.11	0.01	0.02	0.03	0.03	0.07	0.06	0.04	0.05	0.04	0.04
MgO	11.49	9.82	13.04	10.86	13.19	11.36	1.48	3.05	2.07	1.35	6.77	4.66	3.99	3.63	3.44	3.51
CaO	10.52	11.12	9.96	10.60	9.87	10.16	13.68	13.29	13.31	13.50	11.96	12.26	12.80	13.01	12.94	12.98
Na2O	1.54	1.75	1.52	1.55	1.40	1.48	2.21	2.14	2.03	2.09	1.79	1.84	1.93	1.92	1.98	2.04
K2O	0.20	0.16	0.16	0.18	0.17	0.19	0.16	0.16	0.19	0.37	0.22	0.23	0.22	0.19	0.20	0.16
P2O5	0.01	0.00	0.00	0.01	0.01	0.00	0.01	0.00	0.00	0.01	0.01	0.01	0.01	0.01	0.01	0.00
TOTAL	99.47	100.55	99.84	100.16	100.07	99.26	99.66	99.64	99.44	99.59	99.07	96.24	99.24	100.72	100.35	100.71
Zn	37	33	41	35	41	39	9	14	14	18	24	23	18	24	19	15
Cu	12	14	12	12	13	32	43	34	22	23	59	54	47	34	35	31
Ni	300	274	311	300	395	245	79	93	41	30	215	151	120	99	98	93
Co	33	29	38	36	43	30	5	8	7	6	22	17	11	12	12	14
Ga	15	18	13	15	13	14	16	16	19	19	17	17	17	18	19	16
Nb	0	0	0	0	0	0	0	0	0	0	0	0	0	0	0	0
Zr	17	21	19	18	17	17	18	25	22	27	21	23	23	22	24	22
Y	4	3	0	0	3	4	0	0	0	0	0	3	0	0	0	5
Sr	305	332	271	298	272	284	445	444	436	433	361	397	401	398	401	410
Rb	0	0	5	0	0	6	0	0	3	6	5	6	3	5	4	0
U	0	0	0	0	0	0	0	0	0	0	0	0	5	0	0	0
Th	0	0	0	0	0	0	0	0	0	0	0	0	0	0	0	0
Pb	0	0	0	0	0	0	0	0	0	0	0	0	0	0	0	0
Cr	896	740	1108	949	1136	1245	492	601	640	89	765	658	722	659	675	567
V	40	51	80	58	99	57	52	0	0	30	45	39	0	77	16	17
Ba	57	53	48	30	41	48	42	41	57	94	44	60	93	44	58	81
Sc	19	22	32	17	0	10	13	0	19	55	0	25	24	0	9	10
S	150	190	110	100	190	260	180	310	210	380	390	320	300	310	170	210

Sample: IWS	34	35	36	37	38	39	40	41	42	43	44	45	46	47	48	49	50
Height*:	-81.2	-82.9	-84.6	-86.3	-87.7	-89.4	-91.3	-93.0	-94.6	-96.4	-98.1	-99.7	-101.5	-103.4	-105.0	-106.7	-108.5
Rock type:	ln	ln	ln	ln	ln	ln	ma	ma	ma	ma	ma	ma	ma	fpx	fpx	fpx	fpx
SiO2	48.01	47.61	47.90	47.89	47.85	47.81	47.34	47.57	47.71	48.27	48.03	47.98	47.82	51.03	51.11	50.52	48.09
TiO2	0.05	0.04	0.05	0.05	0.05	0.05	0.03	0.01	0.04	0.05	0.02	0.04	0.08	0.24	0.28	0.25	0.25
Al2O3	31.47	31.23	30.25	29.70	29.55	29.52	32.76	34.24	31.67	31.18	33.00	31.53	31.07	5.33	4.58	5.95	10.77
FeO	2.12	1.96	2.14	2.49	2.31	2.63	1.67	1.00	1.63	1.90	1.35	1.69	1.89	12.85	12.61	12.70	10.63
MnO	0.04	0.04	0.04	0.05	0.05	0.06	0.03	0.01	0.02	0.03	0.03	0.03	0.03	0.23	0.21	0.22	0.22
MgO	3.32	3.06	4.13	4.81	5.41	4.89	2.63	0.90	2.47	2.66	1.55	2.38	1.90	22.75	23.13	22.18	18.88
CaO	12.88	13.01	12.80	12.44	12.71	12.59	13.29	13.73	13.26	13.07	13.40	13.26	12.90	4.64	4.70	4.37	5.17
Na2O	2.02	1.95	1.92	1.81	1.85	1.83	1.95	2.09	2.09	2.08	2.16	2.09	2.27	0.69	0.48	0.71	1.01
K2O	0.20	0.30	0.24	0.43	0.18	0.18	0.15	0.13	0.18	0.24	0.18	0.19	0.25	0.10	0.16	0.24	0.33
P2O5	0.00	0.01	0.00	0.01	0.00	0.01	0.00	0.01	0.01	0.00	0.01	0.01	0.01	0.22	0.04	0.04	0.04
TOTAL	100.11	99.21	99.47	99.68	99.96	99.57	99.85	99.69	99.08	99.48	99.73	99.20	98.22	98.08	97.30	97.18	95.39
Zn	18	16	19	20	17	18	12	9	17	14	12	14	17	89	80	86	110
Cu	39	40	34	29	23	21	18	18	113	23	11	15	13	24	30	73	26
Ni	93	98	108	119	120	123	84	23	184	43	29	38	36	541	560	714	565
Co	12	10	12	14	10	16	9	6	6	7	8	7	9	88	83	92	84
Ga	19	17	17	21	15	17	19	18	20	20	14	15	19	6	4	6	11
Nb	0	0	0	0	0	0	0	0	0	0	0	0	0	0	0	0	0
Zr	21	22	22	23	20	23	20	21	25	25	20	24	26	17	17	22	18
Y	0	0	0	0	3	0	0	0	3	0	0	0	3	9	9	6	9
Sr	416	413	411	388	393	385	430	444	438	433	450	447	426	88	70	90	118
Rb	4	4	7	6	3	4	3	0	4	4	3	0	3	0	0	6	4
U	0	0	0	0	0	0	0	0	0	0	0	0	0	0	0	3	0
Th	0	0	0	0	0	0	0	0	0	0	0	0	0	0	0	0	0
Pb	0	0	0	0	0	0	0	0	0	0	0	0	0	3	3	4	0
Cr	295	337	453	642	693	583	347	82	168	175	102	141	389	2694	2949	3585	23787
V	36	64	0	0	40	39	13	0	9	54	48	6	30	172	150	209	305
Ba	69	58	74	53	74	62	64	70	53	88	66	73	61	46	84	135	116
Sc	20	0	20	12	25	11	20	0	0	22	15	0	0	31	36	32	22
S	260	290	90	140	110	110	80	90	115	100	50	85	70	310	270	350	290

Sample: IWS	51	51A	52	53	54	55	56	57	58	59	60	61	62	63	64	65
Height*:	-110.1	-111.8	-112.7	-114.3	-116.0	-117.2	-119.0	-120.5	-122.1	-123.4	-125.4	-127.1	-128.9	-130.6	-132.3	-134.0
Rock type:	fpx	peg	fpx	fpx	fpx	ln	ln	ln	ln	ln	ln	ln	fpx	fpx	fpx	fpx
SiO2	51.32	52.50	51.71	51.44	50.49	49.29	49.19	47.89	48.68	48.74	48.48	48.40	51.46	51.79	52.34	52.22
TiO2	0.22	0.33	0.19	0.19	0.13	0.06	0.04	0.05	0.03	0.03	0.03	0.02	0.24	0.26	0.27	0.28
Al2O3	6.58	6.94	9.85	8.42	14.95	27.22	29.30	22.37	29.12	29.32	29.65	31.81	5.03	6.25	6.14	6.89
FeO	12.83	12.15	11.38	11.7	8.77	3.78	3.00	3.61	2.89	2.76	2.69	1.75	12.75	13.26	13.17	12.93
MnO	0.23	0.21	0.21	0.21	0.18	0.09	0.07	0.08	0.07	0.06	0.06	0.04	0.22	0.23	0.23	0.22
MgO	22.18	21.10	20.16	20.34	16.56	7.21	5.69	13.14	5.53	5.12	4.71	2.72	23.05	21.11	21.28	20.45
CaO	4.54	4.80	5.34	5.36	7.32	11.96	12.45	10.60	12.30	12.48	12.55	13.28	4.34	4.24	4.25	4.48
Na2O	0.74	0.80	0.94	0.89	1.23	1.72	1.77	1.42	1.82	1.82	1.98	2.02	0.56	0.81	0.78	0.86
K2O	0.20	0.57	0.31	0.26	0.20	0.18	0.14	0.14	0.15	0.14	0.15	0.17	0.18	0.31	0.35	0.41
P2O5	0.00	0.01	0.00	0.01	0.01	0.00	0.01	0.01	0.01	0.00	0.01	0.01	0.00	0.14	0.01	0.11
TOTAL	93.84	99.41	99.09	98.83	99.84	101.51	101.66	99.31	101.23	100.47	100.31	100.22	97.83	98.40	98.82	98.85
Zn	82	80	76	80	57	30	24	21	22	22	19	16	83	86	84	85
Cu	36	24	30	21	13	11	11	9	11	9	11	9	8	20	21	27
Ni	636	659	543	563	416	163	127	145	118	109	101	49	517	541	558	518
Co	85	82	75	70	58	26	19	20	17	17	13	8	83	88	89	92
Ga	6	8	6	8	11	17	18	16	15	18	15	17	7	10	8	7
Nb	0	0	0	0	0	0	0	0	0	0	0	0	0	0	0	0
Zr	15	56	26	15	18	20	19	15	17	18	19	17	20	25	26	33
Y	8	9	6	4	0	0	0	0	0	0	0	0	7	9	7	12
Sr	65	85	95	91	168	343	368	309	374	380	385	419	78	67	64	76
Rb	3	12	4	6	5	0	4	4	0	0	3	0	3	9	9	10
U	0	3	0	0	0	0	0	0	0	0	0	0	0	0	0	4
Th	0	0	0	0	0	0	0	0	0	0	0	0	0	0	0	0
Pb	0	0	0	0	0	0	0	0	0	0	0	3	0	0	0	4
Cr	2463	4843	2485	2214	1812	1152	621	710	567	535	520	436	2596	2466	2551	2569
V	173	119	125	140	154	55	59	91	54	80	26	31	116	164	155	143
Ba	64	131	95	84	76	48	50	0	39	52	42	42	78	98	108	134
Sc	27	33	39	17	0	37	0	20	0	0	27	0	41	28	35	29
S	200	160	250	160	30	50	40	40	30	40	40	30	190	70	80	40

Sample: IWS	66	67	68	70	71	72b	72m	73	74	75	76	77	78	79	80	81	85
Height*:	-135.7	-137.3	-138.9	-3.8	0.0	-7.5	-6.9	-24.6	-22.5	-20.8	-19.2	-17.5	-15.9	-14.2	-12.5	-10.8	1.7
Rock type:	fpx	chr	ma	n	fpx	ln	ma	ln	n	n	n	ln	ln	ln	ln	ln	ln
Si02	52.42	23.16	48.39	48.62	49.55	48.27	47.91	48.24	48.51	48.03	48.16	46.49	48.08	47.82	48.38	48.58	48.12
Ti02	0.34	1.23	0.05	0.07	0.30	0.02	0.02	0.03	0.07	0.07	0.06	0.10	0.06	0.06	0.07	0.12	0.06
Al203	6.09	11.61	31.63	25.42	6.78	33.46	32.17	33.11	29.56	27.42	26.97	22.66	28.64	26.42	24.77	16.66	29.40
Fe0	13.04	20.34	1.33	3.78	12.42	0.95	1.38	1.20	2.51	3.49	2.85	4.25	3.38	3.16	3.90	5.93	2.81
Mn0	0.22	0.48	0.02	0.09	0.21	0.01	0.02	0.02	0.05	0.07	0.06	0.08	0.07	0.07	0.09	0.13	0.06
Mg0	20.66	8.13	1.29	8.33	20.75	0.88	1.91	1.99	4.39	5.67	7.66	12.17	5.60	7.03	9.05	15.45	3.81
Ca0	4.02	1.38	13.33	11.45	4.71	13.78	13.25	12.34	12.79	12.12	11.59	9.52	12.66	11.70	11.31	8.90	12.57
Na20	0.77	0.34	2.40	1.67	0.66	2.33	2.27	2.43	2.08	1.87	2.11	1.32	1.85	1.94	1.68	1.15	2.02
K20	0.57	0.04	0.50	0.19	0.31	0.16	0.14	0.93	0.15	0.11	0.15	0.06	0.11	0.10	0.10	0.05	0.17
P205	0.02	0.01	0.01	0.00	0.02	0.00	0.00	0.00	0.01	0.01	0.00	0.00	0.01	0.00	0.01	0.01	0.00
TOTAL	98.15		98.95	99.62	95.71	99.86	99.07	100.29	100.12	98.86	99.61	96.65	100.46	98.30	99.36	96.98	99.02
Zn	94	741	12	28	80	8	12	10	21	28	21	28	26	24	31	41	23
Cu	24	36	11	63	374	8	14	7	18	15	8	16	18	22	16	16	70
Ni	568	1099	9	189	898	15	32	12	91	131	67	174	156	126	166	247	157
C0	85	252	4	22	85	3	8	5	14	21	14	22	19	15	23	30	12
Ga	7	60	20	13	5	18	19	19	17	19	18	16	20	16	16	14	16
Nb	0	0	0	0	0	0	0	0	0	0	0	0	0	0	0	0	0
Zr	43	6	28	19	35	20	18	23	27	23	24	21	21	21	21	21	18
Y	8	0	0	0	8	3	0	0	3	5	0	3	0	0	0	3	3
Sr	52	33	495	317	69	456	436	508	421	347	409	338	409	384	347	287	357
Rb	18	3	6	5	6	3	3	19	0	4	0	0	0	0	0	0	0
U	0	0	0	3	0	0	0	0	0	0	0	0	0	0	3	0	0
Th	3	0	0	0	0	0	0	0	0	0	0	0	0	0	0	0	0
Pb	3	0	0	0	3	0	0	0	0	0	0	0	0	0	0	0	0
Cr	6455	21103	254	804	2355	60	127	116	379	501	378	710	444	620	634	1253	350
V	239	2385	54	79	151	16	76	37	59	32	34	5	73	0	85	94	80
Ba	142	53	76	65	87	39	40	113	59	58	60	64	80	44	19	47	48
Sc	13	0	0	17	49	21	9	12	11	0	0	0	14	0	40	55	13
S	110	30	210	170	12440	70	30	60	160	140	70	170	200	130	170	110	440

Sample: IWS	86	87	88	89	90	91	92	93	94	95	96	97	98	99	100	101
Height*:	3.4	5.1	7.1	9.1	11.3	13.0	14.7	16.4	18.0	19.7	21.4	23.1	24.8	26.5	28.1	30.0
Rock type:	ln	ln	ma	ma	fpx	n	n	n	n	ln	ma	ma	ma	ma	ma	ma
SiO2	48.08	48.02	47.78	45.95	50.42	49.05	49.10	48.11	46.76	48.57	48.32	47.97	48.54	46.32	50.02	50.28
TiO2	0.05	0.05	0.03	0.03	0.25	0.08	0.09	0.06	0.08	0.07	0.09	0.06	0.06	0.03	0.04	0.06
Al203	29.96	29.69	31.89	28.37	7.20	19.80	20.12	25.29	19.09	26.78	31.04	28.11	29.16	27.00	28.73	27.14
FeO	2.53	2.69	1.45	2.82	11.74	6.42	6.15	4.34	5.13	4.17	1.69	3.32	2.54	2.17	1.67	2.12
MnO	0.05	0.06	0.02	0.04	0.21	0.15	0.14	0.10	0.13	0.09	0.03	0.07	0.05	0.05	0.03	0.04
MgO	3.64	3.34	1.48	3.80	21.49	13.23	12.91	8.60	15.02	6.26	1.82	3.22	3.40	3.02	4.01	6.77
CaO	12.67	12.84	13.46	12.45	4.33	9.09	9.55	11.18	10.45	12.15	13.44	12.51	12.59	14.24	14.73	12.08
Na20	2.05	2.00	2.07	1.80	0.78	1.35	1.33	1.59	1.11	1.69	2.00	2.05	2.25	1.71	2.42	2.41
K20	0.17	0.16	0.18	0.19	0.22	0.10	0.15	0.14	0.10	0.18	0.34	0.27	0.20	0.37	0.32	0.31
P205	0.00	0.00	0.01	0.00	0.00	0.00	0.01	0.01	0.00	0.01	0.02	0.01	0.01	0.00	0.00	0.00
TOTAL	99.20	98.85	98.37	95.46	96.64	99.27	99.55	99.42	97.87	99.97	98.79	97.59	98.80	94.91	101.97	101.21
Zn	20	21	11	18	82	48	45	32	41	34	19	27	21	13	13	21
Cu	66	56	37	784	313	32	20	22	21	30	35	38	8	7	10	13
Ni	152	121	66	1313	1032	318	293	195	183	135	51	101	47	29	42	47
CO	13	11	8	26	122	42	40	25	29	23	6	15	12	6	7	10
Ga	18	16	20	19	8	9	8	13	14	16	20	18	20	18	16	16
Nb	0	0	0	0	4	0	0	0	0	0	0	0	0	0	0	0
Zr	20	20	21	17	26	13	17	15	16	20	32	22	21	17	18	20
Y	0	4	0	0	4	0	4	0	3	0	5	3	3	0	3	0
Sr	374	352	385	416	73	185	196	260	229	290	362	321	342	384	364	384
Rb	3	0	3	4	6	0	0	0	0	3	6	4	3	7	4	4
U	0	0	0	0	0	0	0	0	0	0	0	0	0	0	0	0
Th	0	0	0	0	0	0	0	0	0	0	0	0	0	0	0	0
Pb	0	0	0	4	0	0	0	0	0	3	0	0	0	0	0	40
Cr	341	326	83	135	2013	1437	1384	879	799	628	149	206	139	101	115	120
V	31	16	56	33	147	109	110	89	136	101	41	63	17	52	95	26
Ba	56	72	69	63	31	46	51	64	24	51	78	59	49	79	70	61
Sc	0	30	16	0	15	13	15	15	14	27	0	0	8	0	0	0
S	500	410	330	290	4640	1990	120	170	130	140	170	240	240	690	220	60

APPENDIX 2

Microprobe analyses for plagioclase, orthopyroxene, chromite and olivine.

MICROPROBE DATA FOR PLAGIOCLASE

*Height below or above the Merensky Reef

(pos 1) cores
(pos 2) rims
(pos 3) intercumulus phase

Sample: IWS 100
Height*: 28.1

Number	Na_2O	SiO_2	CaO	FeO	Al_2O_3	MgO	K_2O	Pos	Total	An
1	3.11	49.57	15.63	0.36	31.06	0.01	0.12	1	99.86	73
2	2.93	49.73	16.16	0.37	31.21	0.01	0.15	2	100.53	74
3	3.04	49.72	16.06	0.35	30.82	0.01	0.19	1	100.17	73
4	2.83	48.43	16.72	0.38	31.10	0.01	0.13	2	99.60	76
5	3.38	49.55	15.40	0.31	30.24	0.05	0.12	2	99.05	71
6	2.79	49.56	16.45	0.34	31.53	0.01	0.15	1	100.83	76
7	3.00	49.30	16.13	0.28	30.97	0.01	0.19	2	99.88	74
8	2.83	49.32	16.24	0.34	31.16	0.01	0.15	1	100.05	75
9	2.79	48.64	16.57	0.37	30.90	0.01	0.14	2	99.42	76

Sample: IWS 97
Height*: 23.1

Number	Na_2O	SiO_2	CaO	FeO	Al_2O_3	MgO	K_2O	Pos	Total	An
1	2.62	49.22	15.09	0.80	31.17	0.00	0.15	1	99.05	75
2	2.99	50.00	14.99	0.34	31.62	0.00	0.17	2	100.11	72
3	2.70	49.05	15.31	0.40	31.76	0.00	0.14	1	99.36	75
4	3.56	51.48	13.90	0.41	30.68	0.00	0.20	2	100.23	67
5	2.97	50.23	14.31	0.29	31.59	0.00	0.14	1	99.53	72
6	2.89	49.78	14.09	0.30	32.00	0.00	0.13	2	99.19	72
7	2.86	49.90	14.88	0.35	31.77	0.00	0.14	1	99.90	74
8	2.51	48.93	14.83	0.31	32.36	0.00	0.09	2	99.03	76
9	2.93	50.12	14.06	0.38	31.65	0.00	0.14	1	99.28	72
10	3.09	50.36	13.87	0.30	31.63	0.00	0.17	2	99.42	71
11	2.69	48.97	14.76	0.40	31.93	0.00	0.11	1	98.86	75
12	2.89	49.71	14.55	0.34	32.08	0.00	0.11	2	99.68	73
13	3.05	50.05	13.96	0.38	31.20	0.00	0.17	1	98.81	71
14	2.46	47.78	15.95	0.34	32.31	0.00	0.12	2	98.96	77
15	3.15	50.63	14.35	0.33	31.70	0.00	0.19	1	100.35	70

Sample: IWS 94
Height*: 18.0

Number	Na_2O	SiO_2	CaO	FeO	Al_2O_3	MgO	K_2O	Pos	Total	An
1	2.42	49.54	15.83	0.29	31.77	0.01	0.15	1	100.01	77
2	2.43	49.70	15.82	0.34	32.40	0.00	0.13	2	100.82	77
3	2.38	49.28	15.76	0.29	32.38	0.00	0.17	1	100.26	77
4	2.39	48.90	15.42	0.31	31.85	0.00	0.15	2	99.02	77
5	2.41	49.08	16.51	0.33	32.19	0.00	0.18	1	100.70	78
6	2.57	49.95	16.31	0.35	32.07	0.01	0.15	2	101.41	77
7	2.43	49.65	15.72	0.25	32.39	0.00	0.15	1	100.59	77
8	2.47	50.13	15.77	0.25	32.34	0.00	0.13	2	101.09	77
9	2.38	49.63	16.43	0.32	32.50	0.00	0.17	1	101.43	78
10	2.53	49.34	15.50	0.28	31.64	0.00	0.15	2	99.44	76
11	2.19	48.86	15.72	0.23	32.53	0.00	0.14	1	99.67	79
12	2.12	48.74	17.09	0.29	32.53	0.00	0.14	2	100.91	81
13	2.34	49.20	15.19	0.32	31.75	0.00	0.14	1	98.94	77
14	2.54	49.75	16.57	0.28	32.52	0.00	0.15	2	101.81	77
15	2.49	49.42	16.51	0.28	31.86	0.00	0.14	1	100.70	78

Sample: IWS 93
Weight*: 16.4

Number	Na_2O	SiO_2	CaO	FeO	Al_2O_3	MgO	K_2O	Pos	Total	An
1	2.35	47.22	16.94	0.25	31.55	0.01	0.10	1	98.42	79
2	2.49	48.42	16.85	0.29	31.53	0.01	0.15	1	99.74	78
3	2.47	47.83	16.86	0.24	31.50	0.02	0.12	2	99.04	78
4	2.32	48.03	16.81	0.24	31.60	0.01	0.13	1	99.14	79
5	2.27	48.11	17.21	0.23	32.02	0.01	0.10	2	99.95	80
6	2.42	48.42	17.30	0.25	31.68	0.01	0.11	1	100.19	79
7	2.43	48.41	17.04	0.28	31.49	0.00	0.13	2	99.78	78

data
PC045

Sample: IWS 90
Height*: 11.3

Number	Na_2O	SiO_2	CaO	FeO	Al_2O_3	MgO	K_2O	Pos	Total	An
1	3.17	51.07	14.73	0.17	31.66	0.00	0.19	3	100.99	71
2	3.03	50.01	15.04	0.21	32.09	0.00	0.20	3	100.58	72
3	2.97	50.24	15.12	0.15	32.01	0.00	0.21	3	100.70	72
4	2.60	49.47	15.90	0.19	32.48	0.00	0.15	3	100.79	77
5	2.61	49.47	15.70	0.17	32.29	0.00	0.20	3	100.44	76
6	2.59	49.31	14.92	0.12	32.41	0.00	0.17	3	99.52	75
7	3.15	50.22	14.59	0.21	31.66	0.00	0.24	3	100.07	71
8	2.78	48.63	15.27	0.14	32.21	0.00	0.16	3	99.19	74
9	2.84	48.85	15.32	0.14	32.08	0.00	0.11	3	99.34	74
10	2.58	48.65	15.84	0.15	32.74	0.00	0.13	3	109.09	76
11	2.86	49.58	15.44	0.17	32.39	0.00	0.16	3	100.60	74
12	5.38	55.43	10.78	0.11	28.55	0.00	0.29	3	100.54	52
13	2.79	49.83	15.30	0.21	32.30	0.00	0.18	3	100.61	74
14	2.90	50.18	15.89	0.20	32.26	0.00	0.16	3	101.59	74

Sample: IWS 88
Height*: 7.1

Number	Na_2O	SiO_2	CaO	FeO	Al_2O_3	MgO	K_2O	Pos	Total	An
1	2.63	49.47	15.78	0.32	31.35	0.00	0.14	1	99.69	76
2	2.53	49.33	16.04	0.41	31.39	0.00	0.12	2	99.82	77
3	2.66	49.44	15.20	0.34	31.58	0.00	0.14	1	99.36	75
4	2.37	49.78	15.91	0.39	31.64	0.00	0.15	2	100.24	78
5	2.37	48.89	15.93	0.31	31.21	0.00	0.13	1	98.84	78
6	2.55	49.01	16.21	0.32	31.85	0.00	0.13	2	100.07	77
7	2.57	49.48	15.90	0.41	31.45	0.00	0.10	1	99.91	77
8	2.47	47.93	16.44	0.36	32.58	0.00	0.13	2	99.91	78
9	2.55	49.97	15.72	0.39	31.59	0.00	0.13	1	100.35	76
10	2.50	47.94	15.02	0.42	31.58	0.00	0.14	2	97.60	76
11	2.57	49.22	16.06	0.38	31.90	0.00	0.16	1	100.29	76
12	2.40	48.85	16.12	0.36	32.04	0.00	0.12	2	99.89	78
13	2.57	49.75	15.60	0.41	31.21	0.00	0.13	1	99.67	76
14	1.84	54.47	15.01	0.35	28.17	0.00	0.06	2	99.90	81
15	2.61	49.06	16.24	0.34	31.91	0.00	0.17	1	100.33	76

Sample: IWS 86
Height*: 3.4

Number	Na_2O	SiO_2	CaO	FeO	Al_2O_3	MgO	K_2O	Pos	Total	An
1	2.99	49.03	15.54	0.40	31.12	0.00	0.17	1	99.25	73
2	2.99	49.28	15.71	0.40	31.16	0.00	0.16	2	99.70	73
3	2.98	49.50	15.79	0.42	31.12	0.00	0.19	1	100.00	73
4	3.46	50.09	15.09	0.35	30.63	0.00	0.12	2	99.74	70
5	3.90	51.29	12.56	0.28	29.78	0.00	0.30	1	98.11	62
6	3.10	49.45	15.62	0.38	30.88	0.00	0.17	2	99.60	72
7	2.72	48.55	15.85	0.31	31.53	0.00	0.10	1	99.06	75
8	2.80	48.54	16.37	0.31	31.53	0.01	0.14	2	99.70	76
9	2.75	48.72	16.35	0.30	31.43	0.00	0.14	1	99.69	76
10	2.81	48.62	16.32	0.31	31.46	0.00	0.12	2	99.64	75

Sample: IWS 85
Height*: 1.7

Number	Na_2O	SiO_2	CaO	FeO	Al_2O_3	MgO	K_2O	Pos	Total	An
1	2.96	50.69	14.67	0.33	31.97	0.00	0.21	1	100.83	72
2	2.55	49.10	15.21	0.39	32.66	0.00	0.16	2	100.07	75
3	2.58	49.19	15.76	0.25	32.90	0.00	0.10	1	100.78	76
4	2.91	50.25	15.02	0.24	31.11	0.00	0.15	2	99.68	73
5	2.90	50.05	15.71	0.31	32.45	0.00	0.21	1	101.63	74
6	2.69	49.64	15.64	0.32	32.55	0.00	0.19	2	101.03	75
7	2.54	48.03	16.40	0.29	32.24	0.01	0.14	1	99.65	77
8	2.78	49.64	15.57	0.35	32.47	0.01	0.19	2	101.01	74
9	3.00	49.82	15.26	0.31	32.01	0.00	0.17	1	100.57	73
10	2.15	47.28	17.19	0.36	32.78	0.00	0.09	2	99.85	81
11	2.94	49.86	15.57	0.27	32.33	0.00	0.11	1	101.08	74
12	2.95	49.44	15.70	0.32	32.00	0.00	0.15	2	100.56	73
13	3.15	50.26	14.06	0.30	31.91	0.00	0.18	1	99.86	70
14	2.77	49.58	15.88	0.36	32.13	0.00	0.23	2	100.95	75
15	2.69	49.25	16.00	0.33	32.46	0.00	0.14	1	100.89	76

data
PC045

Sample: IWS 71
Height*: 0.0

Number	Na_2O	SiO_2	CaO	FeO	Al_2O_3	MgO	K_2O	Pos	Total	An
1	3.16	50.32	14.37	0.34	30.47	0.00	0.24	3	98.90	70
2	2.87	49.66	15.02	0.33	31.98	0.00	0.20	3	100.06	73
3	2.67	49.20	14.39	0.32	31.99	0.00	0.18	3	98.75	74
4	3.08	49.64	14.05	0.31	30.74	0.00	0.24	3	98.06	70
5	2.38	48.81	14.66	0.33	32.51	0.00	0.16	3	98.85	76
6	3.12	49.72	13.30	0.20	31.92	0.00	0.17	3	98.43	69
7	2.95	49.18	14.07	0.50	31.54	0.04	0.09	3	98.37	72
8	3.19	49.52	12.46	0.83	30.85	0.22	0.14	3	97.21	67
9	3.11	49.88	11.08	0.74	30.25	0.13	0.84	3	96.03	63
10	2.95	48.77	14.33	0.58	30.18	0.13	0.23	3	97.17	72
11	2.83	49.51	14.21	0.33	31.62	0.02	0.18	3	98.70	72
12	2.65	49.02	15.55	0.27	31.73	0.04	0.12	3	99.38	75
13	3.92	51.66	13.34	0.19	30.36	0.00	0.23	3	99.70	64
14	3.63	50.39	13.56	0.41	30.98	0.01	0.21	3	99.19	66

Sample: IWS 72
Height*: -6.9

Number	Na_2O	SiO_2	CaO	FeO	Al_2O_3	MgO	K_2O	Pos	Total	An
1	2.59	49.20	15.60	0.37	31.57	0.00	0.20	1	99.53	76
2	2.69	48.87	15.25	0.42	31.86	0.00	0.17	2	99.26	75
3	2.53	48.84	15.78	0.40	32.33	0.00	0.15	1	100.03	76
4	2.75	49.40	15.63	0.40	32.26	0.00	0.16	2	100.60	75
5	2.50	49.16	15.84	0.47	32.41	0.02	0.12	1	100.52	77
6	2.66	49.16	15.71	0.37	32.07	0.00	0.15	2	100.12	76
7	2.51	48.73	15.56	0.36	32.09	0.00	0.16	2	99.41	76
8	2.89	49.65	14.19	0.42	32.03	0.00	0.15	1	99.33	72
9	2.65	49.27	13.68	0.41	32.38	0.00	0.16	2	98.55	73
10	2.69	48.90	12.89	0.40	31.80	0.00	0.14	1	96.82	72
11	2.78	49.32	14.22	0.36	32.02	0.00	0.15	2	98.85	73
12	2.68	48.40	14.59	0.32	31.13	0.00	0.19	1	97.31	74
13	2.46	48.74	15.28	0.41	31.86	0.00	0.12	2	98.87	76
14	2.70	48.83	15.42	0.46	31.68	0.00	0.17	1	99.26	75

Sample: IWS 80
Height*: -12.5

Number	Na_2O	SiO_2	CaO	FeO	Al_2O_3	MgO	K_2O	Pos	Total	An
1	2.33	48.25	14.72	1.47	29.67	0.617	0.124	1	97.07	77
2	2.52	49.61	16.02	0.29	31.85	0.000	0.154	2	100.44	77
3	2.67	49.46	15.73	0.36	31.43	0.000	0.154	1	99.80	76
4	2.50	49.03	16.16	0.30	31.69	0.000	0.118	2	99.79	77
5	2.55	49.27	16.12	0.23	31.50	0.000	0.159	1	99.82	77
6	2.64	49.43	15.75	0.31	31.65	0.000	0.183	2	99.96	76
7	2.56	49.09	15.73	0.29	31.28	0.000	0.131	1	99.08	76
8	2.59	48.85	15.94	0.30	31.33	0.000	0.107	2	99.11	76
9	2.56	49.48	16.02	0.36	31.70	0.000	0.116	1	100.23	77
10	2.58	48.31	15.49	0.34	31.04	0.000	0.146	2	97.90	76
11	2.78	49.97	15.45	0.34	31.43	0.000	0.186	1	100.15	74
12	2.56	49.06	15.96	0.37	31.76	0.000	0.117	2	99.82	77
13	2.72	49.65	15.54	0.35	31.68	0.000	0.159	1	100.09	77
14	2.76	49.17	14.42	1.09	29.92	0.519	0.132	2	98.00	73
15	2.45	49.17	15.75	0.31	31.94	0.000	0.134	1	99.75	77

Sample: IWS 76
Height*: -19.2

Number	Na_2O	SiO_2	CaO	FeO	Al_2O_3	MgO	K_2O	Pos	Total	An
1	2.80	49.10	15.31	0.35	30.70	0.02	0.17	1	98.45	74
2	2.75	49.15	15.43	0.29	30.89	0.01	0.19	2	98.71	74
3	2.30	48.11	16.65	0.33	31.96	0.00	0.11	1	99.46	79
4	2.47	48.50	16.29	0.31	31.48	0.00	0.12	2	99.17	78
5	2.46	48.67	16.38	0.40	31.49	0.00	0.16	1	99.56	78
6	2.66	49.24	16.31	0.34	31.34	0.01	0.13	2	100.03	76
7	2.79	49.55	15.68	0.39	30.93	0.01	0.16	1	99.46	74
8	2.65	49.10	15.81	0.34	31.06	0.01	0.20	2	99.17	76
9	2.59	48.52	16.10	0.36	31.20	0.01	0.15	1	98.93	76
10	2.63	49.03	16.30	0.33	31.27	0.01	0.15	2	99.72	77

data
PC045

Sample: IWS 74
Height*: -22.5

Number	Na_2O	SiO_2	CaO	FeO	Al_2O_3	MgO	K_2O	Pos	Total	An
1	2.64	48.57	16.48	0.26	31.76	0.01	0.11	1	99.83	72
2	2.80	48.71	16.01	0.33	31.55	0.00	0.13	2	99.53	75
3	2.72	48.71	16.15	0.33	31.31	0.00	0.10	1	99.32	76
4	2.65	48.49	16.23	0.28	31.51	0.00	0.13	2	99.29	76
5	2.76	49.01	16.64	0.30	30.89	0.00	0.12	1	99.72	76
6	2.93	49.23	16.24	0.37	31.14	0.01	0.10	2	100.02	75
7	2.61	48.67	16.28	0.31	31.61	0.01	0.10	1	99.59	77
8	2.50	48.03	16.38	0.37	31.79	0.00	0.13	2	99.20	76
9	2.42	48.16	16.89	0.35	31.80	0.01	0.11	1	99.74	78

Sample: IWS 73
Height*: -24.6

Number	Na_2O	SiO_2	CaO	FeO	Al_2O_3	MgO	K_2O	Pos	Total	An
1	2.66	50.12	14.51	0.41	31.66	0.00	0.16	1	99.52	74
2	2.60	49.41	15.67	0.36	32.00	0.00	0.11	2	100.15	76
3	2.47	50.10	15.65	0.32	31.97	0.00	0.09	1	100.60	77
4	2.44	47.82	16.04	0.37	32.14	0.00	0.12	2	98.93	77
5	2.48	49.80	15.97	0.36	31.97	0.00	0.14	1	100.72	77
6	2.36	48.63	15.68	0.44	32.41	0.02	0.15	2	99.69	78
7	2.54	48.04	15.31	0.34	31.92	0.00	0.14	2	98.29	76
8	2.65	48.98	15.95	0.36	31.90	0.00	0.16	1	100.00	76
9	2.51	48.55	15.87	0.42	32.46	0.01	0.15	2	99.97	77
10	2.66	49.71	15.67	0.35	32.41	0.04	0.09	1	100.93	76
11	2.57	46.74	15.48	0.41	31.97	0.00	0.13	2	97.30	76
12	2.57	48.92	15.74	0.35	32.06	0.00	0.11	1	99.75	77
13	2.59	47.35	15.48	0.38	31.96	0.00	0.11	2	97.87	76
14	2.59	47.71	16.24	0.29	32.43	0.00	0.07	1	99.33	77

Sample: IWS 3
Height*: -29.5

Number	Na_2O	SiO_2	CaO	FeO	Al_2O_3	MgO	K_2O	Pos	Total	An
1	2.51	49.75	16.02	0.21	32.49	0.00	0.10	0	101.08	77
2	2.50	49.30	15.58	0.25	32.30	0.00	0.14	0	100.07	76
3	2.50	49.65	16.14	0.21	32.41	0.00	0.13	0	101.04	77
4	2.56	49.51	16.26	0.23	32.60	0.00	0.13	0	101.29	77
5	2.53	49.26	16.26	0.23	32.68	0.00	0.10	0	101.06	78
6	2.47	49.38	15.59	0.25	32.61	0.00	0.06	0	100.36	77
7	2.75	49.83	15.68	0.20	32.43	0.00	0.11	0	101.00	77
8	2.71	49.36	15.66	0.21	32.22	0.00	0.08	0	100.24	78
9	2.69	49.57	16.02	0.22	32.37	0.00	0.05	0	100.92	77
10	2.62	49.77	16.03	0.15	32.47	0.00	0.09	0	101.13	76
11	2.58	49.16	15.29	0.18	32.16	0.00	0.11	1	99.48	77
12	2.67	49.36	15.98	0.29	32.23	0.00	0.06	2	100.59	76
13	2.69	49.29	15.96	0.19	32.17	0.00	0.12	1	100.42	76
14	2.46	49.30	15.20	0.27	32.57	0.00	0.15	2	99.95	76
15	2.72	49.95	15.85	0.16	32.39	0.00	0.14	1	101.22	77
16	2.70	49.24	14.42	0.27	32.41	0.00	0.13	2	99.17	74
17	2.75	48.78	15.31	0.24	31.82	0.02	0.10	1	99.02	76
18	2.64	49.50	14.19	0.27	32.46	0.01	0.12	2	99.19	75
19	2.63	49.53	14.12	0.20	32.38	0.00	0.12	1	98.98	74
20	2.56	49.41	14.78	0.22	32.40	0.00	0.06	2	99.43	74
21	2.48	49.55	15.76	0.19	32.40	0.00	0.12	1	100.50	76
22	2.50	48.15	16.11	0.18	32.31	0.00	0.12	2	99.37	77
23	2.67	49.36	15.94	0.21	32.39	0.00	0.14	1	100.71	76
24	2.66	49.72	15.07	0.24	32.71	0.00	0.16	2	100.56	76
25	2.51	49.29	16.06	0.21	32.38	0.00	0.13	1	100.58	77
26	2.63	49.56	15.98	0.19	32.34	0.00	0.13	2	100.83	76
27	2.59	49.42	15.19	0.17	32.37	0.00	0.12	1	99.86	76
28	2.55	49.86	14.11	0.19	32.52	0.00	0.11	1	99.34	74
29	2.65	49.88	14.54	0.22	32.44	0.00	0.09	2	99.82	75

data
PC045

Sample: IWS 7
Height*: -35.7

Number	Na_2O	SiO_2	CaO	FeO	Al_2O_3	MgO	K_2O	Pos	Total	An
1	2.76	50.59	15.60	0.27	32.04	0.00	0.09	0	101.35	75
2	2.90	48.89	15.66	0.16	31.24	0.00	0.09	0	98.94	74
3	2.42	49.34	16.14	0.21	32 64	0.00	0.13	0	100.88	78
4	1.92	48.39	16.63	0.24	33.36	0.00	0.08	0	100.62	82
5	2.31	48.58	15.87	0.21	32.06	0.00	0.11	0	99.14	78
6	2.87	49.96	13.71	0.19	31.24	0.00	0.11	1	98.08	72
7	2.59	49.92	13.79	0.25	32.09	0.00	0.15	1	98.79	74
8	2.34	49.34	13.85	0.18	32.16	0.00	0.13	2	98.00	76
9	2.29	49.24	14.45	0.13	32.54	0.00	0.15	2	98.80	77
10	2.17	49.03	14.46	0.21	33.00	0.00	0.10	2	98.97	78

Sample: IWS 10
Height*: -40.8

Number	Na_2O	SiO_2	CaO	FeO	Al_2O_3	MgO	K_2O	Pos	Total	An
1	2.279	49.316	16.375	0.255	31.860	0.017	0.183	1	100.25	79
2	2.306	48.955	16.364	0.244	32.185	0.000	0.145	2	100.17	79
3	2.580	49.530	15.947	0.300	31.668	0.000	0.174	1	100.18	76
4	2.318	48.575	16.465	0.274	31.938	0.010	0.121	2	99.67	79
5	2.287	48.915	16.378	0.228	32.249	0.000	0.135	1	100.15	79
6	2.163	48.309	16.436	0.223	32.268	0.000	0.126	2	99.49	79
7	2.316	48.466	16.071	0.256	32.044	0.000	0.177	1	99.30	79
8	2.029	48.225	16.281	0.276	32.325	0.000	0.118	2	99.22	81
9	2.240	48.089	16.534	0.210	31.599	0.000	0.162	1	98.81	80
10	1.906	47.829	16.747	0.227	32.512	0.000	0.099	2	99.28	82
11	2.422	48.511	15.895	0.225	31.570	0.000	0.155	1	98.76	77
12	2.199	47.556	16.555	0.285	31.541	0.000	0.159	2	98.26	79
13	2.100	48.411	16.705	0.205	32.588	0.000	0.110	1	100.10	80
14	2.193	48.385	16.679	0.220	32.012	0.000	0.139	2	99.60	80
15	2.604	49.214	15.900	0.273	31.673	0.000	0.183	1	99.83	76

Sample: IWS 12
Height*: -44.1

Number	Na_2O	SiO_2	CaO	FeO	Al_2O_3	MgO	K_2O	Pos	Total	An
1	2.442	49.568	16.434	0.334	32.119	0.000	0.114	1	100.98	78
2	2.440	49.164	15.637	0.192	32.099	0.000	0.127	2	99.63	77
3	2.348	48.564	15.882	0.196	32.299	0.000	0.145	1	99.40	78
4	2.561	49.188	15.164	0.240	32.442	0.000	0.159	2	99.73	75
5	2.533	49.145	15.551	0.229	31.531	0.000	0.167	1	99.13	76
6	2.446	49.336	15.081	0.264	32.409	0.000	0.170	2	99.68	76
7	2.369	49.154	14.862	0.217	32.399	0.000	0.164	1	99.13	76
8	2.489	49.448	14.619	0.298	32.397	0.000	0.170	2	99.38	75
9	2.539	49.350	15.340	0.234	32.380	0.000	0.169	1	99.99	76
10	2.478	49.474	15.677	0.228	32.324	0.000	0.136	2	100.28	77
11	2.267	48.782	16.541	0.307	32.434	0.000	0.115	1	100.42	79
12	2.519	48.316	15.493	0.980	31.367	0.158	0.131	2	98.93	76
13	2.299	48.434	16.166	0.225	32.729	0.000	0.153	1	99.97	78
14	2.572	49.540	15.722	0.177	32.000	0.000	0.184	2	100.18	76
15	2.340	49.024	16.572	0.273	32.566	0.000	0.162	1	100.92	78

Sample: IWS 16
Height*: -50.7

Number	Na_2O	SiO_2	CaO	FeO	Al_2O_3	MgO	K_2O	Pos	Total	An
1	2.548	47.994	16.241	0.276	31.669	0.003	0.161	1	98.86	77
2	2.529	48.413	16.598	0.285	31.422	0.010	0.150	2	98.38	77
3	2.710	48.648	16.768	0.283	31.408	0.008	0.162	1	99.95	76
4	2.612	48.173	17.039	0.262	31.558	0.000	0.138	2	99.75	77
5	2.471	48.112	16.739	0.298	31.684	0.009	0.124	1	99.40	78
6	2.542	47.907	16.591	0.263	31.684	0.008	0.140	2	99.11	77
7	2.741	48.606	16.399	0.244	31.052	0.010	0.185	1	99.21	76
8	2.505	48.254	16.959	0.271	31.623	0.000	0.147	2	99.73	78
9	2.778	48.867	16.457	0.271	31.501	0.011	0.112	1	99.97	76
10	2.637	48.724	16.575	0.316	31.502	0.000	0.157	2	99.88	77

data
PC045

Sample: IWS 19
Height*: -55.8

Number	Na_2O	SiO_2	CaO	FeO	Al_2O_3	MgO	K_2O	Pos	Total	An
1	2.699	48.536	16.378	0.286	31.655	0.002	0.166	1	99.68	76
2	2.741	48.914	16.617	0.304	31.492	0.004	0.174	2	100.22	76
3	2.755	48.694	16.202	0.256	31.531	0.010	0.151	1	99.58	76
4	2.509	48.141	16.570	0.299	31.825	0.000	0.121	2	99.44	78
5	2.503	48.415	16.217	0.228	31.760	0.001	0.138	1	99.23	77
6	2.530	47.919	16.418	0.239	31.843	0.000	0.073	2	98.99	77
7	2.607	48.019	16.206	0.283	32.070	0.003	0.080	1	99.24	77
8	2.588	47.701	15.611	0.201	31.054	0.000	0.112	2	97.25	76

Sample: IWS 21
Height*: -59.1

Number	Na_2O	SiO_2	CaO	FeO	Al_2O_3	MgO	K_2O	Pos	Total	An
1	2.469	48.092	16.696	0.382	31.478	0.004	0.106	1	99.19	78
2	2.606	48.586	16.385	0.450	31.008	0.000	0.108	2	99.11	77
3	2.603	48.984	16.813	0.410	31.465	0.004	0.138	1	100.39	77
4	2.732	48.451	16.142	0.404	30.689	0.011	0.140	2	98.55	75
5	2.536	48.661	16.729	0.491	31.231	0.004	0.143	1	99.77	77
6	2.754	49.062	16.566	0.374	31.189	0.000	0.152	2	100.07	76
7	2.671	48.901	16.576	0.322	31.259	0.000	0.094	1	99.80	77
8	2.572	48.318	16.569	0.397	31.130	0.012	0.158	2	99.12	77
9	2.501	48.392	16.668	0.407	31.349	0.007	0.115	1	99.40	78
10	2.541	47.864	16.582	0.396	30.881	0.000	0.125	2	98.37	77

Sample: IWS 23
Height*: -62.6

Number	Na_2O	SiO_2	CaO	FeO	Al_2O_3	MgO	K_2O	Pos	Total	An
1	2.441	47.986	16.334	0.266	32.079	0.000	0.096	1	99.17	78
2	2.610	48.689	16.907	0.248	31.869	0.000	0.148	2	100.43	77
3	2.607	48.669	16.335	0.250	31.754	0.006	0.126	1	99.71	77
4	2.668	48.763	16.728	0.264	31.858	0.008	0.105	1	100.35	78
5	2.714	49.101	16.660	0.284	31.850	0.000	0.134	2	100.73	77
6	2.669	49.070	16.612	0.325	31.969	0.005	0.121	1	100.74	78
7	2.651	48.480	16.652	0.207	31.884	0.000	0.131	2	99.99	78
8	2.374	47.990	17.202	0.191	32.177	0.000	0.132	1	100.05	77
9	2.431	48.391	16.882	0.240	32.173	0.001	0.119	2	100.22	76

Sample: IWS 25
Height*: -65.9

Number	Na_2O	SiO_2	CaO	FeO	Al_2O_3	MgO	K_2O	Pos	Total	An
1	2.37	48.53	16.59	0.20	32.31	0.00	0.14	1	100.14	78
2	2.40	48.27	15.77	0.28	31.95	0.00	0.14	2	98.81	77
3	2.50	48.11	15.40	0.32	31.68	0.00	0.10	2	98.11	76
4	2.55	48.61	16.51	0.23	31.83	0.00	0.14	1	99.87	77
5	2.49	48.63	16.48	0.31	31.72	0.00	0.12	2	99.75	78
6	2.54	48.83	16.56	0.30	31.85	0.00	0.14	1	100.22	77
7	2.56	48.59	16.38	0.32	31.92	0.00	0.12	2	99.89	78
8	2.41	48.43	15.69	0.36	31.85	0.00	0.11	1	98.85	77
9	2.56	48.75	15.78	0.30	31.91	0.00	0.11	2	99.41	76
10	2.52	48.78	15.66	0.23	31.77	0.00	0.15	1	99.31	75
11	2.55	48.67	16.17	0.27	31.80	0.00	0.12	2	99.58	77
12	2.47	48.24	16.01	0.23	31.95	0.00	0.15	1	99.05	77
13	2.43	48.27	15.85	0.24	31.95	0.00	0.11	2	98.86	77

Sample: IWS 27
Height*: -69.3

Number	Na_2O	SiO_2	CaO	FeO	Al_2O_3	MgO	K_2O	Pos	Total	An
1	2.677	48.788	16.512	0.413	31.334	0.000	0.128	1	99.82	76
2	2.631	49.340	16.717	0.435	31.480	0.000	0.129	2	100.71	77
3	2.637	49.096	16.384	0.392	31.440	0.005	0.100	1	100.03	77
4	2.460	48.782	16.940	0.355	31.819	0.001	0.100	2	100.44	78
5	2.650	49.405	16.379	0.452	31.408	0.022	0.107	1	100.39	77
6	2.584	48.802	16.307	0.439	31.053	0.000	0.138	2	99.29	77
7	2.544	47.927	16.254	0.423	31.063	0.003	0.121	2	98.31	77
8	2.650	48.820	16.535	0.433	31.087	0.006	0.096	1	99.60	77
9	2.651	48.997	16.208	0.442	30.621	0.002	0.178	2	99.07	76

data
PC045

Sample: IWS 30
Height*: -74.4

Number	Na_2O	SiO_2	CaO	FeO	Al_2O_3	MgO	K_2O	Pos	Total	An
1	2.477	49.624	16.080	0.282	32.116	0.000	0.150	1	100.71	77
2	2.519	49.219	15.192	0.292	32.206	0.000	0.139	2	99.53	76
3	2.625	49.378	15.191	0.308	32.045	0.000	0.099	1	99.61	75
4	2.518	49.288	16.137	0.266	32.432	0.000	0.100	2	100.71	77
5	2.382	49.043	16.443	0.281	32.222	0.000	0.095	1	100.45	78
6	2.621	49.303	15.931	0.246	32.181	0.000	0.122	2	100.39	76
7	2.496	49.316	15.828	0.310	32.392	0.000	0.077	1	100.39	77
8	2.479	49.550	15.758	0.279	32.367	0.000	0.124	2	100.52	77
9	2.772	49.712	15.704	0.238	31.778	0.000	0.136	1	100.31	75
10	1.859	47.704	17.461	0.238	33.468	0.000	0.050	2	100.75	83
11	2.291	49.094	16.209	0.257	32.391	0.000	0.128	1	100.34	79
12	2.552	49.163	16.148	0.264	32.465	0.000	0.076	2	100.64	77
13	2.528	49.144	15.985	0.282	32.328	0.000	0.103	1	100.34	77
14	2.271	49.374	16.029	0.231	32.127	0.000	0.112	2	100.12	79
15	2.417	49.428	15.376	0.247	32.388	0.000	0.084	1	99.90	77
16	2.483	49.284	16.099	0.249	32.207	0.000	0.121	2	100.33	77
17	2.503	49.385	16.084	0.271	32.379	0.000	0.099	1	100.69	77
18	2.472	49.768	16.079	0.255	32.310	0.000	0.121	2	100.98	77
19	2.632	49.813	15.592	0.284	32.271	0.000	0.144	1	100.72	76
20	2.504	49.187	15.928	0.258	32.345	0.000	0.093	2	100.28	77
21	2.742	49.402	15.926	0.277	32.230	0.000	0.084	1	100.64	76
22	2.551	49.386	15.251	0.221	32.154	0.000	0.078	2	99.62	76
23	2.617	49.780	15.877	0.271	32.103	0.015	0.123	1	100.76	77
24	2.553	49.581	15.112	0.253	32.294	0.000	0.117	1	99.89	76
25	2.381	48.589	15.814	0.303	32.408	0.000	0.123	2	99.59	77
26	2.483	49.638	15.354	0.223	32.069	0.000	0.105	1	99.84	77
27	2.428	49.070	16.058	0.310	32.093	0.000	0.095	2	100.03	76
28	2.583	49.519	15.609	0.299	32.263	0.000	0.117	1	100.35	77
29	2.657	49.381	15.535	0.249	32.079	0.000	0.109	2	99.97	78

Sample: IWS 31
Height*: -76.2

Number	Na_2O	SiO_2	CaO	FeO	Al_2O_3	MgO	K_2O	Pos	Total	An
1	2.588	48.635	15.931	0.282	31.624	0.000	0.158	2	99.19	76
2	2.609	48.842	16.131	0.312	32.292	0.000	0.127	1	100.29	76
3	2.257	48.386	16.343	0.334	32.735	0.000	0.118	2	100.14	79
4	2.183	48.074	16.541	0.299	32.332	0.000	0.155	1	99.56	80
5	2.508	48.500	16.324	0.282	31.922	0.000	0.098	2	99.61	77
6	2.323	48.123	16.397	0.310	32.719	0.000	0.128	1	99.97	79
7	2.388	47.912	16.667	0.270	32.048	0.000	0.149	2	99.40	78
8	2.458	48.883	16.285	0.356	32.702	0.017	0.131	1	100.80	78
9	2.498	48.713	16.242	0.266	32.445	0.000	0.090	2	100.23	77
10	2.577	48.902	16.296	0.308	33.130	0.024	0.118	1	101.32	77
11	2.729	49.270	16.229	0.230	32.625	0.044	0.130	1	101.23	76
12	2.497	48.784	16.078	0.314	32.102	0.001	0.126	2	99.87	77
13	2.347	48.478	16.426	0.254	32.523	0.000	0.109	1	100.10	79

Sample: IWS 33
Height*: -79.5

Number	Na_2O	SiO_2	CaO	FeO	Al_2O_3	MgO	K_2O	Pos	Total	An
1	2.581	49.435	15.998	0.299	32.171	0.000	0.155	1	100.61	76
2	2.343	48.862	15.836	0.290	32.487	0.000	0.166	2	99.96	78
3	2.378	50.865	15.407	0.314	31.204	0.000	0.149	1	100.28	77
4	2.356	48.584	15.729	0.264	32.084	0.000	0.149	2	99.13	78
5	2.537	49.010	15.793	0.292	32.308	0.000	0.126	1	100.04	77
6	2.552	49.160	15.783	0.327	32.485	0.000	0.183	2	100.47	76
7	2.482	49.078	15.873	0.253	32.192	0.000	0.143	1	100.00	77
8	2.263	48.668	15.167	0.223	32.611	0.000	0.191	2	99.10	80
9	2.278	48.158	16.173	0.369	32.738	0.000	0.143	1	99.82	79
10	2.547	49.056	15.767	0.268	32.353	0.000	0.157	2	100.11	76
11	2.438	48.759	15.760	0.295	32.229	0.000	0.151	1	99.60	77
12	2.434	49.092	14.565	0.325	32.409	0.000	0.189	2	98.98	76
13	2.542	48.982	15.944	0.279	32.245	0.000	0.149	1	100.11	77
14	2.121	48.727	14.967	0.277	32.716	0.000	0.126	2	98.90	78
15	2.393	49.133	15.644	0.277	32.265	0.000	0.176	1	98.86	77

data
PC045

Sample: IWS 35
Height*: -82.9

Number	Na_2O	SiO_2	CaO	FeO	Al_2O_3	MgO	K_2O	Pos	Total	An
1	2.51	48.15	16.84	0.32	31.65	0.00	0.04	1	99.51	78
2	2.57	48.03	16.08	0.74	30.97	0.22	0.06	2	98.67	77
3	2.42	47.80	16.88	0.37	31.22	0.00	0.06	1	98.75	79
4	2.34	48.14	17.13	0.35	32.22	0.01	0.04	2	100.23	80
5	2.53	48.09	16.52	0.36	31.16	0.00	0.05	1	98.71	78
6	2.31	47.76	16.72	0.34	31.64	0.00	0.02	2	98.79	80
7	2.50	48.55	16.47	0.37	31.59	0.00	0.04	1	99.52	78
8	2.42	48.09	16.83	0.41	31.51	0.00	0.05	2	99.31	79
9	2.52	48.17	17.00	0.32	31.59	0.00	0.09	1	99.69	78
10	2.58	48.40	16.56	0.38	31.39	0.03	0.03	2	99.37	77

Sample: IWS 36
Height*: -84.6

Number	Na_2O	SiO_2	CaO	FeO	Al_2O_3	MgO	K_2O	Pos	Total	An
1	2.61	49.17	15.95	0.29	32.10	0.00	0.13	1	100.25	79
2	2.48	48.23	16.47	0.33	32.07	0.00	0.14	2	99.75	78
3	2.45	48.41	16.04	0.32	32.34	0.00	0.15	1	99.71	77
4	2.30	48.15	16.56	0.30	32.45	0.00	0.21	2	99.97	79
5	2.48	47.46	16.26	0.36	31.65	0.00	0.15	1	98.36	77
6	2.54	48.62	16.08	0.26	32.08	0.00	0.13	2	99.71	77
7	2.39	48.31	16.35	0.29	32.15	0.00	0.14	1	99.63	78
8	2.42	48.41	15.79	0.34	31.98	0.00	0.16	2	99.10	77
9	2.49	48.11	15.44	0.31	31.84	0.00	0.14	2	98.33	76
10	2.51	48.02	16.26	0.31	32.08	0.00	0.15	1	99.33	77
11	2.56	48.62	16.55	0.31	32.46	0.00	0.11	2	100.61	78
12	2.66	48.13	15.89	0.33	31.72	0.00	0.10	1	98.83	76
13	2.44	47.85	16.54	0.33	32.08	0.00	0.14	2	99.38	78

Sample: IWS 38
Height*: -87.7

Number	Na_2O	SiO_2	CaO	FeO	Al_2O_3	MgO	K_2O	Pos	Total	An
1	2.46	48.37	16.34	0.25	32.13	0.00	0.14	1	99.69	78
2	2.58	48.41	16.24	0.29	31.98	0.00	0.15	2	99.65	77
3	2.48	48.78	15.12	0.24	31.72	0.01	0.16	1	98.51	76
4	2.60	48.87	16.33	0.30	31.77	0.00	0.14	2	100.01	77
5	2.58	48.86	16.44	0.31	31.93	0.00	0.09	1	100.21	77
6	2.53	48.53	15.57	0.29	31.95	0.01	0.10	2	98.98	77
7	2.52	48.03	15.93	0.41	31.50	0.05	0.14	1	98.58	78
8	2.46	48.42	15.35	0.29	31.91	0.00	0.13	2	98.56	77
9	2.53	48.41	16.07	0.32	31.86	0.00	0.14	1	99.33	77
10	2.53	48.11	16.60	0.28	32.05	0.02	0.14	2	99.73	77
11	2.30	48.45	16.06	0.30	32.30	0.00	0.09	1	99.50	77
12	2.74	48.59	15.07	0.22	31.41	0.00	0.14	2	98.17	74
13	2.51	48.62	15.36	0.30	32.06	0.00	0.14	1	98.99	76
14	2.53	48.43	16.28	0.34	31.74	0.00	0.15	2	99.47	77
15	2.43	48.22	16.51	0.30	32.26	0.00	0.14	1	99.86	77

Sample: IWS 41
Height*: -93.0

Number	Na_2O	SiO_2	CaO	FeO	Al_2O_3	MgO	K_2O	Pos	Total	An
1	2.648	49.561	15.742	0.243	32.113	0.000	0.112	1	100.40	76
2	2.589	48.553	16.522	0.232	32.171	0.015	0.090	2	100.15	77
3	2.599	49.145	15.251	0.369	32.213	0.000	0.117	1	99.66	76
4	2.569	49.160	16.244	0.325	32.045	0.000	0.119	2	100.43	77
5	2.551	49.048	16.346	0.252	32.315	0.000	0.097	1	100.58	77
6	2.583	48.577	16.159	0.237	31.915	0.000	0.096	2	99.53	77
7	2.440	48.682	15.785	0.219	32.533	0.000	0.088	1	99.72	77
8	2.544	48.863	13.927	0.289	32.514	0.000	0.103	2	98.21	74
9	2.541	48.919	16.169	0.386	32.603	0.000	0.147	1	100.73	75
10	2.610	48.418	15.630	0.256	31.748	0.000	0.118	2	98.75	76
11	2.542	48.036	16.517	0.319	31.862	0.025	0.111	1	99.38	77
12	2.341	47.820	16.516	0.339	32.183	0.019	0.105	2	99.29	79
13	2.587	49.341	16.194	0.297	32.299	0.015	0.128	1	100.82	77
14	2.351	48.571	16.824	0.336	32.596	0.015	0.119	2	100.78	79

data
PC045

Sample: IWS 42
Height*: -94.6

Number	Na_2O	SiO_2	CaO	FeO	Al_2O_3	MgO	K_2O	Pos	Total	An
1	2.56	49.46	15.46	0.29	31.29	0.00	0.15	1	99.21	76
2	2.47	48.10	15.79	0.27	31.76	0.00	0.15	2	98.54	77
3	2.48	46.85	15.45	0.36	30.86	0.00	0.21	1	96.21	76
4	2.49	47.72	15.56	0.31	31.21	0.00	0.15	2	97.44	77
5	2.50	47.44	15.60	0.33	30.90	0.00	0.16	1	96.93	76
6	2.49	47.75	15.09	0.30	31.25	0.00	0.14	2	97.02	77
7	2.48	48.29	15.72	0.36	31.65	0.00	0.15	1	98.65	77
8	2.63	48.48	14.66	0.27	31.60	0.00	0.12	2	97.76	76
9	2.57	48.30	15.52	0.29	31.29	0.00	0.22	1	98.19	76
10	2.48	48.45	15.83	0.30	31.79	0.00	0.14	2	98.99	77
11	2.59	47.51	15.84	0.31	30.69	0.00	0.14	1	97.08	77
12	2.64	47.16	15.45	0.36	30.80	0.00	0.19	2	96.60	75
13	2.59	48.12	15.42	0.29	30.96	0.00	0.16	2	97.54	76
14	2.46	47.01	15.85	0.31	30.69	0.00	0.17	1	96.49	75

Sample: IWS 45
Height*: -99.7

Number	Na_2O	SiO_2	CaO	FeO	Al_2O_3	MgO	K_2O	Pos	Total	An
1	2.54	48.47	16.89	0.36	31.38	0.00	0.13	1	99.77	78
2	2.66	48.95	16.98	0.38	31.56	0.00	0.15	2	100.68	77
3	2.79	49.31	16.43	0.38	30.80	0.00	0.18	1	99.89	75
4	2.80	49.63	16.39	0.32	31.37	0.00	0.16	2	100.67	75
5	2.54	48.59	17.00	0.35	31.41	0.00	0.15	1	100.04	78
6	2.64	48.85	16.68	0.34	31.11	0.00	0.17	2	99.79	77
7	2.73	48.86	16.80	0.39	31.14	0.00	0.17	1	100.09	76
8	2.43	48.48	17.15	0.37	31.60	0.00	0.16	2	100.19	79
9	2.52	48.52	17.05	0.36	31.37	0.00	0.14	1	99.96	78
10	3.03	49.04	16.37	0.31	30.90	0.01	0.21	2	99.87	74

Sample: IWS 46
Height*: -101.5

Number	Na_2O	SiO_2	CaO	FeO	Al_2O_3	MgO	K_2O	Pos	Total	An
1	2.51	48.18	16.20	0.29	31.56	0.01	0.15	3	98.90	77
2	2.63	49.04	16.72	0.32	31.49	0.00	0.13	3	100.33	77
3	2.89	49.27	16.38	0.32	30.95	0.01	0.15	3	99.97	76
4	2.65	47.92	16.06	0.37	31.10	0.01	0.15	3	98.26	76
5	2.76	48.63	16.32	0.29	30.98	0.00	0.15	3	99.13	75
6	2.81	49.61	16.42	0.40	31.27	0.00	0.18	3	100.69	75
7	2.72	48.40	16.63	0.35	31.53	0.00	0.13	3	99.76	76
8	2.46	47.92	17.34	0.35	31.42	0.01	0.13	3	99.63	79
9	2.53	49.14	17.53	0.42	32.08	0.01	0.12	3	101.83	78

Sample: IWS 50
Height*: -108.5

Number	Na_2O	SiO_2	CaO	FeO	Al_2O_3	MgO	K_2O	Pos	Total	An
1	3.64	52.58	12.85	0.15	30.26	0.00	0.34	3	99.82	64
2	3.73	51.98	12.65	0.17	30.31	0.01	0.31	3	99.16	63
3	3.26	51.31	12.57	0.18	30.41	0.00	0.77	3	98.50	64
4	4.24	53.03	11.04	0.12	29.57	0.01	0.37	3	98.38	57
5	4.05	50.58	11.83	0.16	29.43	0.00	0.33	3	96.38	60
6	4.10	51.65	10.21	0.12	30.01	0.00	0.30	3	96.39	57
7	4.54	53.80	10.52	0.13	28.67	0.00	0.31	3	97.97	55
8	3.63	51.86	9.75	0.17	30.44	0.00	0.27	3	96.12	58
9	4.01	52.38	11.80	0.21	30.02	0.02	0.36	3	98.80	60
10	3.89	52.55	10.57	0.12	29.89	0.02	0.29	3	97.33	59
11	3.92	51.94	12.46	0.11	30.27	0.00	0.25	3	98.95	63

data
PC045

Sample: IWS 51
Height*: -110.1

Number	Na_2O	SiO_2	CaO	FeO	Al_2O_3	MgO	K_2O	Pos	Total	An
1	4.43	52.78	13.10	0.19	29.04	0.00	0.28	3	99.82	61
2	4.89	53.21	12.45	0.16	27.86	0.00	0.32	3	98.89	57
3	4.92	52.91	12.39	0.14	27.76	0.00	0.32	3	98.44	57
4	4.99	54.22	11.97	0.13	27.77	0.00	0.29	3	99.37	56
5	5.02	54.10	12.38	0.12	28.00	0.00	0.35	3	99.97	56
6	5.00	53.63	12.51	0.20	28.63	0.00	0.25	3	100.22	57
7	4.40	53.02	12.13	0.15	28.78	0.00	0.31	3	98.79	59
8	4.41	53.07	12.73	0.20	28.65	0.00	0.29	3	99.35	60

Sample: IWS 52
Height*: -112.7

Number	Na_2O	SiO_2	CaO	FeO	Al_2O_3	MgO	K_2O	Pos	Total	An
1	2.92	49.02	15.08	0.17	31.69	0.00	0.16	3	99.04	73
2	2.84	48.24	15.66	0.18	31.64	0.00	0.16	3	98.72	74
3	2.82	48.02	15.79	0.18	31.73	0.00	0.17	3	98.71	74
4	2.90	49.49	14.38	0.16	31.67	0.00	0.17	3	98.77	72
5	2.97	50.01	14.87	0.25	31.74	0.00	0.15	3	99.99	72
6	2.89	48.59	15.03	0.17	31.72	0.00	0.17	3	98.57	73
7	2.59	49.98	15.20	0.18	32.44	0.00	0.12	3	100.51	75
8	2.90	48.93	15.45	0.18	31.87	0.00	0.15	3	99.48	74
9	2.84	47.89	15.58	0.20	31.67	0.00	0.16	3	98.34	74
10	3.20	50.21	14.37	0.20	31.45	0.00	0.19	3	99.62	70
11	2.80	48.96	15.55	0.24	32.13	0.00	0.17	3	99.85	74
12	2.96	49.11	14.95	0.19	31.99	0.00	0.17	3	99.37	72
13	2.83	49.04	15.69	0.16	32.05	0.00	0.16	3	99.93	74

Sample: IWS 54
Height*: -116.0

Number	Na_2O	SiO_2	CaO	FeO	Al_2O_3	MgO	K_2O	Pos	Total	An
1	3.94	51.41	13.74	0.14	29.70	0.00	0.37	3	99.30	64
2	3.88	51.92	13.71	0.13	29.48	0.00	0.39	3	99.51	64
3	2.96	49.15	16.13	0.14	31.21	0.00	0.16	3	99.75	74
4	2.71	48.13	16.03	0.17	31.34	0.01	0.13	3	98.51	76
5	2.81	49.02	16.46	0.16	31.51	0.00	0.12	3	100.08	75
6	3.89	51.13	14.03	0.15	29.80	0.00	0.23	3	99.23	65
7	3.08	50.04	15.82	0.14	31.05	0.00	0.14	3	100.27	73
8	2.75	48.94	16.33	0.20	31.67	0.00	0.14	3	100.03	76
9	4.22	52.91	13.32	0.18	29.18	0.01	0.16	3	99.98	62
10	3.34	50.81	15.17	0.23	30.70	0.00	0.19	3	100.44	70

Sample: IWS 56
Height*: -119.0

Number	Na_2O	SiO_2	CaO	FeO	Al_2O_3	MgO	K_2O	Pos	Total	An
1	2.42	49.05	14.66	0.21	32.70	0.00	0.14	1	99.18	76
2	2.66	48.70	15.53	0.25	32.49	0.00	0.19	2	99.82	75
3	2.53	48.52	16.17	0.24	32.29	0.00	0.14	1	99.89	77
4	2.61	49.48	16.00	0.24	32.50	0.00	0.13	2	100.96	76
5	2.62	49.28	16.04	0.21	32.47	0.00	0.17	2	100.79	76
6	2.64	49.53	16.80	0.30	32.43	0.00	0.19	1	101.89	77
7	2.28	47.56	16.00	0.29	32.98	0.00	0.15	2	99.26	78
8	2.48	49.62	14.81	0.27	32.35	0.00	0.17	1	99.70	76
9	2.47	48.11	16.21	0.29	32.37	0.00	0.18	2	99.63	77
10	2.39	49.02	16.02	0.26	32.61	0.00	0.15	1	100.45	78
11	2.57	48.25	16.09	0.26	32.59	0.00	0.16	2	99.92	76
12	2.37	48.68	16.18	0.27	32.70	0.00	0.15	1	100.35	78
13	2.23	48.35	16.17	0.28	33.17	0.00	0.13	2	100.33	79
14	2.57	47.71	15.98	0.22	32.14	0.00	0.17	1	98.79	76

data
PC045

Sample: IWS 59
Height*: -123.7

Number	Na_2O	SiO_2	CaO	FeO	Al_2O_3	MgO	K_2O	Pos	Total	An
1	2.62	50.94	15.65	0.37	31.73	0.00	0.19	1	101.50	75
2	2.09	49.38	15.99	0.32	32.62	0.00	0.13	2	100.53	80
3	2.23	49.91	15.56	0.34	32.14	0.00	0.15	1	100.33	78
4	2.35	49.60	15.99	0.25	31.32	0.02	0.16	2	99.69	78
5	2.56	49.90	15.72	0.27	31.55	0.00	0.13	1	100.13	76
6	2.45	50.28	15.66	0.30	31.97	0.01	0.16	2	100.83	77
7	2.36	49.47	16.49	0.37	31.61	0.02	0.14	1	100.46	78
8	2.36	49.75	16.17	0.40	32.07	0.01	0.14	2	100.90	78
9	2.49	49.99	15.96	0.35	31.34	0.01	0.14	1	100.28	77
10	2.29	49.63	15.84	0.29	31.97	0.00	0.14	2	100.16	78
11	2.35	49.63	15.40	0.38	31.49	0.00	0.14	1	99.39	77
12	2.46	49.10	16.17	0.40	31.32	0.02	0.21	2	99.68	77
13	2.45	49.96	15.38	0.37	31.56	0.01	0.16	1	99.89	78
14	2.52	50.16	15.72	0.36	31.99	0.00	0.19	2	100.94	77
15	2.45	49.70	15.31	0.38	31.69	0.00	0.17	1	99.70	76

Sample: IWS 60
Height*: -125.4

Number	Na_2O	SiO_2	CaO	FeO	Al_2O_3	MgO	K_2O	Pos	Total	An
1	2.54	49.06	16.60	0.28	31.71	0.00	0.14	1	100.33	77
2	2.29	48.55	17.07	0.29	32.24	0.03	0.15	2	100.62	79
3	2.40	48.56	16.68	0.29	31.99	0.00	0.15	1	100.07	78
4	2.47	49.12	16.92	0.25	32.19	0.01	0.14	2	101.10	78
5	2.57	49.21	16.88	0.31	31.99	0.01	0.18	1	101.15	77
6	2.49	49.42	16.51	0.28	31.97	0.01	0.13	2	100.81	77
7	2.52	49.09	16.86	0.32	31.92	0.01	0.13	1	100.85	78
8	2.68	49.55	16.48	0.30	31.64	0.02	0.15	2	100.82	76
9	2.55	49.42	16.75	0.32	31.70	0.01	0.17	1	100.92	77
10	2.52	59.50	13.13	0.20	25.35	0.04	0.09	2	100.83	73

Sample: IWS 61
Height*: -127.1

Number	Na_2O	SiO_2	CaO	FeO	Al_2O_3	MgO	K_2O	Pos	Total	An
1	2.47	50.17	16.41	0.30	32.30	0.00	0.14	1	101.79	78
2	2.64	48.09	15.78	0.23	30.95	0.00	0.15	2	97.84	76
3	2.43	48.06	16.26	0.26	31.41	0.00	0.13	1	98.55	78
4	2.45	48.37	15.99	0.28	31.74	0.00	0.14	2	98.97	77
5	2.57	47.56	15.91	0.27	30.95	0.00	0.15	1	97.41	76
6	1.72	47.07	17.91	0.29	33.30	0.00	0.09	2	100.38	84
7	2.54	48.86	16.22	0.31	31.52	0.00	0.17	1	99.62	77
8	2.38	47.49	16.32	0.29	31.34	0.00	0.09	2	97.91	78
9	2.71	50.26	16.10	0.30	32.14	0.00	0.15	1	101.66	76
10	2.44	48.17	16.33	0.27	31.55	0.00	0.13	2	98.89	78
11	2.55	48.60	16.25	0.16	31.70	0.00	0.17	2	99.43	77
12	2.54	49.27	16.21	0.34	32.03	0.00	0.14	1	100.53	77
13	2.62	48.21	16.24	0.26	31.53	0.00	0.14	2	99.00	76
14	2.56	48.41	16.06	0.27	31.29	0.00	0.17	1	98.76	76

Sample: IWS 64
Height*: -132.3

Number	Na_2O	SiO_2	CaO	FeO	Al_2O_3	MgO	K_2O	Pos	Total	An
1	2.62	48.96	16.13	0.20	31.55	0.00	0.12	3	99.58	76
2	2.77	49.35	16.28	0.18	31.30	0.00	0.14	3	100.02	75
3	2.81	49.40	16.17	0.18	31.50	0.00	0.14	3	100.20	75
4	2.79	48.89	16.40	0.21	31.09	0.00	0.16	3	99.54	75
5	2.82	49.20	16.29	0.18	30.95	0.00	0.14	3	99.58	75
6	3.00	50.31	15.54	0.15	31.32	0.00	0.16	3	100.48	73
7	3.33	50.50	15.04	0.21	30.04	0.00	0.18	3	99.30	70
8	3.38	50.24	15.02	0.19	30.05	0.00	0.18	3	99.06	70
9	3.01	49.63	16.00	0.23	30.78	0.00	0.13	3	99.78	74
10	2.97	49.52	15.94	0.20	30.87	0.00	0.13	3	99.63	74

data
PC045

Sample: IWS 66
Height*: -135.7

Number	Na_2O	SiO_2	CaO	FeO	Al_2O_3	MgO	K_2O	Pos	Total	An
1	5.08	55.93	11.2	0.11	28.84	0.00	0.31	3	101.54	54
2	5.08	54.84	10.98	0.16	28.88	0.00	0.36	3	100.30	53
3	4.24	52.35	12.44	0.14	29.96	0.00	0.27	3	99.40	60
4	4.36	53.33	13.05	0.14	30.31	0.01	0.23	3	101.43	61

Sample: IWS 68
Height*: -138.9

Number	Na_2O	SiO_2	CaO	FeO	Al_2O_3	MgO	K_2O	Pos	Total	An
1	2.60	48.69	16.45	0.31	31.52	0.00	0.08	1	99.65	77
2	2.35	47.88	17.09	0.40	31.74	0.00	0.11	2	99.57	79
3	2.43	47.56	16.98	0.36	31.66	0.01	0.11	1	99.11	79
4	2.52	48.16	17.00	0.28	31.80	0.01	0.14	2	99.91	78
5	2.44	48.26	16.77	0.33	31.59	0.02	0.12	1	99.53	78
6	2.47	47.72	16.84	0.33	31.64	0.00	0.13	2	99.13	78
7	2.47	48.35	16.85	0.33	31.49	0.01	0.13	1	99.63	78
8	2.38	48.38	16.95	0.29	31.69	0.00	0.12	2	99.81	79
9	2.87	49.41	16.07	0.39	31.18	0.00	0.06	1	99.98	75
10	2.81	49.13	15.84	0.32	31.04	0.01	0.11	2	99.26	75

data
PC045

MICROPROBE DATA FOR ORTHOPYROXENES

*Height below or above the Merensky Reef

Sample: IWS 93
Height*: 16.4

Number	1	2	3	4	5	6	7	8	9	10
SiO_2	54.65	54.78	54.09	54.92	54.98	54.71	55.38	55.09	55.53	55.07
Al_2O_3	1.11	1.14	1.06	1.04	1.03	1.00	1.03	1.11	0.94	0.95
Na_2O	0.01	0.03	0.03	0.03	0.02	0.01	0.03	0.01	0.02	0.02
MgO	29.22	28.14	27.30	28.52	27.81	28.17	28.01	27.95	28.23	28.10
FeO	12.86	12.59	12.02	12.44	12.42	13.07	12.60	12.63	12.82	12.77
MnO	0.27	0.26	0.23	0.23	0.24	0.24	0.25	0.25	0.24	0.26
NiO	0.00	0.00	0.00	0.00	0.00	0.00	0.00	0.00	0.00	0.00
CaO	0.91	1.42	2.61	1.24	1.76	0.88	1.44	1.11	0.93	0.88
TiO_2	0.14	0.14	0.10	0.13	0.13	0.17	0.19	0.15	0.17	0.17
CrO_2	0.47	0.46	0.48	0.50	0.46	0.46	0.43	0.45	0.47	0.43
TOTAL	99.64	98.96	97.92	99.05	98.85	98.25	99.36	98.75	99.35	99.65
Mg. No.	0.80	0.80	0.80	0.80	0.80	0.79	0.79	0.79	0.79	0.80

Sample: IWS 90
Height*: 11.3

Number	1	2	3	4	5	6	7	8	9	10
SiO_2	55.09	54.46	55.44	55.25	55.63	55.79	55.76	55.50	55.00	54.88
Al_2O_3	1.14	0.93	0.97	1.03	1.02	0.79	0.95	1.00	1.26	1.37
Na_2O	0.03	0.02	0.02	0.04	0.02	0.02	0.03	0.01	0.01	0.03
MgO	30.32	29.46	30.16	29.83	30.75	30.69	30.26	30.61	30.03	29.51
FeO	13.10	12.44	11.89	11.80	11.89	11.88	10.89	11.54	12.28	12.27
MnO	0.28	0.26	0.22	0.27	0.22	0.23	0.25	0.28	0.28	0.23
NiO	0.09	0.10	0.08	0.11	0.07	0.08	0.10	0.10	0.09	0.07
CaO	0.72	1.49	1.45	1.43	1.13	0.87	0.92	0.80	0.69	1.32
TiO_2	0.10	0.16	0.10	0.09	0.09	0.12	0.10	0.10	0.07	0.07
CrO_2	0.38	0.35	0.45	0.45	0.45	0.44	0.42	0.47	0.48	0.43
TOTAL	101.25	99.67	100.78	100.30	101.27	100.91	99.68	99.42	100.19	100.18
Mg. No.	0.80	0.81	0.82	0.82	0.82	0.82	0.83	0.83	0.81	0.81

Sample: IWS 87
Height*: 5.1

Number	1	2	3	4	5	6	7	8	9	10
SiO_2	53.25	53.40	52.96	52.75	53.22	52.99	55.58	55.34	55.01	55.59
Al_2O_3	0.87	0.93	0.88	0.84	0.91	0.77	0.93	0.93	0.91	1.01
Na_2O	0.02	0.02	0.04	0.03	0.01	0.01	0.02	0.02	0.01	0.01
MgO	27.28	26.59	26.71	26.45	26.44	26.47	27.15	27.19	27.12	27.21
FeO	15.50	15.29	15.46	15.15	15.45	15.27	15.62	15.32	15.19	15.63
MnO	0.28	0.26	0.30	0.32	0.29	0.31	0.34	0.35	0.30	0.31
NiO	0.00	0.00	0.00	0.00	0.00	0.00	0.00	0.00	0.00	0.00
CaO	0.00	0.00	0.00	0.00	0.00	0.00	0.00	0.00	0.00	0.00
TiO_2	0.00	0.00	0.00	0.00	0.00	0.00	0.00	0.00	0.00	0.00
CrO_2	0.30	0.27	0.31	0.31	0.30	0.28	0.24	0.24	0.29	0.23
TOTAL	97.50	96.76	96.66	95.85	96.62	96.10	99.88	99.39	98.83	99.99
Mg. No.	0.76	0.76	0.76	0.26	0.77	0.76	0.76	0.76	0.76	0.76

Sample: IWS 86
Height*: 3.4

Number	1	2	3	4	5	6	7	8	9	10
SiO_2	52.42	54.42	54.59	54.20	54.88	54.91	54.85	54.32	54.21	54.56
Al_2O_3	2.46	1.36	1.22	0.66	0.83	0.82	1.06	0.98	1.03	1.06
Na_2O	0.01	0.02	0.00	0.03	0.02	0.01	0.03	0.01	0.08	0.04
MgO	26.21	26.69	26.87	26.56	27.19	27.04	25.96	27.19	25.61	25.47
FeO	15.43	15.48	15.30	15.35	15.43	15.31	14.30	15.31	14.54	14.90
MnO	0.29	0.34	0.28	0.28	0.27	0.32	0.27	0.31	0.28	0.31
NiO	0.00	0.00	0.00	0.00	0.00	0.00	0.00	0.00	0.00	0.00
CaO	0.94	0.96	0.88	0.81	0.87	0.85	2.47	0.87	2.04	2.13
TiO_2	0.23	0.26	0.26	0.30	0.22	0.27	0.22	0.23	0.24	0.23
CrO_2	0.29	0.30	0.31	0.29	0.25	0.31	0.30	0.30	0.35	0.36
TOTAL	98.28	99.83	99.71	98.48	99.71	99.84	99.46	99.52	98.38	98.70
Mg. No.	0.75	0.75	0.76	0.76	0.76	0.76	0.76	0.75	0.75	0.76

Sample: IWS 71
Height*: 0.0

Number	1	2	3	4	5	6	7	8	9	10
SiO_2	54.45	54.72	54.90	55.30	54.65	54.94	54.97	54.97	54.70	54.08
Al_2O_3	1.15	1.21	1.20	0.97	1.25	1.50	1.34	1.25	1.10	0.87
Na_2O	0.01	0.02	0.01	0.03	0.04	0.02	0.03	0.02	0.04	0.05
MgO	29.13	29.29	29.29	29.26	28.95	29.46	29.33	29.50	29.16	28.36
FeO	13.25	13.26	13.49	13.63	12.94	12.75	12.91	12.92	13.51	12.80
MnO	0.32	0.23	0.26	0.31	0.27	0.29	0.30	0.25	0.30	0.25
NiO	0.11	0.10	0.13	0.10	0.11	0.10	0.09	0.11	0.10	0.11
CaO	1.37	0.91	0.78	0.82	1.39	1.08	1.33	1.15	0.82	1.90
TiO_2	0.14	0.18	0.20	0.19	0.16	0.14	0.15	0.17	0.22	0.22
CrO_2	0.39	0.48	0.38	0.31	0.43	0.47	0.46	0.47	0.34	0.31
TOTAL	100.32	100.40	100.64	100.92	100.19	100.75	100.91	100.81	100.29	98.95
Mg. No.	0.79	0.80	0.79	0.79	0.80	0.80	0.80	0.80	0.79	0.80

Sample: IWS 80
Height*: -12.5

Number	1	2	3	4	5	6	7	8	9	10
SiO_2	54.11	54.01	54.21	51.60	54.31	53.87	53.67	53.09	53.01	53.01
Al_2O_3	1.51	0.98	1.11	1.06	1.35	1.29	1.24	1.12	1.26	1.19
Na_2O	0.00	0.00	0.00	0.00	0.00	0.00	0.00	0.00	0.00	0.00
MgO	29.53	28.89	28.70	28.72	29.41	28.93	28.76	29.09	28.82	28.87
FeO	13.43	13.89	14.10	13.57	13.63	13.59	13.26	13.62	13.26	13.21
MnO	0.27	0.27	0.30	0.28	0.26	0.24	0.27	0.26	0.26	0.24
NiO	0.08	0.09	0.09	0.07	0.08	0.08	0.09	0.10	0.07	0.09
CaO	0.71	1.06	0.83	0.83	0.83	1.11	1.88	0.95	1.45	1.51
TiO_2	0.09	0.17	0.19	0.21	0.11	0.12	0.12	0.13	0.19	0.14
CrO_2	0.44	0.34	0.33	0.42	0.42	0.44	0.46	0.44	0.47	0.46
TOTAL	100.17	99.70	99.86	96.76	100.40	99.67	99.75	98.80	98.79	98.72
Mg. No.	0.80	0.80	0.80	0.80	0.81	0.80	0.79	0.79	0.79	0.79

Sample: IWS 78
Height*: -15.9

Number	1	2	3	4	5	6	7	8	9	10
SiO_2	53.95	54.47	54.72	54.78	54.76	54.54	55.18	54.73	53.81	54.12
Al_2O_3	1.12	1.17	1.18	1.30	1.32	1.38	1.47	1.45	1.36	1.39
Na_2O	0.16	0.30	0.09	0.02	0.02	0.03	0.03	0.05	0.12	0.12
MgO	28.46	27.86	27.72	27.01	26.71	25.62	26.94	26.85	24.84	25.16
FeO	13.69	13.23	13.26	13.21	12.83	12.32	13.61	13.37	12.01	12.40
MnO	0.28	0.26	0.27	0.24	0.24	0.27	0.26	0.27	0.24	0.26
NiO	0.00	0.00	0.00	0.00	0.00	0.00	0.00	0.00	0.00	0.00
CaO	0.85	0.85	0.92	1.62	2.36	3.41	0.86	0.87	4.02	3.36
TiO_2	0.21	0.21	0.20	0.19	0.17	0.16	0.16	0.15	0.15	0.11
CrO_2	0.43	0.40	0.42	0.44	0.42	0.38	0.48	0.45	0.52	0.50
TOTAL	99.15	98.75	98.78	98.81	98.83	98.11	98.99	97.74	97.07	97.42
Mg. No.	0.79	0.79	0.78	0.78	0.78	0.78	0.78	0.79	0.78	0.78

Sample: IWS 74
Height*: -22.5

Number	1	2	3	4	5	6	7	8	9	10
SiO_2	53.57	53.24	53.23	53.46	53.61	53.78	54.15	54.28	54.10	53.95
Al_2O_3	0.92	1.13	1.08	1.20	1.14	1.23	1.16	1.18	1.21	1.19
Na_2O	0.01	0.01	0.01	0.01	0.00	0.01	0.03	0.02	0.01	0.01
MgO	26.13	25.44	25.50	25.79	25.72	25.47	25.44	25.62	25.60	25.74
FeO	17.23	16.69	16.93	16.97	16.90	16.82	17.18	16.80	16.85	16.83
MnO	0.30	0.31	0.31	0.29	0.31	0.29	0.32	0.28	0.30	0.27
NiO	0.00	0.00	0.00	0.00	0.00	0.00	0.00	0.00	0.00	0.00
CaO	0.00	0.00	0.00	0.00	0.00	0.00	0.00	0.00	0.00	0.00
TiO_2	0.00	0.00	0.00	0.00	0.00	0.00	0.00	0.00	0.00	0.00
CrO_2	0.24	0.25	0.31	0.32	0.27	0.31	0.28	0.31	0.30	0.28
TOTAL	100.40	97.07	97.37	98.04	97.95	97.92	98.56	98.49	98.37	98.27
Mg. No.	0.73	0.73	0.73	0.73	0.73	0.72	0.73	0.73	0.73	0.73

Sample: IWS 3
Height*: -29.5

Number	1	2	3	4	5	6	7	8	9	10
SiO_2	54.53	54.22	54.22	54.32	54.06	54.73	55.36	54.72	54.98	54.42
Al_2O_3	1.44	1.38	1.26	1.16	1.19	1.10	1.23	1.26	1.02	0.96
Na_2O	0.03	0.03	0.00	0.00	0.00	0.00	0.01	0.00	0.00	0.00
MgO	29.77	28.70	29.47	29.62	29.59	29.55	29.61	29.73	29.88	29.68
FeO	11.34	11.10	11.43	11.71	11.70	11.39	11.56	11.61	11.57	11.68
MnO	0.26	0.25	0.25	0.26	0.25	0.26	0.27	0.24	0.26	0.28
NiO	0.06	0.07	0.07	0.07	0.09	0.08	0.08	0.08	0.08	0.06
CaO	1.99	2.69	1.57	0.89	0.98	1.78	1.44	1.50	1.19	1.35
TiO_2	0.06	0.10	0.10	0.11	0.12	0.17	0.13	0.10	0.18	0.14
CrO_2	0.49	0.44	0.40	0.40	0.40	0.45	0.46	0.43	0.41	0.40
TOTAL	99.97	98.98	98.77	98.54	98.38	99.51	100.15	99.67	99.57	98.97
Mg. No.	0.82	0.82	0.82	0.82	0.82	0.82	0.82	0.82	0.82	0.82

Sample: IWS 7
Height*: -35.7

Number	1	2	3	4	5	6	7	8	9	10
SiO_2	54.82	54.39	53.76	54.98	54.90	54.79	54.47	54.89	55.08	50.49
Al_2O_3	1.29	1.19	1.13	1.43	1.24	1.33	1.29	1.39	1.31	1.61
Na_2O	0.02	0.01	0.00	0.00	0.02	0.00	0.03	0.01	0.00	0.02
MgO	30.01	29.41	29.22	30.31	29.75	30.05	29.22	29.38	29.92	32.85
FeO	12.17	11.94	11.96	12.06	11.86	11.92	11.70	11.58	11.88	13.20
MnO	0.29	0.23	0.24	0.26	0.22	0.23	0.21	0.21	0.22	0.25
NiO	0.08	0.07	0.07	0.09	0.10	0.08	0.08	0.09	0.11	0.09
CaO	0.90	0.91	0.76	0.80	1.36	0.98	1.41	1.76	1.13	1.32
TiO_2	0.18	0.14	0.17	0.06	0.15	0.14	0.21	0.17	0.13	0.11
CrO_2	0.47	0.47	0.47	0.45	0.43	0.46	0.47	0.46	0.44	0.51
TOTAL	100.23	98.76	97.78	100.44	100.03	99.98	99.09	98.94	100.22	100.42
Mg. No.	0.81	0.81	0.81	0.82	0.82	0.82	0.82	0.82	0.82	0.81

Sample: IWS 10
Height*: -40.8

Number	1	2	3	4	5	6	7	8	9
SiO_2	54.37	54.67	54.62	54.37	54.13	54.33	54.23	54.05	54.82
Al_2O_3	1.47	1.48	1.53	1.49	1.54	1.51	1.52	1.30	1.34
Na_2O	0.01	0.00	0.01	0.04	0.03	0.00	0.01	0.00	0.01
MgO	30.06	30.02	29.77	29.53	29.33	29.94	29.96	29.92	30.12
FeO	11.54	11.81	11.64	11.42	11.33	11.69	11.80	11.45	11.28
MnO	0.22	0.19	0.18	0.18	0.22	0.21	0.21	0.22	0.23
NiO	0.08	0.09	0.09	0.09	0.07	0.07	0.07	0.08	0.09
CaO	1.48	0.77	1.12	1.72	1.80	1.00	0.91	0.73	0.82
TiO_2	0.13	0.19	0.12	0.15	0.15	0.08	0.10	0.14	0.17
CrO_2	0.50	0.36	0.50	0.48	0.44	0.44	0.50	0.22	0.28
TOTAL	99.86	99.58	99.58	99.47	99.04	99.27	99.31	98.11	99.16
Mg. No.	0.82	0.82	0.82	0.82	0.82	0.83	0.82	0.82	0.83

Sample: IWS 12
Height*: -44.1

Number	1	2	3	4	5	6	7	8	9	10
SiO_2	54.48	54.80	55.16	54.76	54.96	55.20	54.48	54.86	55.22	55.33
Al_2O_3	0.99	1.14	1.06	1.09	1.07	1.06	1.37	1.1	1.10	1.10
Na_2O	0.00	0.00	0.00	0.00	0.00	0.01	0.00	0.00	0.00	0.00
MgO	30.47	29.96	30.21	29.91	30.17	29.83	30.35	29.54	30.12	30.43
FeO	12.37	12.06	12.21	12.39	12.02	12.14	12.04	11.88	12.15	12.12
MnO	0.23	0.22	0.26	0.25	0.26	0.23	0.24	0.26	0.28	0.23
NiO	0.06	0.07	0.06	0.06	0.08	0.70	0.07	0.08	0.04	0.07
CaO	0.64	1.04	0.82	0.78	0.90	1.18	0.65	1.20	0.88	1.01
TiO_2	0.12	0.14	0.08	0.10	0.12	0.08	0.07	0.14	0.10	0.09
CrO_2	0.44	0.46	0.44	0.46	0.44	0.36	0.44	0.43	0.40	0.34
TOTAL	99.73	99.98	100.30	99.80	100.02	100.79	99.71	99.53	100.29	100.72
Mg. No.	0.81	0.82	0.82	0.81	0.82	0.81	0.82	0.82	0.82	0.82

Sample: IWS 19
Height*: -55.8

Number	1	2	3	4	5	6	7
SiO_2	54.11	39.29	39.39	39.11	39.19	39.10	38.96
Al_2O_3	1.18	0.12	0.13	0.12	0.15	0.08	0.09
Na_2O	0.01	0.01	0.00	0.01	0.03	0.01	0.03
MgO	27.76	40.90	40.47	40.56	40.66	40.76	40.90
FeO	12.21	19.63	19.51	19.39	19.34	19.36	19.41
MnO	0.27	0.25	0.23	0.27	0.28	0.25	0.24
NiO	0.00	0.00	0.00	0.00	0.00	0.00	0.00
CaO	0.00	0.00	0.00	0.00	0.00	0.00	0.00
TiO_2	0.00	0.00	0.00	0.00	0.00	0.00	0.00
CrO_2	0.37	0.00	0.00	0.00	0.00	0.01	0.03
TOTAL	95.91	100.20	99.73	99.46	99.65	99.57	99.66
Mg. No.	0.80	0.78	0.78	0.79	0.79	0.79	0.78

Sample: IWS 20
Height*: -57.4

Number	1	2	3	4	5	6	7	8	9	10
SiO_2	55.40	55.34	55.48	55.14	55.15	55.00	55.11	55.26	55.28	55.39
Al_2O_3	0.78	1.58	1.52	1.55	1.44	1.58	1.58	1.39	1.51	1.55
Na_2O	0.00	0.01	0.01	0.02	0.01	0.03	0.02	0.05	0.00	0.00
MgO	30.42	28.41	28.29	28.73	28.91	28.34	28.89	28.11	29.20	29.25
FeO	12.48	12.41	12.36	12.32	12.63	11.81	12.33	11.54	12.47	12.52
MnO	0.24	0.25	0.24	0.21	0.22	0.22	0.23	0.23	0.23	0.22
NiO	0.00	0.00	0.00	0.00	0.00	0.00	0.00	0.00	0.00	0.00
CaO	0.00	0.00	0.00	0.00	0.00	0.00	0.00	0.00	0.00	0.00
TiO_2	0.00	0.00	0.00	0.00	0.00	0.00	0.00	0.00	0.00	0.00
CrO_2	0.10	0.43	0.46	0.43	0.39	0.44	0.44	0.42	0.44	0.44
TOTAL	99.42	98.43	98.36	98.40	98.75	96.42	98.60	97.00	99.13	99.37
Mg. No.	0.81	0.81	0.80	0.81	0.80	0.81	0.81	0.82	0.81	0.81

Sample: IWS 23
Height*: -62.6

Number	1	2	3	4	5	6	7	8	9	10
SiO_2	55.24	55.26	55.62	55.10	55.50	55.66	55.10	55.19	55.52	55.29
Al_2O_3	1.19	1.18	1.28	1.25	1.24	1.30	1.30	1.30	1.26	1.25
Na_2O	0.01	0.00	0.00	0.00	0.00	0.01	0.02	0.01	0.00	0.00
MgO	29.23	28.64	28.75	28.91	28.91	28.90	28.64	28.57	28.75	28.86
FeO	12.46	12.70	12.67	12.83	12.77	13.00	12.80	12.93	12.95	12.02
MnO	0.23	0.26	0.23	0.21	0.25	0.24	0.22	0.20	0.26	0.22
NiO	0.00	0.00	0.00	0.00	0.00	0.00	0.00	0.00	0.00	0.00
CaO	0.00	0.00	0.00	0.00	0.00	0.00	0.00	0.00	0.00	0.00
TiO_2	0.00	0.00	0.00	0.00	0.00	0.00	0.00	0.00	0.00	0.00
CrO_2	0.46	0.45	0.42	0.43	0.41	0.43	0.47	0.44	0.43	0.43
TOTAL	98.82	98.49	98.97	98.70	99.08	99.54	98.55	98.64	99.17	98.07
Mg. NO.	0.81	0.80	0.80	0.80	0.80	0.80	0.81	0.81	0.80	0.81

Sample: IWS 24
Height*: - 64.2

Number	1	2	3	4	5	6	7	8
SiO_2	53.45	53.68	54.48	54.22	54.67	54.58	53.92	53.94
Al_2O_3	1.23	1.22	1.29	1.24	1.20	1.26	1.23	1.25
Na_2O	0.01	0.01	0.01	0.02	0.00	0.00	0.02	0.02
MgO	26.49	26.58	26.76	26.63	26.75	26.85	26.91	27.07
FeO	16.08	16.35	16.64	16.30	15.89	16.24	15.94	15.88
MnO	0.30	0.30	0.33	0.34	0.30	0.30	0.26	0.32
NiO	0.07	0.08	0.07	0.10	0.09	0.10	0.10	0.08
CaO	1.00	0.95	0.91	0.76	0.89	0.97	0.97	1.00
TiO_2	0.19	0.22	0.18	0.22	0.21	0.22	0.16	0.17
CrO_2	0.34	0.34	0.36	0.34	0.33	0.37	0.34	0.31
TOTAL	99.16	99.73	101.03	100.17	100.33	100.89	99.85	100.04
Mg. No	0.75	0.74	0.74	0.74	0.75	0.75	0.75	0.75

Sample: IWS 26
Height*: -67.6

Number	1	2	3	4	5	6	7	8	9	10
SiO_2	53.89	54.15	54.05	54.21	54.27	53.75	54.37	54.28	54.50	54.21
Al_2O_3	1.01	0.91	0.99	1.08	1.05	0.97	0.90	0.93	0.93	0.92
Na_2O	0.02	0.01	0.01	0.03	0.02	0.00	0.00	0.01	0.02	0.01
MgO	26.02	25.46	25.61	25.28	25.38	25.38	25.32	25.57	25.62	25.69
FeO	17.79	17.80	17.19	17.01	17.03	17.50	17.70	17.64	17.41	17.68
MnO	0.36	0.03	0.33	0.34	0.34	0.33	0.34	0.37	0.34	0.33
NiO	0.00	0.00	0.00	0.00	0.00	0.00	0.00	0.00	0.00	0.00
CaO	0.00	0.00	0.00	0.00	0.00	0.00	0.00	0.00	0.00	0.00
TiO_2	0.00	0.00	0.00	0.00	0.00	0.00	0.00	0.00	0.00	0.00
CrO_2	0.35	0.35	0.35	0.36	0.33	0.37	0.28	0.31	0.31	0.34
TOTAL	99.44	98.71	98.53	98.31	98.42	98.30	98.91	99.11	99.13	99.18
Mg. No.	0.72	0.71	0.73	0.72	0.72	0.72	0.71	0.72	0.72	0.72

Sample: IWS 30
Height*: -74.4

Number	1	2	3	4	5	6	7	8	9	10
SiO_2	53.80	54.16	53.57	54.28	54.31	54.13	54.32	55.71	53.34	53.78
Al_2O_3	0.91	1.39	1.23	1.02	1.14	1.25	0.97	1.05	1.08	1.01
Na_2O	0.02	0.07	0.01	0.00	0.01	0.02	0.00	0.00	0.00	0.00
Mgo	28.25	25.61	27.60	27.71	27.68	27.37	27.73	27.63	27.57	26.81
FeO	15.07	13.69	15.27	15.35	14.95	14.95	15.48	15.01	15.59	14.94
MnO	0.26	0.28	0.30	0.28	0.30	0.29	0.29	0.31	0.32	0.29
NiO	0.08	0.08	0.10	0.11	0.09	0.09	0.08	0.10	0.08	0.09
CaO	1.52	4.23	1.28	0.89	1.27	1.37	0.79	0.91	0.74	2.06
TiO_2	0.13	0.12	0.20	0.20	0.18	0.12	0.21	0.20	0.10	0.54
CrO_2	0.45	0.56	0.47	0.47	0.49	0.52	0.39	0.43	0.47	0.89
TOTAL	100.49	100.19	100.03	100.31	100.42	100.11	100.26	101.35	99.29	100.41
Mg. No.	0.76	0.76	0.76	0.77	0.77	0.77	0.76	0.77	0.76	0.76

Sample: IWS 31
Height*: -76.2

Number	1	2	3	4	5	6	7	8	9	10
SiO_2	54.30	54.49	54.06	54.47	54.60	54.61	54.53	54.78	54.52	54.39
Al_2O_3	0.81	0.79	0.80	0.82	0.85	0.88	0.86	0.89	1.04	1.10
Na_2O	0.01	0.01	0.00	0.02	0.02	0.03	0.02	0.05	0.02	0.02
MgO	27.33	26.96	26.73	26.45	26.46	26.49	26.40	26.45	27.09	27.03
FeO	16.05	15.90	15.55	15.84	15.85	15.87	15.84	16.01	14.99	14.90
MnO	0.29	0.32	0.26	0.30	0.31	0.33	0.27	0.29	0.30	0.27
NiO	0.00	0.00	0.00	0.00	0.00	0.00	0.00	0.00	0.00	0.00
CaO	0.00	0.00	0.00	0.00	0.00	0.00	0.00	0.00	0.00	0.00
TiO_2	0.00	0.00	0.00	0.00	0.00	0.00	0.00	0.00	0.00	0.00
CrO_2	0.23	0.24	0.23	0.19	0.20	0.17	0.22	0.19	0.41	0.41
TOTAL	99.02	98.71	97.63	98.09	98.29	98.38	98.14	98.66	98.37	98.12
Mg. No.	0.75	0.75	0.75	0.74	0.74	0.75	0.75	0.75	0.76	0.76

Sample: IWS 33
Height*: -79.5

Number	1	2	3	4	5	6	7	8	9	10
SiO_2	54.73	55.05	55.17	55.04	54.92	54.57	53.51	54.76	54.85	54.82
Al_2O_3	0.86	0.88	0.90	0.95	0.94	0.99	0.89	1.06	1.04	0.92
Na_2O	0.00	0.00	0.01	0.00	0.01	0.01	0.01	0.03	0.01	0.00
MgO	27.83	27.31	27.28	27.09	27.06	27.03	27.01	26.73	26.74	26.81
FeO	15.51	15.28	15.56	15.37	15.28	15.93	16.04	16.08	16.14	16.20
MnO	0.33	0.30	0.32	0.32	0.33	0.31	0.29	0.31	0.30	0.29
NiO	0.00	0.00	0.00	0.00	0.00	0.00	0.00	0.00	0.00	0.00
CaO	0.00	0.00	0.00	0.00	0.00	0.00	0.00	0.00	0.00	0.00
TiO_2	0.00	0.00	0.00	0.00	0.00	0.00	0.00	0.00	0.00	0.00
CrO_2	0.30	0.30	0.34	0.32	0.32	0.33	0.36	0.38	0.37	0.37
TOTAL	99.56	99.12	99.58	99.09	98.86	99.17	98.11	99.35	99.45	99.41
Mg. No.	0.76	0.76	0.75	0.76	0.76	0.75	0.75	0.75	0.77	0.76

Sample: IWS 36
Height*: -84.6

Number	1	2	3	4	5	6	7	8
SiO_2	54.04	53.55	54.43	53.60	54.10	54.10	53.85	53.47
Al_2O_3	1.08	1.10	1.22	1.13	1.09	1.11	1.16	1.11
Na_2O	0.01	0.01	0.01	0.02	0.01	0.02	0.00	0.01
MgO	27.32	26.67	26.98	26.51	26.73	26.80	26.61	26.39
FeO	15.16	14.96	15.14	15.12	15.21	14.91	14.95	14.78
MnO	0.30	0.27	0.27	0.28	0.26	0.29	0.30	0.28
NiO	0.09	0.09	0.11	0.08	0.12	0.10	0.11	0.10
CaO	1.59	1.30	1.14	1.35	1.35	1.71	1.65	1.83
TiO_2	0.19	0.21	0.16	0.16	0.29	0.18	0.08	0.20
CrO_2	0.40	0.42	0.45	0.44	0.42	0.45	0.43	0.42
TOTAL	100.18	98.58	99.91	98.69	99.58	99.67	99.14	98.59
Mg. No.	0.76	0.76	0.76	0.76	0.76	0.76	0.77	0.76

Sample: IWS 38
Height*: -87.7

Number	1	2	3	4	5	6	7	8	9	10
SiO_2	54.69	54.18	52.91	54.24	54.29	54.26	54.63	53.59	53.56	53.55
Al_2O_3	1.10	1.07	1.14	1.14	0.98	0.98	0.93	1.07	1.05	1.06
Na_2O	0.01	0.01	0.04	0.03	0.01	0.00	0.02	0.02	0.03	0.04
MgO	29.42	28.60	28.34	28.51	28.64	29.15	28.59	28.77	28.41	27.91
FeO	14.54	14.04	13.84	13.97	14.12	14.63	14.21	14.06	13.78	13.62
MnO	0.29	0.26	0.28	0.31	0.27	0.28	0.30	0.32	0.30	0.27
NiO	0.08	0.08	0.10	0.08	0.08	0.11	0.09	0.10	0.09	0.07
CaO	0.87	0.16	2.03	1.37	1.33	0.79	1.36	1.19	1.50	2.50
TiO_2	0.13	0.15	0.18	0.15	0.13	0.15	0.12	0.15	0.16	0.16
CrO_2	0.44	0.47	0.54	0.55	0.48	0.45	0.51	0.51	0.51	0.50
TOTAL	101.57	99.02	99.40	100.35	100.33	100.80	100.76	99.78	99.39	99.68
Mg. No.	0.78	0.78	0.77	0.78	0.78	0.78	0.78	0.78	0.77	0.78

Sample: IWS 47
Height*: -103.4

Number	1	2	3	4	5	6	7	8	9	10
SiO_2	54.46	54.73	54.94	54.09	54.92	55.13	55.02	54.90	55.43	55.15
Al_2O_3	1.19	1.51	1.34	1.41	1.30	1.43	1.33	1.42	1.40	1.42
Na_2O	0.04	0.01	0.01	0.06	0.01	0.02	0.01	0.05	0.00	0.01
MgO	28.35	28.36	28.39	27.26	28.82	28.45	28.39	27.67	28.46	28.45
FeO	12.41	12.67	12.73	12.14	12.86	12.63	12.97	12.49	12.94	12.96
MnO	0.25	0.24	0.25	0.23	0.26	0.21	0.28	0.26	0.24	0.25
NiO	0.00	0.00	0.00	0.00	0.00	0.00	0.00	0.00	0.00	0.00
CaO	0.00	0.00	0.00	0.00	0.00	0.00	0.00	0.00	0.00	0.00
TiO_2	0.00	0.00	0.00	0.00	0.00	0.00	0.00	0.00	0.00	0.00
CrO_2	0.46	0.55	0.60	0.58	0.54	0.54	0.53	0.58	0.48	0.57
TOTAL	97.16	98.07	98.26	95.77	98.71	98.41	98.53	97.37	98.95	98.56
Mg. No.	0.80	0.80	0.80	0.80	0.79	0.80	0.79	0.80	0.80	0.80

Sample: IWS 48
Height*: -105.0

Number	1	2	3	4	5	6	7	8	9	10
SiO_2	53.93	54.32	54.80	54.85	54.62	55.27	55.34	55.30	54.80	54.95
Al_2O_3	1.09	0.99	0.87	0.99	0.99	0.88	0.80	1.00	0.94	0.90
Na_2O	0.00	0.01	0.02	0.01	0.02	0.00	0.01	0.00	0.01	0.08
MgO	28.78	28.06	28.22	28.10	27.90	28.86	28.56	28.20	27.88	27.44
FeO	13.54	13.29	13.29	13.31	12.78	13.08	13.77	13.90	13.78	12.89
MnO	0.26	0.25	0.25	0.26	0.27	0.27	0.33	0.29	0.26	0.27
NiO	0.00	0.00	0.00	0.00	0.00	0.00	0.00	0.00	0.00	0.00
CaO	0.69	1.18	1.29	1.05	1.66	0.71	0.83	0.80	1.03	2.51
TiO_2	0.14	0.19	0.20	0.20	0.21	0.20	0.21	0.22	0.23	0.21
CrO_2	0.29	0.41	0.36	0.40	0.46	0.41	0.35	0.36	0.33	0.41
TOTAL	98.72	98.70	99.30	99.17	98.91	99.68	99.85	100.07	99.26	99.66
Mg. No.	0.79	0.79	0.79	0.79	0.80	0.28	0.78	0.78	0.78	0.79

Sample: IWS 50
Height*: -108.5

Number	1	2	3	4	5	6	7	8	9
SiO_2	54.93	55.51	52.85	52.94	55.07	55.10	54.77	53.24	52.37
Al_2O_3	0.99	1.12	1.00	1.08	1.01	1.24	1.39	1.29	1.17
Na_2O	0.03	0.04	0.06	0.03	0.03	0.04	0.03	0.03	0.06
MgO	30.58	30.54	29.38	29.27	29.71	30.15	28.69	29.41	29.03
FeO	12.98	13.10	12.67	12.65	12.92	12.99	12.11	12.75	12.31
MnO	0.26	0.25	0.26	0.27	0.28	0.26	0.26	0.28	0.26
NiO	0.06	0.06	0.05	0.07	0.06	0.09	0.07	0.07	0.07
CaO	1.20	0.71	1.91	1.55	1.29	0.71	2.59	1.59	2.17
TiO_2	0.11	0.12	0.13	0.13	0.12	0.12	0.10	0.14	0.12
CrO_2	0.45	10.48	0.52	0.51	0.55	0.52	0.59	0.54	0.58
TOTAL	101.59	101.93	98.83	98.50	101.04	101.22	100.64	99.34	98.11
Mg. No.	0.81	0.81	0.81	0.82	0.82	0.81	0.81	0.81	0.83

Sample: IWS 52
Height*: -112.7

Number	1	2	3	4	5	6	7	8	9	10
SiO_2	54.92	55.05	54.80	55.04	54.70	54.88	54.97	55.03	54.81	54.40
Al_2O_3	1.18	1.47	1.32	1.34	1.10	0.96	1.10	1.21	1.28	1.28
Na_2O	0.00	0.03	0.00	0.03	0.01	0.00	0.00	0.03	0.00	0.00
MgO	30.27	28.16	29.63	28.18	29.47	29.53	29.30	29.13	29.16	29.41
FeO	12.74	11.87	12.57	11.62	12.54	12.46	12.26	12.23	12.42	12.38
MnO	0.26	0.25	0.26	0.22	0.24	0.26	0.25	0.21	0.26	0.22
NiO	0.06	0.07	0.08	0.08	0.07	0.07	0.07	0.07	0.07	0.06
CaO	0.97	2.90	0.89	3.16	0.99	0.83	1.16	1.61	1.54	1.06
TiO_2	0.07	0.06	0.06	0.10	0.07	0.07	0.10	0.10	0.12	0.09
CrO_2	0.46	0.57	0.49	0.52	0.50	0.49	0.48	0.42	0.47	0.48
TOTAL	100.93	100.43	100.10	100.29	99.69	99.55	99.69	100.04	100.13	99.38
Mg. No.	0.81	0.81	0.81	0.82	0.82	0.81	0.81	0.81	0.81	0.81

Sample: IWS 54
Height*: -116.0

Number	1	2	3	4	5	6	7	8	9	10
SiO_2	53.85	54.76	54.78	55.08	55.31	54.39	54.55	54.65	54.09	55.14
Al_2O_3	0.88	0.78	1.01	0.95	0.91	0.95	0.95	1.04	0.91	0.99
Na_2O	0.07	0.04	0.02	0.03	0.03	0.03	0.02	0.04	0.02	0.01
MgO	29.30	29.19	29.40	29.69	30.00	29.24	29.40	28.61	29.22	29.72
FeO	12.99	12.75	12.71	12.88	12.68	12.54	13.03	12.62	12.89	13.38
MnO	0.26	0.25	0.26	0.24	0.24	0.23	0.25	0.26	0.26	0.26
NiO	0.07	0.06	0.07	0.08	0.08	0.07	0.06	0.08	0.09	0.09
CaO	1.21	1.24	1.19	0.69	0.96	1.10	1.19	2.17	1.35	0.95
TiO_2	0.16	0.21	0.24	0.30	0.20	0.21	0.14	0.18	0.16	0.21
CrO_2	0.46	0.43	0.49	0.48	0.47	0.56	0.49	0.50	0.45	0.40
TOTAL	99.25	99.71	100.17	100.42	100.88	99.32	100.08	100.15	99.45	101.15
Mg. No.	0.80	0.81	0.81	0.82	0.81	0.81	0.80	0.79	0.81	0.81

Sample: IWS 56
Height*: -119.0

Number	1	2	3	4	5	6	7	8	9
SiO_2	54.60	54.43	55.15	54.05	54.62	54.43	54.03	53.78	53.80
Al_2O_3	0.88	1.05	1.04	1.14	1.05	1.05	0.99	0.95	0.97
Na_2O	0.02	0.01	0.04	0.04	0.01	0.01	0.02	0.00	0.01
MgO	29.75	28.60	28.64	28.79	29.17	28.84	28.95	28.71	28.78
FeO	13.53	12.76	12.57	12.81	13.16	12.85	13.35	12.98	12.76
MnO	0.30	0.29	0.29	0.24	0.29	0.25	0.28	0.25	0.23
NiO	0.07	0.05	0.06	0.07	0.06	0.07	0.08	0.06	0.06
CaO	0.91	1.45	1.76	1.25	1.23	1.42	0.86	1.31	1.48
TiO_2	0.21	0.19	0.19	0.17	0.17	0.12	0.19	0.17	0.18
CrO_2	0.46	0.47	0.49	0.53	0.46	0.49	0.43	0.48	0.46
TOTAL	100.73	99.31	99.23	99.09	100.22	99.53	99.18	98.69	98.7
Mg. No.	0.80	0.80	0.80	0.80	0.79	0.80	0.79	0.79	0.80

Sample: IWS 57
Height*: -120.5

Number	1	2	3	4	5	6	7	8	9	10
SiO_2	54.81	54.62	54.34	54.55	54.62	55.08	54.83	54.29	54.89	54.54
Al_2O_3	0.88	0.69	0.88	0.99	0.89	0.89	0.85	1.01	0.85	0.93
Na_2O	0.00	0.01	0.01	0.02	0.02	0.01	0.02	0.03	0.02	0.01
MgO	28.48	28.07	28.13	27.74	27.46	27.85	28.12	27.65	28.01	27.86
FeO	13.43	13.64	13.55	13.22	13.24	13.46	13.40	13.44	13.65	13.56
MnO	0.28	0.27	0.26	0.29	0.26	0.27	0.26	0.27	0.27	0.31
NiO	0.00	0.00	0.00	0.00	0.00	0.00	0.00	0.00	0.00	0.00
CaO	0.00	0.00	0.00	0.00	0.00	0.00	0.00	0.00	0.00	0.00
TiO_2	0.00	0.00	0.00	0.00	0.00	0.00	0.00	0.00	0.00	0.00
CrO_2	0.44	0.35	0.44	0.51	0.43	0.36	0.42	0.54	0.38	0.45
TOTAL	98.32	97.65	97.61	97.32	96.92	97.92	97.90	97.23	98.07	97.66
Mg. No.	0.79	0.79	0.79	0.78	0.79	0.78	0.79	0.79	0.78	0.79

Sample: IWS 60
Height*: -125.4

Number	1	2	3	4	5	6	7	8
SiO_2	54.23	54.94	55.16	53.80	54.39	53.94	53.76	54.34
Al_2O_3	0.91	0.97	0.90	0.98	0.99	0.89	0.94	0.93
Na_2O	0.01	0.01	0.01	0.02	0.01	0.03	0.01	0.01
MgO	27.11	27.08	27.41	26.98	27.32	27.16	27.53	27.36
FeO	13.93	13.52	14.10	14.03	14.05	13.89	13.88	13.95
MnO	0.28	0.28	0.31	0.26	0.31	0.26	0.27	0.29
NiO	0.00	0.00	0.00	0.00	0.00	0.00	0.00	0.00
CaO	0.00	0.00	0.00	0.00	0.00	0.00	0.00	0.00
TiO_2	0.00	0.00	0.00	0.00	0.00	0.00	0.00	0.00
CrO_2	0.35	0.38	0.38	0.43	0.45	0.37	0.40	0.40
TOTAL	96.82	97.18	98.27	96.50	97.52	96.54	96.63	97.28
Mg. No.	0.77	0.78	0.78	0.77	0.77	0.77	0.78	0.78

Sample: IWS 62
Height*: -128.9

Number	1	2	3	4	5	6	7	8	9	10
SiO_2	54.41	54.99	54.52	54.26	54.67	55.11	54.42	54.61	54.46	54.43
Al_2O_3	0.61	0.59	0.60	0.61	0.64	0.63	0.57	0.65	0.65	0.73
Na_2O	0.02	0.03	0.02	0.04	0.04	0.03	0.03	0.04	0.04	0.03
MgO	27.54	27.43	27.19	27.21	27.18	27.33	27.37	27.25	27.30	27.22
FeO	14.00	13.88	13.78	13.79	13.92	14.03	13.91	14.50	14.39	14.09
MnO	0.02	0.02	0.02	0.02	0.02	0.02	0.02	0.02	0.02	0.02
NiO	0.00	0.00	0.00	0.00	0.00	0.00	0.00	0.00	0.00	0.00
CaO	0.00	0.00	0.00	0.00	0.00	0.00	0.00	0.00	0.00	0.00
TiO_2	0.00	0.00	0.00	0.00	0.00	0.00	0.00	0.00	0.00	0.00
CrO_2	0.39	0.42	0.38	0.40	0.36	0.31	0.39	0.31	0.34	0.42
TOTAL	96.99	97.35	96.51	96.33	96.83	97.46	96.71	97.38	97.20	96.91
Mg. No.	0.77	0.77	0.78	0.77	0.78	0.77	0.77	0.78	0.77	0.78

Sample: IWS 64
Height*: -132.3

Number	1	2	3	4	5	6	7	8	9	10
SiO_2	54.14	54.02	54.32	54.13	54.88	54.87	54.85	54.77	54.32	54.30
Al_2O_3	1.23	1.12	1.14	1.22	1.06	1.07	1.05	1.26	1.15	1.25
Na2O	0.04	0.03	0.03	0.05	0.03	0.03	0.06	0.03	0.04	0.04
MgO	28.75	28.70	28.56	28.87	29.10	28.74	28.87	28.17	27.93	27.95
FeO	12.74	12.97	13.09	13.17	13.17	13.43	13.40	12.77	13.13	12.90
MnO	0.29	0.27	0.26	0.28	0.25	0.30	0.30	0.27	0.29	0.29
NiO	0.08	0.06	0.09	0.09	0.09	0.07	0.10	0.07	0.09	0.10
CaO	2.11	1.67	1.71	1.19	1.07	1.45	1.04	2.08	1.81	1.71
TiO_2	0.15	0.13	0.18	0.13	0.11	0.11	0.12	0.11	0.11	0.09
CrO_2	0.52	0.49	0.47	0.57	0.48	0.50	0.50	0.53	0.52	0.48
TOTAL	100.05	99.46	99.85	99.7	100.24	100.57	100.29	99.95	99.39	99.11
Mg. No.	0.80	0.79	0.80	0.79	0.80	0.79	0.79	0.79	0.79	0.79

Sample: IWS 65
Height*: -134.0

Number	1	2	3	4	5	6	7	8	9
SiO_2	53.93	55.01	54.86	54.68	54.85	54.28	54.49	54.27	54.73
Al_2O_3	1.10	0.78	0.75	1.16	1.16	1.09	1.00	0.88	1.06
Na_2O	0.02	0.01	0.03	0.03	0.02	0.04	0.01	0.03	0.04
MgO	28.38	28.47	28.43	28.26	28.74	28.14	28.86	28.36	28.41
FeO	14.33	14.17	14.29	14.30	14.14	13.70	14.19	14.08	14.04
MnO	0.25	0.29	0.29	0.29	0.28	0.26	0.27	0.27	0.22
NiO	0.08	0.06	0.08	0.07	0.07	0.07	0.07	0.06	0.07
CaO	1.47	1.72	1.79	1.43	1.40	2.08	1.14	1.44	1.65
TiO_2	0.19	0.15	0.13	0.07	0.10	0.09	0.11	0.13	0.11
CrO_2	0.45	0.35	0.35	0.43	0.47	0.48	0.42	0.41	0.49
TOTAL	100.20	101.01	101.00	100.72	101.23	100.23	100.56	99.93	100.82
Mg. No.	0.78	0.78	0.78	0.77	0.78	0.79	0.78	0.78	0.79

MICROPROBE DATA FOR CHROMITE

* Height below or above the Merensky Reef

	Sample: IWS 6.1 Height*: -109.2					Sample: IWS 51A Height*: -111.8			
Number	1	2	3	4	5	1	2	3	4
TiO_2	1.09	0.95	1.04	3.15	1.00	1.55	1.75	1.43	1.05
FeO	29.97	29.95	29.28	32.70	30.39	31.07	30.33	30.31	32.39
Fe_2O_3	17.04	16.51	16.19	14.67	20.31	16.57	14.67	16.22	16.04
MgO	2.39	2.70	2.96	1.35	2.43	1.92	2.79	1.96	0.69
CaO	0.00	0.00	0.00	0.00	0.00	0.00	0.00	0.00	0.00
MnO	0.38	0.36	0.36	0.35	0.36	0.45	0.37	0.42	0.48
Al_2O_3	9.19	9.17	10.48	6.77	8.03	5.67	5.90	6.09	5.72
Cr_2O_3	38.58	40.79	38.31	38.41	38.53	43.07	45.54	41.84	43.85
V_2O_5	0.57	0.54	0.56	0.59	0.56	0.75	0.52	0.62	0.49
TOTAL	99.22	100.97	99.18	97.99	101.63	101.05	101.88	98.91	100.71
Cr/(Cr + Al)	0.81	0.82	0.26	0.85	0.83	0.88	0.89	0.87	0.88
$Cr/(Fe^{2+}+Fe^{3+})$	0.82	0.88	0.84	0.81	0.76	0.90	1.01	0.90	0.91
$Fe^{3+}/(Fe^{3+}+Al+Cr)$	0.26	0.25	0.25	0.24	0.30	0.25	0.22	0.25	0.24
$Mg(Mg+Fe^{2+})$	0.07	0.08	0.09	0.04	0.07	0.06	0.08	0.06	0.02

	Sample: IWS 50 Height*: -108.5					
Number	1	2	3	4	5	6
TiO_2	1.06	1.29	1.14	0.96	1.05	1.10
FeO	25.66	25.76	27.39	28.44	27.56	24.22
Fe_2O_3	9.79	10.31	12.41	12.19	9.87	10.18
MgO	5.65	6.03	3.70	3.47	4.69	6.43
CaO	0.00	0.00	0.00	0.00	0.00	0.00
MnO	0.34	0.34	0.42	0.41	0.31	0.34
Al_2O_3	11.99	10.59	8.92	8.54	10.81	11.59
Cr_2O_3	44.70	47.11	42.96	45.74	46.73	44.71
V_2O_5	0.41	0.34	0.37	0.38	0.42	0.34
TOTAL	99.61	101.78	97.30	100.14	101.44	98.91
Cr/(Cr + Al)	0.79	0.82	0.83	0.84	0.81	0.79
$Cr/(Fe^{2+}+Fe^{3+})$	1.26	1.31	1.08	1.13	1.25	1.30
$Fe^{3+}/(Fe^{3+}+Al+Cr)$	0.15	0.15	0.19	0.18	0.15	1.15
$Mg(Mg+Fe^{2+})$	0.18	0.19	0.12	0.11	0.14	0.21

PC091

	Sample: IWS 67 Height*: -137.3						Sample: IWS 66 Height*: -135.7				
Number	1	2	3	4	5	6	1	2	3	4	5
TiO_2	0.71	0.72	0.69	0.80	0.82	0.87	1.84	1.85	1.81	2.09	1.52
FeO	21.13	20.09	21.30	21.38	21.38	22.22	28.40	28.83	27.59	27.38	27.94
Fe_2O_3	8.10	9.12	7.58	7.78	7.44	6.76	13.52	12.98	14.37	12.04	10.94
MgO	9.89	9.03	9.13	8.95	8.90	8.69	3.80	4.02	3.93	4.37	4.44
CaO	0.00	0.00	0.00	0.00	0.00	0.00	0.00	0.00	0.00	0.00	0.00
MnO	0.29	0.28	0.26	0.26	0.25	0.31	0.35	0.39	0.36	0.37	0.35
Al_2O_3	15.79	15.77	15.96	15.93	15.75	15.89	7.79	7.91	7.85	10.04	9.35
Cr_2O_3	44.43	41.69	45.96	44.89	45.22	46.57	43.15	45.31	41.17	40.29	45.97
V_2O_5	0.48	0.49	0.44	0.41	0.41	0.44	0.55	0.49	0.54	0.52	0.50
TOTAL	99.83	97.18	101.31	100.41	100.17	101.74	99.40	101.76	97.62	97.09	101.01
Cr/(Cr + Al)	0.74	0.73	0.74	0.24	0.74	0.75	0.85	0.85	0.84	0.80	0.83
$Cr/(Fe^{2+}+Fe^{3+})$	1.52	1.43	1.59	1.54	1.57	1.61	1.03	1.08	0.98	1.02	1.18
$Fe^{3+}/(Fe^{3+}+Al+Cr)$	0.12	0.14	0.11	0.11	0.11	0.10	0.21	0.20	0.23	0.19	0.17
$Mg(Mg+Fe^{2+})$	0.32	0.31	0.30	0.30	0.29	0.28	0.11	0.12	0.12	0.14	0.14

	Sample: IWS 65 Height*: -134.0					
Number	6	7	8	1	2	3
TiO_2	1.07	1.57	1.64	0.04	0.02	0.00
FeO	26.62	29.58	29.58	30.04	30.94	30.88
Fe_2O_3	11.57	12.64	12.75	20.30	19.31	19.38
MgO	4.55	3.20	3.09	0.98	1.04	1.04
CaO	0.00	0.00	0.00	0.00	0.00	0.00
MnO	0.35	0.33	0.35	0.43	0.45	0.45
Al_2O_3	9.96	7.11	7.01	5.63	5.79	5.78
Cr_2O_3	43.80	46.04	45.53	40.05	43.06	42.87
V_2O_5	0.47	0.67	0.61	0.27	0.22	0.26
TOTAL	98.39	101.14	100.56	97.74	100.84	100.67
Cr/(Cr + Al)	0.81	0.87	0.87	0.88	0.88	0.88
$Cr/(Fe^{2+}+Fe^{3+})$	1.15	1.09	1.08	0.79	0.86	0.85
$Fe^{3+}/(Fe^{3+}+Al+Cr)$	0.17	0.19	0.20	0.31	0.28	0.28
$Mg(Mg+Fe^{2+})$	0.15	0.10	0.09	0.03	0.03	0.03

PC091

	Sample: IWS UG2 Height*: -111.0					Sample: IWS BB1 Height*: -26.1					
Number	1	2	3	4	5	1	2	3	4	5	6
TiO_2	0.74	0.89	0.91	0.91	0.83	1.90	1.76	1.74	1.84	1.91	2.09
FeO	20.98	20.86	20.05	20.67	20.55	26.12	25.22	25.62	25.63	25.95	25.91
Fe_2O_3	6.65	7.28	8.09	7.62	7.61	15.65	16.21	16.58	15.99	16.94	17.09
MgO	9.01	8.88	9.28	9.05	9.27	5.35	5.82	5.63	5.61	5.35	5.53
CaO	0.00	0.00	0.00	0.00	0.00	0.00	0.00	0.00	0.00	0.00	0.00
MnO	0.27	0.28	0.31	0.29	0.29	0.34	0.35	0.37	0.36	0.35	0.36
Al_2O_3	16.05	15.83	15.77	15.83	16.35	10.11	10.52	10.37	10.29	10.00	10.21
Cr_2O_3	45.93	44.45	43.59	44.28	44.41	39.11	38.32	38.43	38.65	37.60	36.99
V_2O_5	0.14	0.07	0.09	0.09	0.08	0.28	0.21	0.25	0.23	0.24	0.29
TOTAL	99.13	97.85	97.31	98.01	98.64	97.40	96.84	97.38	97.06	96.69	96.82
Cr/(Cr + Al)	0.74	0.73	0.73	0.74	0.73	0.80	0.78	0.79	0.79	0.79	0.78
$Cr/(Fe^{2+}+Fe^{3+})$	1.66	1.58	1.55	1.57	1.58	0.94	0.92	0.91	0.93	0.88	0.86
$Fe^{3+}/(Fe^{3+}+Al+Cr)$	0.09	0.11	0.12	0.11	0.11	0.24	0.25	0.25	0.25	0.26	0.27
$Mg(Mg+Fe^{2+})$	0.30	0.29	0.32	0.30	0.31	0.17	0.19	0.18	0.18	0.17	0.18

PC091

MICROPROBE DATA FOR OLIVINE

*Height below or above the Merensky Reef

Sample: IWS 10
Height*: -40.8

Number	1	2	3	4	5	6	7	8	9	10	11	12	13	14	15
SiO_2	38.72	39.22	38.79	38.21	39.00	38.13	38.93	38.87	39.39	37.68	39.38	39.15	38.87	39.33	39.21
Al_2O_3	0.00	0.00	0.00	0.00	0.00	0.00	0.00	0.00	0.00	0.00	0.00	0.00	0.00	0.00	0.00
Na_2O	0.00	0.00	0.00	0.00	0.00	0.00	0.00	0.00	0.00	0.00	0.00	0.00	0.00	0.00	0.00
MgO	41.77	41.23	40.99	41.16	41.06	40.87	40.92	41.35	41.50	41.77	41.73	41.62	41.50	41.61	41.78
FeO	17.96	18.11	18.17	17.84	18.17	18.40	18.43	17.64	18.04	18.04	18.06	17.86	18.03	17.96	18.35
MnO	0.22	0.22	0.22	0.19	0.22	0.24	0.21	0.24	0.25	0.19	0.20	0.25	0.20	0.23	0.21
NiO	0.32	0.36	0.34	0.35	0.34	0.36	0.37	0.35	0.30	0.36	0.34	0.36	0.35	0.33	0.34
CaO	0.00	0.00	0.00	0.01	0.00	0.00	0.01	0.00	0.00	0.00	0.01	0.00	0.00	0.00	0.01
TiO_2	0.04	0.04	0.04	0.04	0.02	0.04	0.03	0.02	0.01	0.03	0.03	0.03	0.03	0.03	0.05
TOTAL	99.03	99.18	98.55	97.80	98.81	98.04	98.90	98.47	99.49	98.07	99.02	99.27	98.98	99.49	99.95

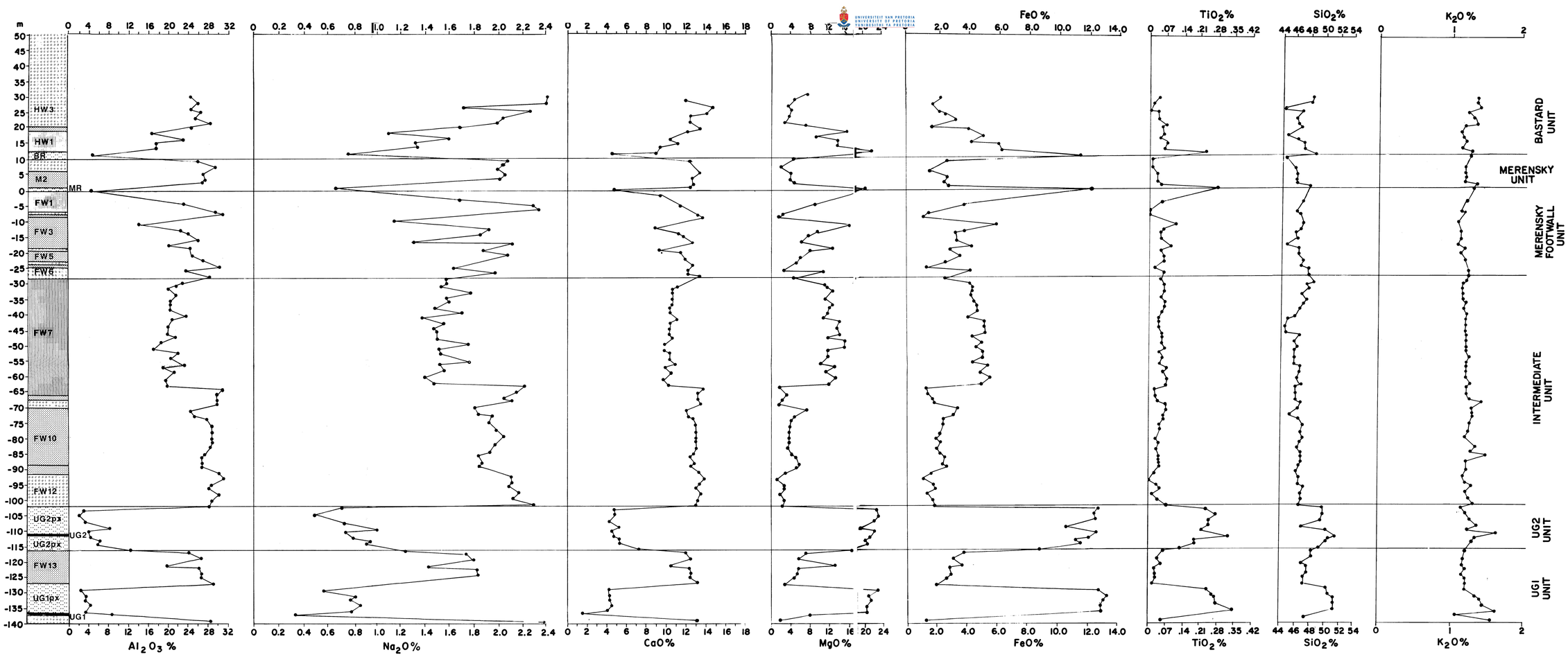

FIGURE 7.1

MAJOR ELEMENTS VS STRATIGRAPHIC HEIGHT

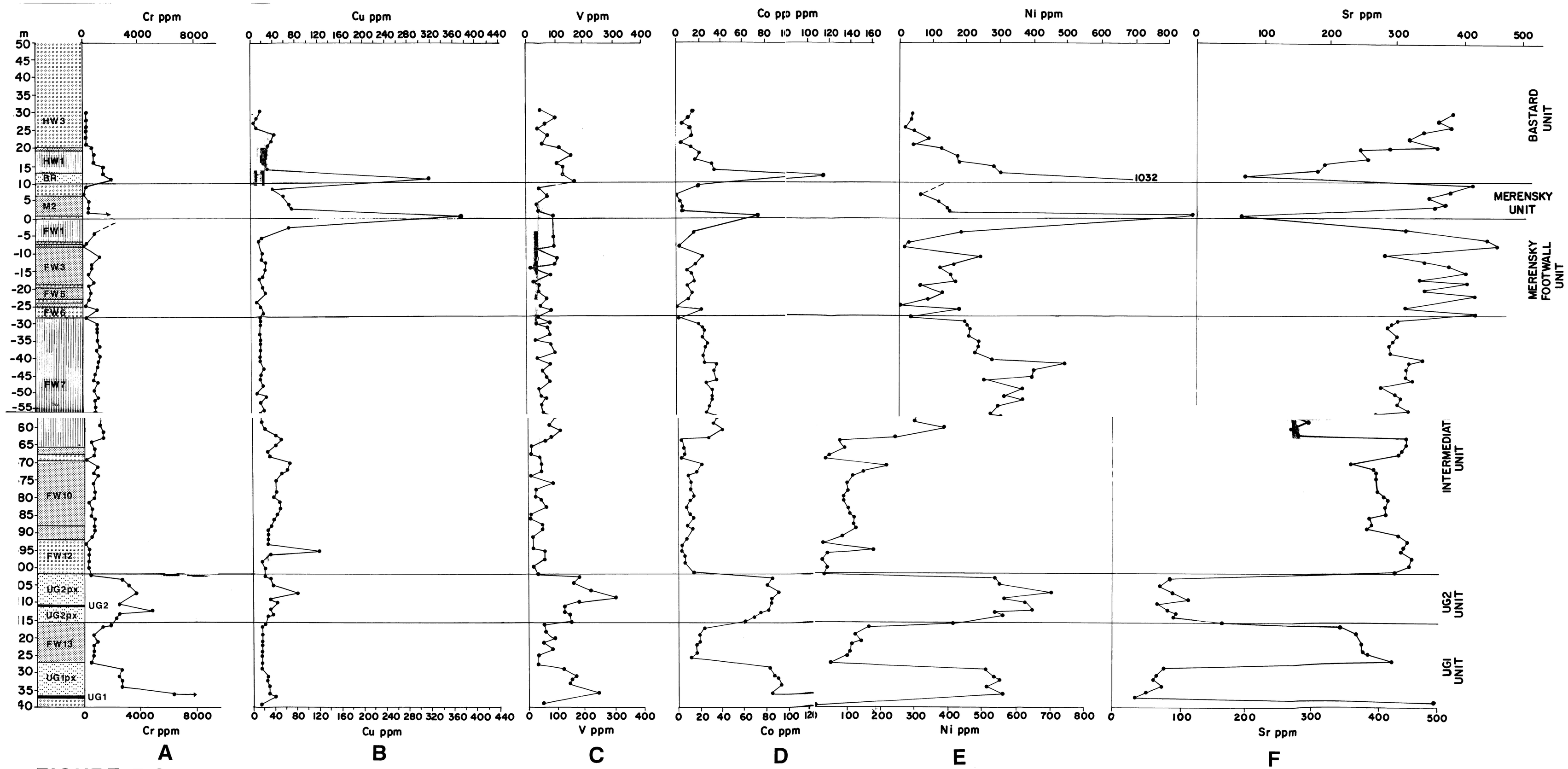

FIGURE 7.2

TRACE ELEMENTS VS. STRATIGRAPHIC HEIGHT